

U.S. Department of Commerce National Telecommunications and Information Administration

Institute for Telecommunication Sciences NTIA Technical Report

A Comparative Analysis of Multiple Knife-Edge Diffraction Methods

Nicholas DeMinco, Paul M. McKenna, and Robert T. Johnk

October 2025
Boulder,
Colorado
its.ntia.gov

Institute for Telecommunication Sciences
NTIA Technical Report
NTIA TR-26-580
October 2025

A Comparative Analysis of Multiple Knife-Edge Diffraction Methods

Nicholas DeMinco, Paul M. McKenna, and Robert T. Johnk



United States Department of Commerce

National Telecommunications and Information Administration

Institute for Telecommunication Sciences 325 Broadway, Boulder, CO 80305 its.ntia.gov

Approved for public release. Distribution is unlimited.

About the Institute for Telecommunication Sciences

The <u>Institute for Telecommunication Sciences</u> (ITS) is the research and engineering laboratory of the <u>National Telecommunications and Information Administration</u> (NTIA), an agency of the <u>U.S. Department of Commerce</u> (DoC). ITS manages the telecommunications technology research programs of NTIA and the DoC-owned Table Mountain Radio Quiet Zone. ITS works closely with other NTIA Line Offices to support Administration and Agency needs.

The mission of ITS is to ADVANCE innovation in communications technologies, INFORM spectrum and communications policy for the benefit of all stakeholders, and INVESTIGATE our Nation's most pressing telecommunications challenges through research that employees are proud to deliver.

ITS publishes fundamental research communications as part of its Technology Transfer efforts. We are committed to ensuring that our publications are substantive, technically sound, accurate, and clear. A rigorous peer review process, documented in the "ITS Publications Handbook Volume I: Policies (Third Edition)," safeguards the scientific integrity of ITS technical publications, journal articles, and conference papers. The principles for technical peer review of manuscripts guide parallel peer review processes for the publication of software and datasets.

ITS reports authored by NTIA employees are subject to <u>17 U.S.C. §105</u> are U.S. Government works and generally not subject to copyright protection in the United States. ITS publications, including software and datasets, are freely and openly available at <u>its.ntia.gov</u> or <u>github.com/NTIA</u>.

Principal NTIA Formal Publication Series Published by ITS

NTIA Technical Report (TR): Important contributions to existing knowledge of less breadth than a monograph, such as results of completed projects and major activities.

NTIA Technical Memorandum (TM): Technical information typically of less breadth than an NTIA Technical Report. The series includes data, preliminary project results, and information for a specific, limited audience.

NTIA Special Publication (SP): Conference proceedings; bibliographies; course and instructional materials; or major scientific studies mandated by Congress.

NTIA Monograph (MG): A scholarly, professionally oriented publication dealing with state-of-the-art research, or an authoritative treatment of a broad area. Expected to have long-lasting value.

NTIA Handbook (HB): Information pertaining to technical procedures; reference and data guides; and formal user's manuals that are expected to be pertinent for a long time.

For more information about NTIA fundamental research publications, contact the ITS Publications Office at 325 Broadway, Boulder, CO, 80305 Tel. 303-497-3572 or email ITSinfo@ntia.gov.

Disclaimer

Identification of commercial products or services in this report does not imply recommendation or endorsement by the National Telecommunications and Information Administration, Department of Commerce, or the U.S. Government.

Contents

Figures	vii
Tables	xi
Variables and Acronyms	xiii
1. Introduction	1
2. Description of the Multiple Knife-Edge Diffraction Problem	5
3. Diffraction Computation Methods	71220212427282830
4. Description of the 50 Multiple Knife-Edge Diffraction Scenarios Considered for the Analysis	
5. Comparison of Alternative Computation Methods with the Vogler Method 5.1 Comparisons of Loss Predictions for the Vogler Method and the Alternative Methods 5.2 Comparisons of Execution Times and Path Loss Predictions for the Vogler Method and the Alternative Methods.	45
6. Comparisons of Alternative Computation Methods with Measured Data 6.1 Comparisons to Measured Data from Deygout's Original Paper 6.2 Comparisons of Predictions to Measured Data for the 63rd Street Paths 6.3 Comparisons of Predictions to Measured Data for the Table Mountain Field Site and Radio Quiet Zone	59 59 63
7. Conclusions	72
8. References	75
Appendix A. The Bullington Mathematical Algorithm	77
Appendix B. The Epstein-Peterson Mathematical Algorithm	79
Appendix C. The Deygout Mathematical Method	

81
82
83
84
85
85
87
89
90
91

Figures

Figure	e 1. Six knife-edge diffraction scenario illustrating knife-edge heights and distance locations with two sub-path knife edges M_2 and M_6	6
Figure	e 2: Vogler's geometry and notation for multiple knife-edge diffraction for <i>N</i> diffraction knife edges	8
Figure	ϵ 3: Definition of height h for the Fresnel-Kirchhoff diffraction parameter $ u$.11
Figure	e 4. Knife-edge diffraction gain (dB) as a function of the dimensionless Fresnel-Kirchhoff diffraction parameter ν	.12
Figure	s 5. Incident shadow boundary and ray-path geometry for a typical diffraction scenario, with angles in radians	.14
Figure	e 6. The incident shadow boundary and ray path for a single knife edge, with angles in radians	.14
Figure	\approx 7: The Fresnel transition function $FTFx$ magnitude	.17
Figure	e 8: A four-knife-edge example of the graphical approach for the Bullington method.	.19
Figure	9: A four-knife-edge example for the graphical approach for the Epstein- Peterson method	.20
Figure	e 10: A four-knife-edge example for the graphical approach to the Deygout method.	.22
Figure	e 11: A four-knife-edge example for the graphical approach to the Giovaneli method.	.25
Figure	e 12: Six knife-edge diffraction example for Bullington method with sub-path knife edges M2 and M6.	.29
Figure	e 13: Six knife-edge diffraction example for Epstein-Peterson method with sub-path knife edges M2 and M6	.30
Figure	e 14: Six-knife-edge diffraction example for Deygout method with sub-path knife edges M2 and M6.	.31
Figure	e 15. Six knife-edge diffraction examples for Giovaneli method with sub-path knife edges M2 and M6.	.34
Figure	e 16: Six knife-edge diffraction scenario (Case 3) with two sub-path knife edges, M2 and M6	.36
Figure	e 17: Five-knife-edge diffraction scenario (Case 8) with one sub-path knife edge, <i>M</i> 2	.37

Figure	e 18: Four-knife-edge diffraction scenario (Case 13) with one sub-path knife edge, <i>M</i> 3.	37
Figure	19: Three-knife-edge diffraction scenario (Case 18) with no sub-path knife edges.	41
Figure	20: Two-knife-edge diffraction scenario (Case 23) with no sub-path knife edges.	41
Figure	21: Six-knife-edge ascending scenario (Case 28) with one sub-path knife edge, <i>M</i> 5, and one grazing knife edge, <i>M</i> 1	42
Figure	22: Six-knife-edge descending scenario (Case 33) with one sub-path knife edge, <i>M</i> 2, and one grazing knife edge, <i>M</i> 6	42
Figure	e 23: Six-knife-edge ascending scenario (Case 38) with two sub-path knife edges: M2 and M3	43
Figure	e 24: Six-knife-edge descending scenario (Case 43) with two sub-path knife edges: M4 and M5	43
Figure	25: Six-knife-edge ascending and descending scenario (Case 48) with no sub-path knife edges.	44
Figure	26: Attenuation ratio comparison to Vogler method for four alternative methods with all knife edges. Attenuation ratio (dB) = alternative method (dB) – Vogler method (dB)	45
Figure	27: Attenuation ratio comparison to the Vogler method for three alternative methods with all knife edges. Attenuation ratio (dB) = alternative method (dB) – Vogler method (dB)	46
Figure	28: Attenuation ratio comparison to the Vogler method for three alternative methods with major three knife edges. Attenuation ratio (dB) = alternative method (dB) – Vogler method (dB).	47
Figure	29: Attenuation ratio comparison to the Vogler method for three alternative methods with no sub-path knife edges. Attenuation ratio (dB) = alternative method (dB) – Vogler method (dB).	47
Figure	30: Attenuation ratio comparison to Vogler method for three variations of the Deygout method. Attenuation ratio (dB) = Deygout method (dB) – Vogler method (dB)	48
Figure	231: Attenuation ratio comparison to Vogler method for six variations of the Epstein-Peterson method. Attenuation ratio (dB) = Epstein-Peterson method (dB) – Vogler method (dB).	49
Figure	32: Attenuation ratio comparison to the Vogler method for four variations of the Epstein-Peterson method (two curves with largest errors removed for clarity). Attenuation ratio (dB) = Epstein-Peterson method (dB) - Vogler	Ε0
	method (dB).	50

Figure	the Giovaneli method. Attenuation ratio (dB) = Giovaneli method (dB) – Vogler method (dB)	50
Figure	34: Attenuation ratio comparison to Vogler method of the alternative methods that result in the lowest attenuation ratio. Attenuation ratio (dB) = alternative method (dB) – Vogler method (dB)	51
Figure	35: Attenuation ratio and Fresnel transition function product versus case number for Epstein-Peterson method with all knife edges. Attenuation ratio (dB) = Epstein-Peterson method (dB) - Vogler method (dB)	52
Figure	36: Attenuation ratio and Fresnel transition-function product versus case number for Epstein-Peterson method with no sub-path knife edges. Attenuation ratio (dB) = Epstein-Peterson method (dB) – Vogler method (dB).	53
Figure	37: Attenuation ratio and Fresnel transition function product versus case number for Giovaneli method with no sub-path knife edges. Attenuation ratio (dB) = Giovaneli method (dB) – Vogler method (dB)	53
Figure	38: Attenuation ratio and Fresnel transition function product versus case number for the Deygout method with no sub-path knife edges. Attenuation ratio (dB) = Deygout method (dB) - Vogler method (dB)	52
Figure	39. Comparison of execution times of the four alternative methods to the Vogler method for 50 different cases.	55
Figure	40: Epstein-Peterson loss prediction compared to measured data for the 10 paths in Deygout's original paper. Attenuation ratio (dB) = Epstein-Peterson method (dB) – measured data (dB)	61
Figure	41: Deygout loss prediction compared to measured data for the 10 paths in Deygout's original paper. Attenuation ratio (dB) = Deygout method (dB) - measured data (dB)	62
Figure	42: Giovaneli loss prediction compared to measured data for the 10 paths in Deygout's original paper. Attenuation ratio (dB) = Giovaneli method (dB) – measured data (dB).	62
Figure	43: Terrain contour for the short (north) path along 63rd Street, 12 km northeast of city center, Boulder, CO.	64
Figure	44: Terrain contour for the long (south) path along 63rd Street, 12 km northeast of city center, Boulder, CO.	65
Figure	45: Short propagation path and ITS transmitter van on 63rd Street	65
Figure	46. Loss prediction of alternative methods compared to Vogler loss prediction for short and long paths along 63rd Street. Attenuation ratio (dB) = alternative method (dB) – Vogler method (dB)	66

Figure	e 47. Prediction of basic transmission loss with Epstein-Peterson, Deygout, and Giovaneli loss prediction methods compared to measured data loss for the 63rd Street short path with receiver antenna at a distance of 1.38 km	67
Figure	e 48: Prediction of basic transmission loss with Epstein-Peterson, Deygout, and Giovaneli loss prediction methods compared to measured data loss for the 63rd Street long path with receiver antenna at a distance of 7.11 km	67
Figure	e 49: The Table Mountain Field Site Plateau Road diffraction path	68
Figure	e 50. Terrain contour for the Table Mountain Field Site Plateau Road path	69
Figure	e 51: Comparisons of three prediction methods to data that was measured at the Table Mountain Field Site Plateau Road path at a distance 400 meters from the transmitter using Table 22 scenario data.	70
Figure	e 52: Comparisons of three prediction methods to data that was measured at the Table Mountain Field Site Plateau Road path at a distance of 400 meters from the transmitter using Table 23 scenario data	71

Tables

Table 1: Parameters and computation results for Epstein-Peterson example of Figure 9	21
Table 2: Parameters and computation results for Deygout example of Figure 10	23
Table 3: Parameters and computation results for Giovaneli example of Figure 11	26
Table 4: Horizon parameter determination for the six diffraction knife edges	29
Table 5: Results for six knife-edge examples for the Epstein-Peterson method	30
Table 6: Computation of Fresnel-Kirchhoff diffraction parameter $ u$ and diffraction loss to determine the primary knife edge	32
Table 7: Computation of Fresnel-Kirchhoff diffraction parameter ν and diffraction loss to determine the secondary knife edge on the left side of the primary knife edge.	32
Table 8. Computation of Fresnel-Kirchhoff diffraction parameter $ u$ and diffraction loss for the third-level knife edge on the left side of the primary knife edge and the right side of the secondary knife edge $M1$	32
Table 9. Computation of Fresnel-Kirchhoff diffraction parameter ν and diffraction loss for three edges to determine the secondary knife edge on the right side of the primary knife edge.	33
Table 10. Computation of the Fresnel-Kirchhoff diffraction parameter ν and diffraction loss for the third-level knife edges $M4$ and $M6$ on the right side of the primary knife edge and each side of the secondary knife edge $M5$	33
Table 11. Computation of the Fresnel-Kirchhoff diffraction parameter $ u$ and diffraction loss for the Giovaneli method.	35
Table 12: Height and distance parameters for Cases 1 through 25	38
Table 13: Height and distance parameters for Cases 26 through 50	39
Table 14. Parameters of the computer used to perform the comparisons of execution times of the four alternative methods to the Vogler method for 50 different cases.	55
Table 15. Execution times in milliseconds for the Vogler method and the four alternative loss prediction methods for Cases 1 through 25 of Table 12	56
Table 16. Execution times in milliseconds for the Vogler method and the four alternative loss prediction methods for Cases 26 through 50 of Table 13	56

Table 17. Path loss predictions in decibels (dB) greater than free space for the Vogler method and the four alternative loss prediction methods for Cases 1 through 25 of Table 12.	57
Table 18. Path loss predictions in decibels (dB) greater than free space for the Vogler method and the four alternative loss prediction methods for Cases 26 through 50 of Table 13	58
Table 19. Descriptions of the 10 paths from Deygout's original paper	60
Table 20. Diffraction knife-edge height and diffraction-edge distance description of each diffraction edge for the short path on 63rd Street.	63
Table 21. Diffraction edge height and diffraction edge distance description of long path on 63rd Street.	64
Table 22. Frequency, antenna type, and antenna height data for the Table Mountain Field Site Plateau Road diffraction path measurements for first set of data for Figure 51.	68
Table 23. Frequency, antenna type, and antenna height data for the Table Mountain Field Site Plateau Road diffraction path measurements for second set of data for Figure 52.	69
Table 24. Terrain data for the Table Mountain Field Site path	70

Variables and Acronyms

C(v) and $S(v)$	widely tabulated Fresnel Cosine and Sine integrals with real arguments
$d_1 - d_{n+1}$	distances between consecutive knife edges by index number 1 through $n+1$
d_i	distance to the i^{th} knife edge from the base of the transmitter antenna
d_r	distance of the receiver antenna with respect to the transmitter antenna
d_R	distance from the base of the knife edge under consideration to the base of the receiver antenna
d_T	distance from base of the transmitter antenna to the base of the knife edge under consideration
E_0	free-space electric field strength in the absence of both the ground and knife- edge environments
E	electric field strength in the presence of both the ground and knife-edge environments
Knife edge 1	first knife edge for $n=1$ to the right of the transmitter at distance d_1 with subsequent knife edges $d_2,d_3\cdots d_{n+1}$ numbered consecutively up to the receiver
Knife edge 2	knife edge for $n=2$ located at a distance d_1+d_2 from the transmitter
Knife edge 3	knife edge for $n=3$ located at a distance $d_1+d_2+d_3$ from the transmitter
Knife edge 4	knife edge for $n=4$ located at a distance $d_1+d_2+d_3+d_4$ from the transmitter
Knife edge 5	knife edge for $n=5$ located at a distance $d_1+d_2+d_3+d_4+d_5$ from the transmitter
Knife edge 6	last knife edge for $n=6$ and located at a distance $d_1+d_2+d_3+d_4+d_5+d_6$ from the transmitter, adjacent to the receiver
FAMKE	First Analysis Multiple Knife Edge computer program by Vogler
FTFP	Fresnel transition function product; product of all the individual Fresnel transition functions for a multiple knife-edge scenario
FTF(x)	Fresnel transition function that compensates for the error encountered in the diffraction computation when the ray path is in the transition zone
F(v)	diffraction integral computation for a single knife edge with Fresnel-Kirchhoff diffraction parameter ν
GTD	geometrical theory of diffraction method
h	height of the knife edge above a reference line drawn between the reference height of the transmitter and receiver antennas; referred to as the effective height of the knife edge
Δh_i	adjustment for modifying the height of the i^{th} knife edge for nonzero transmitter and receiver antenna heights
h_1 through h_n	actual heights of the diffraction knife edges by index number 1 through \emph{n}
h_1' through h_n'	effective knife-edge heights of the diffraction knife edges by index number 1 through n
h_r	height of the receiver antenna

 h_t height of the transmitter antenna

ITS Institute for Telecommunication Sciences
ITU International Telecommunication Union

J(v) approximate equation for the diffraction loss for a single diffraction knife edge

km unit distance in thousands of meters

k propagation constant $k = \frac{2\pi}{\lambda}$

 λ wavelength of the radio frequency f given by $\lambda = c/f$, where c is the speed of

light in meters per second and f is the radio frequency in Hertz

L(dB) diffraction loss in decibels

LOS line-of-sight

 L_d^1 (dB) exact expression for the single knife-edge diffraction loss

 M_1-M_n index numbers to specify the names of the diffraction knife edges NLOS non-line-of-sight or beyond line-of-sight; as in the diffraction region

NTIA National Telecommunications and Information Administration

PAMKE Partitioned Analysis Multiple Knife Edge computer program by Vogler

mathematical constant 3.141593... and the ratio of the circumference of a

circle divided by its diameter

RCVR receiver

r first Fresnel zone radius that indicates the size of the Fresnel zone clearance

 $\theta_1,\,\theta_2,\,...,\,\theta_N$ diffraction angles that can be calculated from the knife-edge heights and the

separation distances

 ϕ angle of the incident shadow boundary ϕ_{ray} angle of the incident ray to the next edge UTD Uniform Theory of Diffraction method

 v_1 lower limit for Vogler's diffraction integral for a single diffraction knife edge v_i Fresnel-Kirchhoff diffraction parameter for the i^{th} knife edge in a multiple

knife-edge scenario

 u_m Fresnel-Kirchhoff diffraction parameter for the m^{th} knife edge and the lower

limit of the multiple integrals in the Vogler diffraction computation

x FTF(x) x is a function of the deviation of the ray path and incident shadow boundary

 $\phi_{ray} - \phi'$ and L the distance between the diffraction knife edge and the

observation point

XMTR transmitter

A Comparative Analysis of Multiple Knife-Edge Diffraction Methods

Nicholas DeMinco, ¹ Paul M. McKenna, ¹ and Robert T. Johnk²

Abstract: The results of a thorough comparative analysis of alternative graphical prediction methods for multiple knife-edge diffraction are presented and compared to the method developed by Vogler. The Vogler multiple knife-edge diffraction loss is rigorous and verified with measured data, but too computationally intensive for use in a propagation model that predicts area coverage over irregular terrain. Mathematical algorithms were developed for alternative graphical prediction methods for diffraction paths with up to six knife edges, resulting in methods that are many orders of magnitude faster. This is important for use in propagation models that predict area coverage over irregular terrain for many radial directions from the transmitter. A technique for selecting the best alternative method is proposed. Graphical techniques and mathematical algorithms are also described. Comparisons of the Vogler method to the alternative methods are included. Some comparisons to measured data are also presented.

Keywords:

diffraction, electromagnetic diffraction, electromagnetic wave propagation, multiple knife-edge diffraction, non-line-of-sight, radio frequency propagation, radio-wave propagation, Vogler method

1. Introduction

A comparative analysis of different multiple knife-edge diffraction methods was performed to support various radio wave propagation models under development at the Institute for Telecommunication Sciences (ITS). The goal was to investigate faster methods for computing multiple knife-edge diffractions for the non-line-of-sight (NLOS) environment. The results of ongoing analysis and measurement efforts will be used to develop diffraction loss computation techniques for radio-wave propagation predictions in a variety of NLOS environments.

L.E. Vogler developed a rigorous multiple knife-edge diffraction method in the 1980s [1], [2]. That method has been verified by comparison to measured data to be accurate, but it

¹ The author is with the Institute for Telecommunication Sciences, National Telecommunications and Information Administration, U.S. Department of Commerce, Boulder, CO 80305.

² The author was formerly with the Institute for Telecommunication Sciences, National Telecommunications and Information Administration, U.S. Department of Commerce, Boulder, CO 80305.

requires excessive run times for many knife edges. Faster methods are currently needed for propagation models that compute basic transmission loss predictions in situations where many computations are required in different radial directions over many knife edges. Faster alternative methods for computing multiple knife-edge diffractions are approximations to the rigorous method. They obtain solutions by compositions of single knife-edge diffraction results. This report compares the accuracy of four faster methods to Vogler's more rigorous method.

All of the alternative diffraction computation methods are approximations and are based on the Fresnel-Kirchhoff scalar theory of diffraction. The Kirchhoff boundary conditions are also approximate and only apply to scalars. This diffraction analysis is based on the classical approach of the Fresnel-Kirchhoff scalar theory of optics for a single knife edge. The assumption is made that the knife edge is a perfectly absorbing screen place normal to the direction of propagation extending to infinity in both directions and vertically downwards. In a multiple knife-edge scenario, the losses for each edge will be combined using the alternative multiple knife-edge methods. There are a number of alternative methods for computing diffraction loss over multiple knife edges. Each method has its own unique procedure for computing diffraction loss.

The original motivation for this analysis effort was to determine which alternative diffraction computation method to use to compute diffraction loss over multiple knife edges based on criteria to be discussed in this report. A selection technique to determine the optimum alternative diffraction computation method is based on the relative geometric location of the incident shadow boundary and the ray path from one knife edge to the next.

This report describes the alternative multiple knife-edge diffraction computation methods graphically. Mathematical algorithms for diffraction paths with up to six knife edges were developed for each method so that they can be implemented in a computer program. Comparisons of each of the alternative multiple knife-edge diffraction computation methods to Vogler's analytically rigorous multiple knife-edge diffraction solution were performed. Techniques for determining the best alternative method to use for multiple knife-edge diffraction computations were proposed for various scenario configurations. Some limited comparisons with existing measured data for each of the methods are also presented.

Four alternative diffraction methods were investigated: Bullington [3], Epstein-Peterson [4], Deygout [5], and Giovaneli [6]. All four are graphical techniques, where the analyst must identify the most important knife edges through educated guesswork. Graphical procedures for each of the methods can be obtained from the cited references and are described in Section 3 of this report.

Mathematical algorithms had to be developed for these graphical methods to implement them in a computer program. This enabled comparison of each alternative diffraction method to Vogler's rigorous diffraction method to determine a suitable method for the NLOS propagation scenarios. Descriptions of the graphical techniques and the mathematical algorithms are presented for each of the methods.

The Bullington method is the simplest to implement, but the least accurate and therefore unsuitable even with only two knife edges. The other three methods claim to have improved accuracy when compared to Bullington's method, with only a slight increase in complexity [4]-[6]. Of those, the Epstein-Peterson method is the simplest and most straightforward to

implement. It maintains reasonable diffraction loss prediction accuracy for some scenarios. The Deygout method is an improvement over the Epstein-Peterson method. The Giovaneli method corrects the error in diffraction angle in Deygout's method by using a diffraction angle that more closely coincides with that used for the geometrical theory of diffraction (GTD) [6].

Various modifications were made to each of these alternative methods, including deleting the sub-path knife edges (defined in Section 2) and using only the major three knife edges. This led to three additional methods to include as candidate methods for consideration for each of the four original methods. A special correction based on the GTD was also used with the Epstein-Peterson method [7] for some cases. The major three knife edges for Epstein-Petersen and Deygout methods are determined by selecting the three knife edges whose Fresnel-Kirchhoff parameter ν is the largest. The major three edges for the Giovaneli method are determined by constructing a line from the main (tallest) edge through the peaks of the other edges and selecting the smallest absolute value of slope on each side of the main edge. All these methods need to be compared to the rigorous L.E. Vogler method to determine the superior alternative for a wide variety of scenarios. Comparisons to measured data will also aid in the determination of the best alternative methods to use for diffraction computations.

Section 2 describes the multiple knife-edge diffraction problem and the geometry of the knife-edge locations in a diffraction scenario for zero and nonzero antenna heights. The subpath knife edges were also defined. The first Fresnel zone radius will also be defined.

Section 4 describes the Vogler method for multiple knife edges and the Fresnel diffraction integral method for a single knife edge. The alternative diffraction methods will also be described with graphical examples of how each of these alternative diffraction methods compute the diffraction loss. Summary comments on the alternative diffraction methods are included.

Section 3.3 Provides a technique for selecting the best alternative diffraction loss computation method to obtain the best estimate of diffraction loss. Section 3.4 includes examples of alternative computation methods with six knife edges to provide more detail on the computation complexity when up to six knife edges are included.

Section 4 introduces 50 multiple knife-edge diffraction scenarios that include many variations of varying distances between knife edges, different knife-edge heights, and different height-to-distance ratios for the knife-edge geometries. The scenarios are listed in tabular form. Section 5 includes the figures to graphically illustrate each scenario.

Section 5 compares losses of the alternative computation methods with the Vogler method for the 50 scenarios of Section 4. The results are illustrated in multiple figures. Discussions of the results are also included. Section 5 also includes the execution time comparisons of the Vogler method and the alternative methods for the 50 cases listed in Section 4.

Section 6 contains the results of comparisons of the alternative computation methods with measured data. The results of Deygout's classic original paper are presented here with comparisons to the loss predictions of the alternative computation methods. Comparisons of the losses of alternative prediction methods to data measured by ITS for two separate measurement programs are also presented.

Section 7 contains conclusions for the study and summarizes the results.

Section 8 is a list of references.

Appendices Appendix A through Appendix D provide the mathematical details of all alternative computation method algorithms for up to six multiple knife edges. These algorithms were coded in a computer program.

2. Description of the Multiple Knife-Edge Diffraction Problem

A common procedure used to compute propagation loss over irregular terrain is to determine the locations and heights of the significant terrain features and represent each feature as a knife edge. A sequence of knife edges is then cast as a multiple knife-edge problem.

First, it is necessary to be able to define the geometrical representation of the scenarios. All method development will assume that the database contains up to n knife edges where n=6 is the maximum number of knife edges. Figure 1 shows that the knife edges have index numbers assigned consecutively from left to right as M_1 through M_n with their respective heights h_1 through h_n . Distances d_1 through d_{n+1} represent the distance between the first knife edge and the transmitter, the distances between adjacent knife edges, and the distance between the last knife edge and the receiver. Knife edge 1 is the first knife edge to the right of the transmitter antenna. Subsequent knife edges are numbered consecutively up to the receiver antenna. For n=6, knife edge 6 is adjacent to the receiver antenna. The knife-edge location for the i^{th} knife edge represents the distance from the transmitter antenna and is given by:

$$d_i = \sum_{k=1}^i d_k \tag{1}$$

The receiver is located at:

$$d_r = \sum_{k=1}^{n+1} d_k \tag{2}$$

Knife edge 1 is located at a distance d_1 from the transmitter, knife edge 2 is located at a distance d_1+d_2 from the transmitter, knife edge 3 is located at a distance $d_1+d_2+d_3$ from the transmitter, etc.

For nonzero transmitter and receiver antenna heights, all knife-edge heights are referenced to a baseline drawn between the transmitter and receiver antennas, and are a linear function of the distance of the knife edge from the transmitter and the difference between the transmitter and receiver heights. This determines the slope of the baseline.

The equation for adjusting this height as a function of distance for the i^{th} knife edge is

$$\Delta h_i = (h_r - h_t) \frac{d_i}{d_r} + h_t \tag{3}$$

where h_r is the transmitter antenna height and h_t is the receiver antenna height.

Figure 1 shows a sub-path knife edge, a knife edge between two knife edges whose peak is below a line drawn between the previous knife edge and the next knife edge. Knife edges M_2 and M_6 are sub-path knife edges. A sub-path knife edge can also occur between the transmitter antenna and the second knife edge or the next-to-last knife edge and the receiver

antenna. If the first knife edge or last knife-edge peak is below a ray represented by a line drawn between the transmitter antenna to the second knife-edge peak, or a line drawn from the next-to-last knife-edge peak and the receiver antenna respectively, then the first or last knife-edge peak is a sub-path knife edge. In Figure 1 M_6 is an example of this type of knife edge, since it is between the next-to-last knife-edge peak and the receiver antenna.

If a sub-path knife edge occurs between two knife edges, and causes the first Fresnel zone to be obstructed, then the sub-path knife edge should be included in the analysis. If the sub-path knife edge does not interfere with the first Fresnel zone, then this knife edge can be neglected in the computation of diffraction loss.

The first Fresnel zone radius, r, is given by [8]

$$r = \sqrt{\frac{\lambda d_T d_R}{d_T + d_R}} \tag{4}$$

where d_T is the distance from the first knife edge to the sub-path knife edge, and d_R is the distance from the sub-path knife edge to the other knife edge, and λ is the wavelength defined as $\lambda = c/f$. All dimensions are in either meters or kilometers.

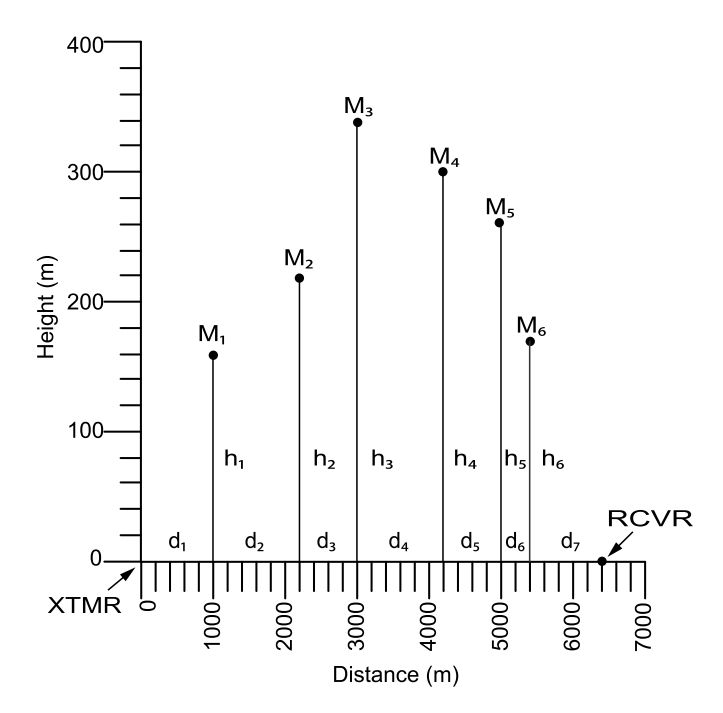


Figure 1. Six knife-edge diffraction scenario illustrating knife-edge heights and distance locations with two sub-path knife edges M_2 and M_6 .

3. Diffraction Computation Methods

The Vogler method is a mathematically rigorous analytical computation technique that uses higher order mathematical techniques but is computationally burdensome. All of the alternative diffraction methods were originally graphical techniques, and they are usually computed manually. Mathematical algorithms were developed to enable the four alternative methods to be run on a computer. This section will first briefly describe the Vogler method, the Fresnel integral method, and then the graphical procedures for each of the alternative methods with an example. Finally, six knife-edge diffraction computation examples for the use of the algorithms in Appendices A through D are presented and each of the four alternative computation methods discussed for these examples.

3.1 The Vogler Method

ITS developed and validated computer code to reproduce multiple knife-edge attenuation results quoted for the First Analysis Multiple Knife Edge (FAMKE) computer program by Vogler and Partitioned Analysis Multiple Knife Edge (PAMKE) computer program by Vogler. FAMKE and PAMKE Vogler methods in [1] and [2]. The practical basis for both methods is the numerical evaluation of the repeated integrals of the complementary error function with a complex argument. The new implementation uses a more robust method of numerical evaluation for these functions developed by Gautschi [9].

The original Vogler work [2] takes work by Furutsu [10] as its starting point and approximates irregular terrain as a series of rounded diffracting obstacles. Furutsu's solution used a generalized residue series, which, unfortunately, is slowly convergent as the obstacles' radii tend to zero. Using transformations of the residue series solution to integrals, Vogler derived a multiple knife-edge diffraction solution involving multiple integrals over successive knife edges and introduced a series representation for these integral functions that is amenable to numerical solution [1], [11]. Whitteker [12] later independently validated Vogler's results by computing numerical values and comparing them to certain analytical results in [1] and [2]. In a later paper [11], Vogler derives a multiple knife-edge diffraction method using Fresnel-Kirchhoff theory and shows that this is equivalent to that method and the results developed in [2].

Equation 18 in [2] is the result of Vogler's derivation using the Fresnel-Kirchhoff theory. This equation is an expression for the diffraction attenuation for multiple knife edges. Figure 2 illustrates Vogler's geometry and notation for the multiple knife-edge diffraction problems for N knife edges.

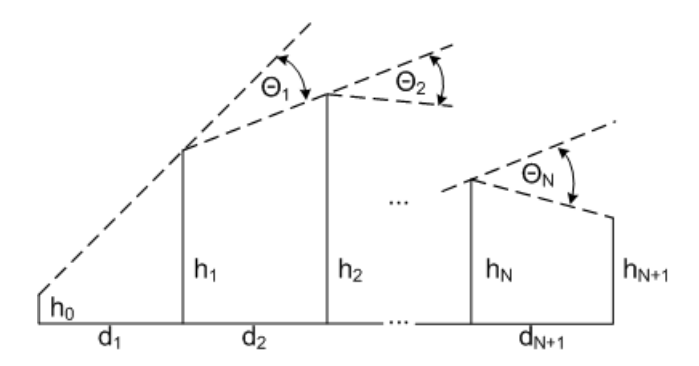


Figure 2: Vogler's geometry and notation for multiple knife-edge diffraction for N diffraction knife edges.

There are N+1 separation distances between knife edges indicated by $d_1, d_2 \cdots d_{n+1}$. The heights of the N knife edges are designated as $h_1, h_2 \cdots h_{n+1}$ where the heights of the transmitter and receiver antennas are h_0 and h_{n+1} , respectively. The diffraction angles $\theta_1, \theta_2, \ldots, \theta_N$ can be calculated from the knife edge heights and separation distances. Equation 18 in [2] is

$$\frac{E}{E_0} = \left(\frac{1}{\pi}\right)^{\frac{N}{2}} \int_{\nu_1}^{\infty} \dots \int_{\nu_N}^{\infty} e^{-(\nu_1^2 + \dots + \nu_N^2)} d\nu_1 \dots d\nu_N \tag{5}$$

where E_0 is the free-space electric field strength in the absence of both the ground and the knife edges, v_1 is the Fresnel-Kirchhoff diffraction parameter for knife edge 1 and v_N is the Fresnel-Kirchhoff diffraction parameter for knife edge N. The Fresnel-Kirchhoff diffraction parameter is defined in [2].

The lower limits of the multiple integrals are given by explicit expressions in terms of the geometry of the knife-edge heights and separation distances of Figure 2. An explanation of the rigorous mathematical derivations for the Vogler method is very complex and beyond the scope of this paper, but a brief description will be presented to communicate its complexity. The complex derivations are described in [1] and [2].

For (5) with N knife edges, it is necessary to evaluate N integrals where each of these integrals must be transformed into an expression suitable for numerical evaluation [2]. This is accomplished by expanding the expression in each of the integrals into its power series [11]. The computation for attenuation is a series of terms involving functions that are repeated integrals of the error function defined in [13]. Reference [13] also contains a number of computation algorithms for computing these functions. Closed form solutions exist for certain special cases for only two or three knife edges where the tops of the knife edges graze the straight line between the source and receiver, so that the diffraction angles θ_i defined in Figure 2 are all equal to zero. For N greater than or equal to three knife edges and nonzero diffraction angles θ_i , no closed form solution exists.

Reference [1] discusses how many repeated integrals of the error function are required to achieve reasonable accuracy in computing the attenuation function. Vogler determined that for 10 diffraction knife edges, 160 repeated integrals were required for three-decimal place accuracy in the numeric ratio representing the diffraction attenuation [1]. This numeric ratio is

a number that is always less than or equal to one. For six diffraction knife edges, one hundred repeated integrals were required to get four-decimal place accuracy [1]. This is extremely costly in terms of computation time even with modern computers.

Vogler's multiple knife-edge computation for *N* greater than or equal to 2 knife edges results in terms involving the product of complex multiple complementary error functions that have complex arguments (dimensionless diffraction parameters). These results are difficult to separate into real and imaginary parts for computing the magnitude of the diffraction loss. The principal restriction in this approach is that the source, knife edges, and receiver be sufficiently separated from one another.

Equation (5) reduces to the case of the Fresnel diffraction integral for a single knife edge when N=1 and is given by:

$$\frac{E}{E_0} = \left(\frac{1}{\pi}\right)^{\frac{1}{2}} \int_{\nu_1}^{\infty} e^{-\nu_1^2} d\nu_1 \tag{6}$$

Vogler's rigorous diffraction loss computation method [1], [2] is very accurate when compared to measured data, but computationally intensive when compared to any of the four alternative multiple knife-edge diffraction methods investigated. A faster radio wave propagation model is needed that computes diffraction loss for many diffraction knife edges. This is important for multiple knife-edge computation of diffraction loss over many knife edges when the methods are used in a propagation model that predicts area coverage. Comparisons of run times with up to 6 diffraction knife edges between the Vogler method and the alternative methods of Epstein-Peterson, Deygout, and Giovaneli resulted in run times more than three orders of magnitude (up to 1000:1) greater than the alternative methods. Section 5.2 contains comparisons of execution times between the Vogler method and the alternative methods.

3.2 Diffraction Computation Method for a Single Knife Edge

This diffraction analysis is based on the classical approach of the Fresnel-Kirchhoff scalar theory of optics for a single knife edge. The assumption is made that the knife edge is a perfectly absorbing screen placed normal to the direction of propagation extending to infinity in both directions and vertically downwards. In a multiple knife-edge scenario, the losses for each knife edge will be combined using the alternative multiple knife-edge methods. The single knife-edge diffraction computation can be represented in terms of a real diffraction parameter ν and computed using the widely tabulated Fresnel Cosine and Sine integrals with real arguments [13]. $F(\nu)$ is the complex Fresnel integral defined previously and ν is the dimensionless Fresnel-Kirchhoff diffraction parameter. This differs from Vogler's derivation and subsequent reduction to a single knife edge, because of a change of variables from ν_1 to $\frac{\pi t^2}{2}$ and integrations from $\int_{\nu_1}^{\infty} e^{-\nu \frac{2}{1}} d\nu_1$ to $\int_0^{\nu} e^{j\frac{\pi t^2}{2}} dt$ for a simpler representation in terms of $F(\nu)$.

$$F(\nu) = \int_{0}^{\nu} \cos\left(\frac{\pi t^2}{2}\right) dt + j \int_{0}^{\nu} \sin\left(\frac{\pi t^2}{2}\right) dt = C(\nu) + jS(\nu)$$
(7)

where

$$C(-z) = -C(z)$$
 and $S(-z) = -S(z)$.

The exact expression for the single knife-edge diffraction loss, L_d^1 (dB), is [8], [14]:

$$L_d^1(dB) = -20 \log \left(\left| \frac{1+j}{2} F(\nu) \right| \right)$$

$$= -20 \log \left(\frac{\sqrt{\left(1 - C(\nu) - S(\nu)\right)^2 + \left(C(\nu) - S(\nu)\right)^2}}{2} \right) = J(\nu)$$
(8)

This expression is easy to evaluate since there are very reasonable computation time methods for evaluating the Fresnel Cosine and Sine integrals.

An even simpler approximate equation also exists for the diffraction integral and is given by $J(\nu)$ in terms of ν for $\nu \ge -0.78$ [8]. The Fresnel diffraction integral can be approximated by the following expression [8]:

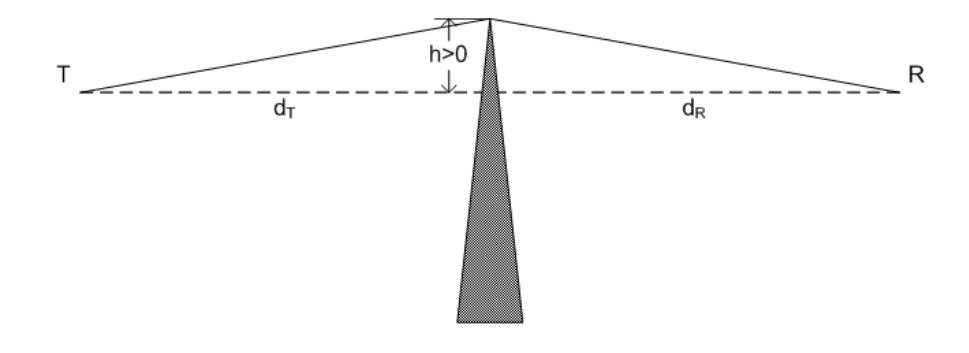
$$\frac{E}{E_0} = J(\nu) = 6.9 + 20\log\left(\sqrt{(\nu - 0.1)^2 + 1.0} + \nu - 0.1\right)$$
(9)

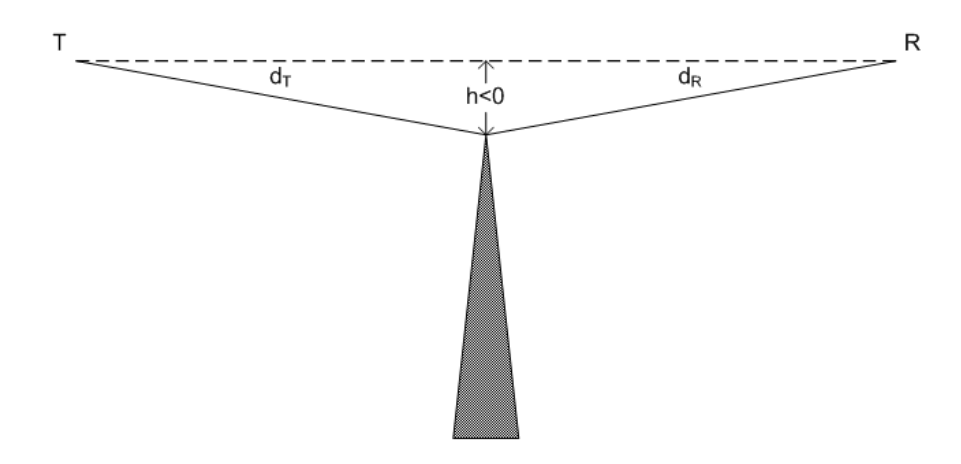
where E is the electric field strength of the diffracted wave and E_0 is the free-space field strength in the absence of both the ground and the knife edge. $J(\nu)$ is the diffraction loss in dB for $\nu \geq -0.78$. For $\nu < -0.78$, $J(\nu)$ oscillates about 0 dB and the magnitude is always less than or equal to 1.3 dB [8]. As shown in Figure 3, the parameter ν is computed from the height of the knife edge h above a reference line drawn between the reference height of the transmitter and receiver antennas, the distance from the transmitter antenna to the base of the knife edge d_T , and the distance from the base of the knife edge to the receiver antenna, d_R , and λ , the wavelength in meters. The parameter ν is given by [8]:

$$v = h \sqrt{\frac{2(d_T + d_R)}{\lambda d_T d_R}} \tag{10}$$

Figure 3 defines the knife-edge height parameter h in (10) and shows how it can be positive, negative, or zero depending on the height of the knife edge relative to the height of a line between the two terminals or between the source or receiver. Figure 3 also defines the variables in the above equation for the Fresnel diffraction parameter v.

Figure 4 is a plot of the knife-edge diffraction gain in dB as a function of the Fresnel-Kirchhoff diffraction parameter ν . For values of $\nu \geq -0.78$, (9) is used to compute the knife-edge diffraction gain in dB. For values of $\nu < -0.78$, (8) is used to compute the knife-edge diffraction gain.





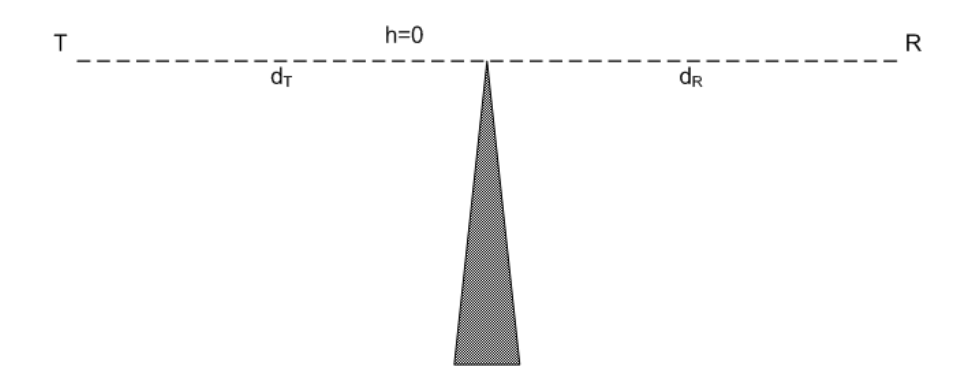


Figure 3: Definition of height h for the Fresnel-Kirchhoff diffraction parameter v.

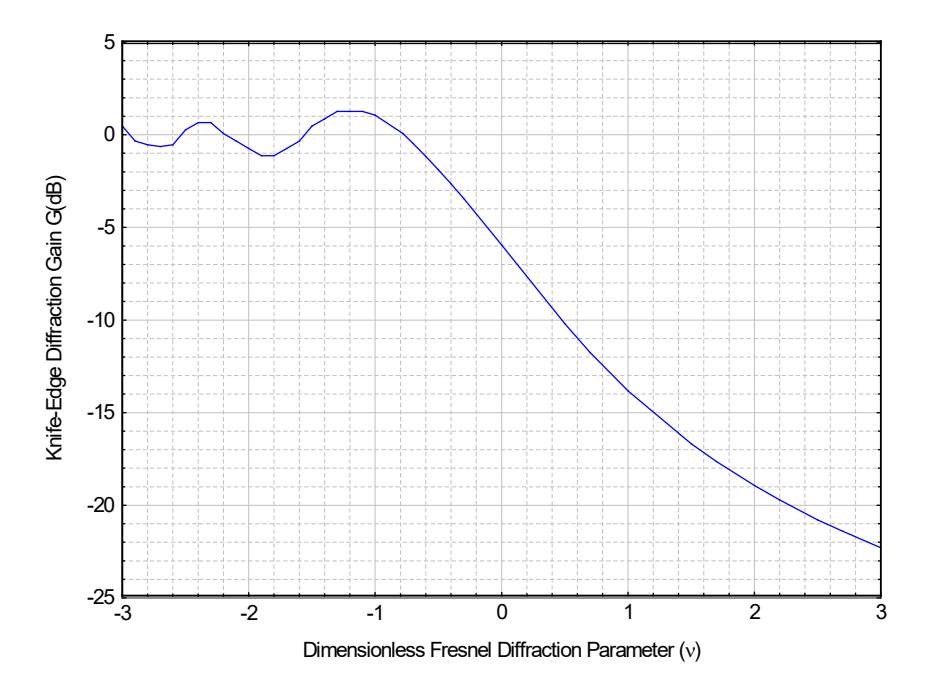


Figure 4. Knife-edge diffraction gain (dB) as a function of the dimensionless Fresnel-Kirchhoff diffraction parameter ν .

3.3 Alternative Diffraction Loss Computation Methods for Multiple Knife Edges

There are a number of alternative methods for computing diffraction loss over multiple knife edges. Each method has its own unique procedure for computing diffraction loss. However, they all 1) determine the field of each knife edge from the field of the preceding knife edge, and 2) use the algebraic approximation to the Fresnel diffraction integral and the Fresnel-Kirchhoff diffraction parameter, defined in (9) and (10), to compute the diffraction loss over each knife edge. They differ in how they compute the Fresnel-Kirchhoff diffraction parameter ν for each knife edge, since the effective height computation of each of the diffraction knife edges is also different for each of the methods. They all add the diffraction losses of the multiple knife edges to obtain the total diffraction loss. The field at any particular knife edge arises solely from the total field from the preceding knife edge.

The alternative methods described in this paper cascade terrain obstructions using multiple knife edges and use Fresnel-Kirchhoff theory for computing knife-edge diffraction loss. The diffraction analysis in this paper is based on the classical approach of the Fresnel-Kirchhoff scalar theory of optics. While computationally efficient, these methods are inherently error prone.

Ray-based diffraction methods such as the geometrical theory of diffraction (GTD) or uniform theory of diffraction (UTD) take into account polarization of the electromagnetic wave, whereas Fresnel-Kirchhoff diffraction methods do not [15]. Ray-based methods such as UTD and GTD will give the same results as Fresnel knife-edge diffraction when the interior wedge angle of the perfectly absorbing knife edge is zero and becomes a knife edge [15]. Imagine

two sides of a triangle forming a wedge. As the interior angle between the two sides of a wedge is reduced to zero, the sides of the triangle will be flat against each other, and the result will appear as a knife edge.

Fresnel-Kirchhoff multiple knife-edge diffraction assumes that each knife edge is uniformly illuminated by the previous knife edge. In reality, the field in the shadow of each knife edge that illuminates successive knife edges is not generally uniform, and as a result, cascading knife edges in the alternative methods are not rigorously correct [15].

While these alternative methods are not correct in a rigorous sense, they do result in reasonably accurate computations for many terrain scenarios simulated as perfectly absorbing knife edges. They also show reasonable agreement (Epstein-Peterson ±6 dB, Deygout ±3 dB, and Giovaneli ±2 dB) compared with measured data [4]-[6], [14]-[16]. A perfectly absorbing knife edge absorbs all of incident field energy, and there are no scattered, transmitted, or reflected fields [15]. The assumption of a perfectly absorbing knife edge eliminates the dependence on polarization and makes the computation much simpler [15]. The computation results are very close (within ±6 dB for the three alternative methods) to those of the rigorous computation methods such as Vogler [2] and [17]. A rigorous analysis for an absorbing knife edge results in a diffraction coefficient that is the same for both polarizations (horizontal and vertical) of the electric field [18]. As a result, the scalar Fresnel-Kirchhoff approximations can be used to determine the complex amplitude of the diffracted field [18].

Vogler compared his results to the GTD, the Epstein-Peterson method, and the Deygout method for five equally spaced knife edges having the same value of the diffraction angle at each knife edge [2]. Good agreement (within ± 6 dB maximum or ± 2 dB minimum) was obtained for the alternative methods except for small diffraction angles. The larger deviation of diffraction loss for small diffraction angles computed with the Epstein-Peterson and Deygout method is due to the proximity of the incident shadow boundary to the incident ray path as shown in Figure 6, where the error in diffraction loss should increase. The large deviation is due to the proximity of the ray path from one knife edge to the next being in the transition zone, the small angular area near the incident shadow boundary. Figure 6 illustrates the incident shadow boundary for the first two knife edges as $\phi = \phi' + \pi$. The angle $\theta = \phi_{ray} - \phi$ is the difference between angle of the incident ray path for the next knife edge ϕ_{ray} and the angle of the incident shadow boundary ϕ . The angles are in radians.

Figure 6 uses the same angle designations as Figure 5 but is the case for a single edge. The angle $\theta = \phi_{ray} - \phi$ is now the difference between angle of the incident ray path to the receiver ϕ_{ray} and the angle of the incident shadow boundary ϕ . The angles are in radians.

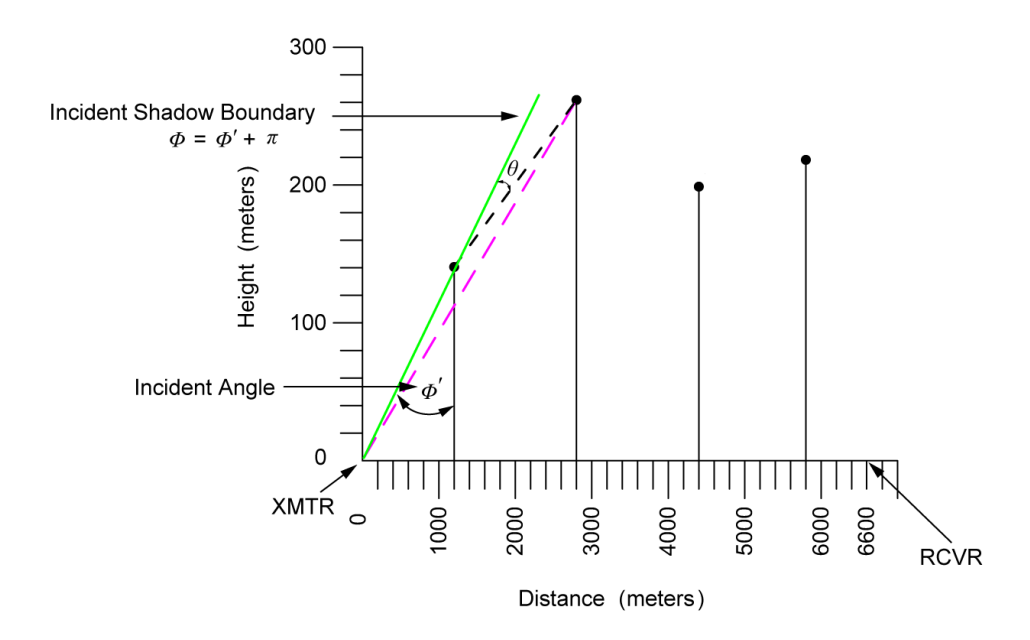


Figure 5. Incident shadow boundary and ray-path geometry for a typical diffraction scenario, with angles in radians.

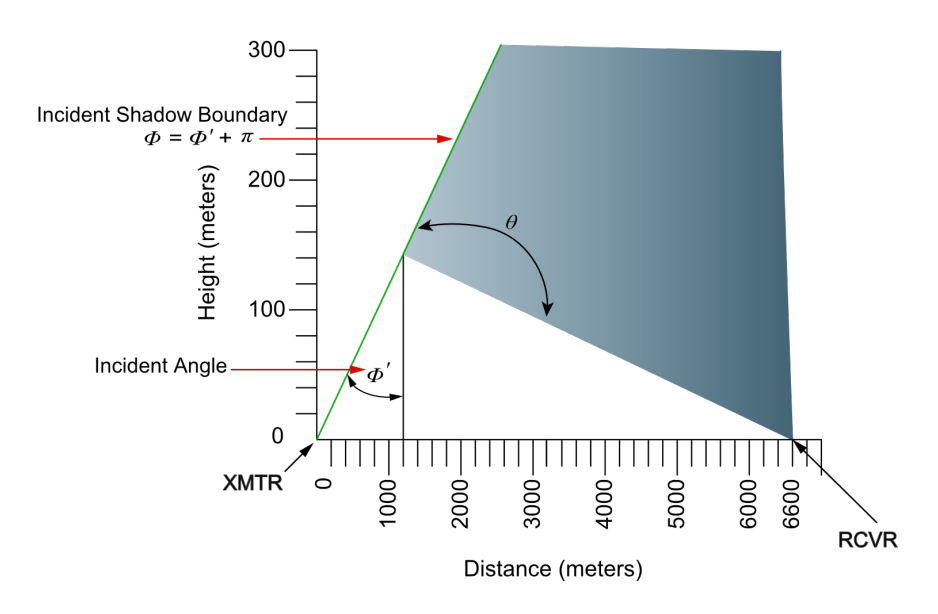


Figure 6. The incident shadow boundary and ray path for a single knife edge, with angles in radians.

These alternative methods use values of the Fresnel integral to establish the diffraction loss when the field points are in the transition region or on the incident shadow boundaries. The GTD method has a singularity at the incident shadow boundary, but the UTD method uses a Fresnel transition function to compensate for this singularity at the incident shadow boundary [15]. When the incident ray from one knife edge to the next lies along or near the incident shadow boundary and hence is not a so-called ray path, the GTD method has a problem predicting the diffraction loss, but the UTD method can accurately predict the diffraction loss because it includes the Fresnel transition function [16]. The alternative methods use the

Fresnel integral and incur an error inversely proportional to the angular difference of the ray path from the incident shadow boundary.

When grazing incidence occurs (i.e., directly on a shadow boundary), a 6 dB diffraction loss results [16]. This is appropriate only for plane waves when the incident field is the so-called ray field [16], [19]. It is no longer correct to add the diffraction losses of the individual knife edges for the grazing incidence case to determine the total loss over multiple knife edges as is done using the alternative methods. For grazing loss over two successive knife edges, the alternative methods would result in a total loss of 12 dB [16], [19]. The spectral theory of diffraction (a more rigorous method) shows the correct loss to be some value between 6 and 12 dB, where the exact value depends on the spacing of the knife edges [16], [19].

One reason for the differences between the Vogler method and the four alternative methods is that the ray path from one knife edge to the next consecutive knife edge is in the transition region, and near the incident or reflection shadow boundary. Computations of these ray path angles and shadow boundaries confirm this for the examples presented in Sections 5 and 6. Figure 6 shows the incident shadow boundary and ray path from one diffraction knife edge to the next knife edge.

The ray path is just the line drawn between one diffraction knife edge and the next consecutive diffraction knife edge. The incident shadow boundary is obtained by adding 180 degrees to the incident ray angle from the previous knife edge or transmitter with reference to the vertical line representing the knife edge or transmitter. The reflection shadow boundary is obtained by subtracting the same incident ray angle from 180 degrees. The reflection shadow boundary is usually far removed from the ray paths and hence does not align with the ray paths and causes a problem. However, the incident shadow boundary can occur close to or align with the ray path to the next knife edge. When the ray path approaches the incident shadow boundary, the value of diffraction loss from the computation of diffraction loss using the GTD approaches infinity, since the denominator approaches zero. The UTD corrects this problem by multiplying the mathematical equation for the GTD prediction by the Fresnel transition function [20].

Preliminary results of this analysis show where each of the alternative multiple knife-edge methods investigated can be used in place of the rigorous Vogler diffraction method to reduce computation time while maintaining suitable accuracy. It was shown that no one alternative method can cover all scenario variations. Which alternative diffraction method works best in a given scenario depends on how a method treats sub-path obstacles and the alignment of the ray path from one knife edge to the next knife edge with the shadow boundaries at the knife edges.

Electromagnetic fields are smooth and continuous everywhere, and as a result, discontinuities across incident shadow boundaries do not occur in nature but do occur in the mathematics of the GTD [21]. The denominator of the mathematical equation for the GTD approaches zero in the transition region as it nears the incident shadow boundary. The Fresnel transition function approaches zero at the same rate that the denominator in the mathematical expression for the GTD approaches zero, resulting in a finite diffraction loss prediction at the incident shadow boundary and in the transition region located near the incident shadow boundary [21]. The Fresnel transition function has a maximum value of one. The mathematical details of the computation of the incident and reflection shadow

boundaries and the respective transition regions about these boundaries are given in [17] and [21].

When applying any of the alternative methods with the Fresnel-Kirchhoff multiple knife-edge diffraction, one should avoid the transition regions and incident shadow boundaries. It would be appropriate to use a different alternative method that avoids the shadow boundaries and transition regions when the ray path from one knife edge to the next knife edge is in the transition region for one particular alternative method but not for a different one. The alternative methods are different enough in their geometric constructions and the procedure and order of computing individual knife-edge diffraction loss that one method would avoid having this ray along the shadow boundary even though another method would cause it to occur along the incident shadow boundary.

If the transition region were unavoidable, then it would help in the diffraction loss prediction to have this ray as far as possible from the incident shadow boundary to reduce the magnitude of the error. A technique will be proposed to determine which alternative method avoids the shadow boundaries or has the maximum deviation of the ray path from the incident shadow boundary. Selection of the method with the largest angular deviation from the incident shadow boundary will improve the accuracy of the diffraction loss prediction.

The first approach investigated for selecting a more accurate diffraction method was to use the method or methods that have the largest angular deviation between the ray path and the incident shadow boundary. This angular deviation did not account for the separation distance between adjacent knife edges or the wavelength for the radio frequency. The argument of the Fresnel transition function was also investigated as a means to judge what magnitude of angular separation would produce a minimal diffraction error. It is a function of the wavelength and the distance, L, from the diffraction knife edge to the observation point (separation between adjacent knife edges).

The second approach used the magnitude of the Fresnel transition function (FTF), which is proportional to the magnitude of the correction needed to keep the mathematical expression for the GTD finite and is therefore a good indicator of the accuracy of a diffraction loss prediction. This second approach used the Fresnel transition function to judge what magnitude of angular separation would produce a minimal diffraction loss error. It is a function of the wavelength and the distance, L, from the knife edge to the observation point (separation between adjacent knife edges). This second approach will be described using a step-by-step procedure.

It was finally determined that the best approach was to compute the Fresnel transition function argument and the Fresnel transition function magnitude ((11) and (12)) for each knife edge and then form the Fresnel transition function product (*FTFP*) for all the knife edges in a subject scenario. The magnitude of the *FTFP* is proportional to the magnitude of the correction needed to keep the mathematical expression for the GTD finite, and is therefore an indication of the accuracy of a diffraction loss prediction. The *FTFP* is obtained by computing *FTF* using (11) and (12) for each knife edge and multiplying the magnitudes of each individual *FTF* together to form the *FTFP*. The *FTFP* is a relative prediction of the accuracy of an alternative loss prediction when comparing two alternative loss prediction methods, but it is not an absolute value of loss prediction. It is an indication of determining which alternative method would result in a better loss prediction.

The method having the highest value for the *FTFP* is the one with the least diffraction loss prediction error. The Fresnel transition function for one knife edge is given by [21]:

$$FTF(x) = 2j\sqrt{x}e^{jx} \int_{\sqrt{x}}^{\infty} e^{-ju^2} du$$
 (11)

The argument x of FTF(x) is given by [21]:

$$x = \frac{2\pi}{\lambda} L \cos^2 \left[\frac{\phi_{ray} - \phi}{2} \right] \tag{12}$$

where $\phi_{ray} - \phi$ in Figure 4 represents the deviation between the ray path and the incident shadow boundary, $\phi = \phi' + \pi$, and L is the distance from the diffraction knife edge to the observation point, which is actually the distance from the diffracting knife edge to the next knife edge. The wavelength is obtained from the operating frequency. A plot of the FTF(x) is shown in Figure 7.

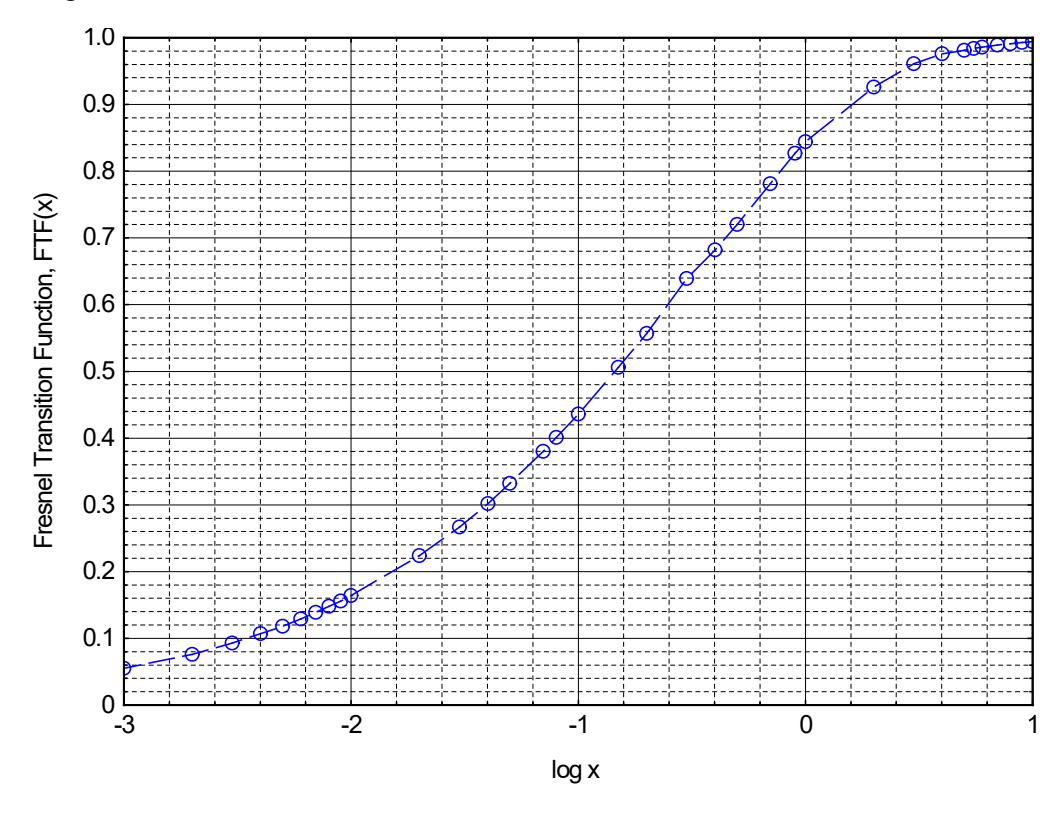


Figure 7: The Fresnel transition function FTF(x) magnitude.

As the argument of the Fresnel transition function varies from very small values (\sim 1.0 E⁻⁶) to 10.0, the Fresnel transition function varies from approximately .05 to 1.0 (Figure 7). Examples of this computation of FTFP(x) with comparisons to attenuation ratio will be discussed in Section 5 for 50 cases. The evaluation of FTF(x) can be performed using (11), but it is easier to use Figure 7 with sufficient accuracy after using (12) to calculate x, and $\log x$. A procedure for computing x, FTF(x), and FTFP(x) is listed below.

- Referring to Figure 4, compute x from (12) the argument of FTF(x) using parameters defined in (12), the parameters $\phi = \phi' + \pi$ and L, where ϕ is the incident shadow boundary, and L is the distance from the diffraction knife edge to the observation point, which is the distance from the diffracting knife edge to the next knife edge,
- The angle $\theta = \phi_{ray} \phi$ is the difference between the angle of the incident ray path for the next knife edge, ϕ_{ray} , and the angle of the incident shadow boundary ϕ .
- The wavelength λ is obtained from the operating frequency.
- Compute x from (12), compute $\log x$ from x, and then compute FTF(x) from Figure 7 using $\log x$.
- Repeat the four steps above for each diffraction edge.
- Compute the product of all diffraction edges, FTFP(x), by multiplying all the individual FTF(x) computations together.

The FTF(x) value of 1.0 indicates that for a single diffraction edge the ray path to the next edge is far away from the incident shadow boundary and that the computation of the diffraction loss will be better than an edge with an FTF(x) value less than 1.0. The FTFP(x) of 1.0 indicates that the total computation of using the product of the FTF(x) for all edges using a particular alternative method will be better than an alternative method that has an FTFP(x) less than 1.0 or less than the other alternative method.

3.3.1 The Bullington Method

For the Bullington method [3], multiple knife edges are replaced by an equivalent single knife edge with an effective height represented by the height of a triangle constructed by drawing a line from each of the antennas through the top of the knife-edge peak that blocks the line-of-sight (LOS) path from each of the antennas. This is equivalent to the horizon from each of the antennas.

Figure 8 is an example of graphical construction using the Bullington method for four knife edges. A line is drawn from the transmitter antenna through the first knife-edge peak that blocks the LOS path from the transmitter antenna. This is the knife edge with the maximum slope with respect to the transmitter antenna. A line is then drawn from the receiver antenna through the last knife-edge peak that blocks the LOS from the receiver antenna. This is the knife-edge peak with the maximum slope with respect to the receiver antenna. The intersection of the two lines locates the height and distances to use for computing the Fresnel-Kirchhoff diffraction parameter ν .

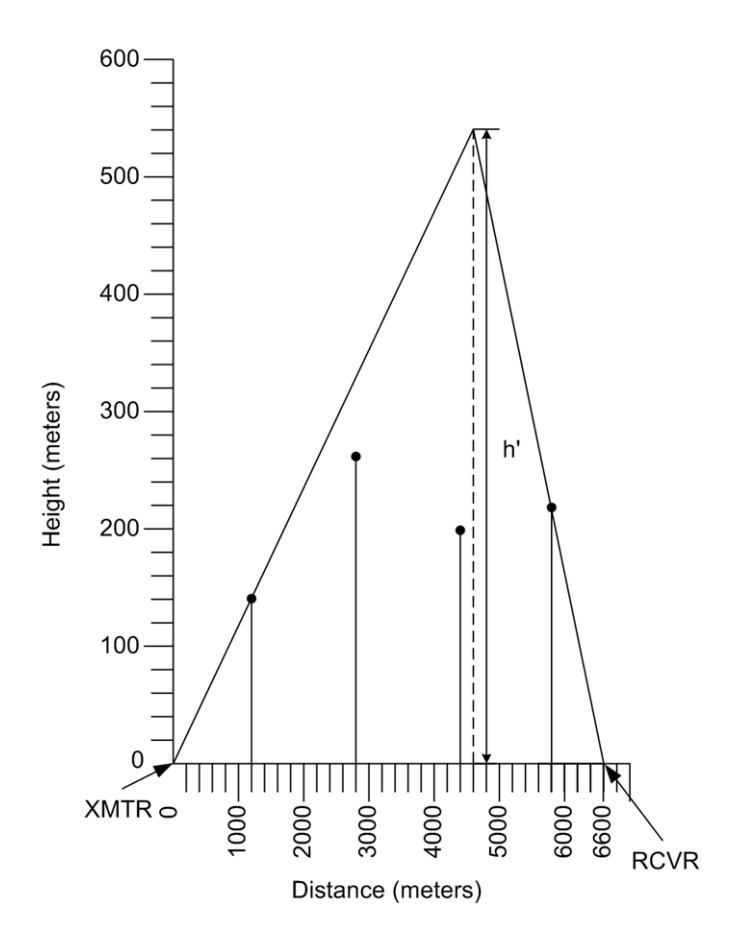


Figure 8: A four-knife-edge example of the graphical approach for the Bullington method.

The height and distances are determined graphically or by solving simultaneous equations in Appendix A that represent the two sloping lines. The distance from the transmitter antenna to this equivalent knife edge d_T and the distance from the equivalent knife edge to the receiver antenna d_{TR} are used with this effective height h' to determine the diffraction parameter and the diffraction loss using the equations in Appendix A. In this example, the effective height h' is 550 meters. The frequency is 1500 MHz with a wavelength of 0.2 meters. The distance d_T is 4600 meters, and the distance d_R is 6600 – 4600 = 2000 meters. The Fresnel-Kirchhoff diffraction parameter ν is computed as 46.6 from (10) for this equivalent knife edge and the diffraction loss is computed using (9) for $J(\nu)$ and is equal to 46.3 dB. This is the total diffraction loss for the Bullington method.

The Bullington method construction oversimplifies the computation of the diffraction loss because it only uses two edges. This results in a low estimation of the diffraction loss and an optimistic value for signal level. A comparison of the diffraction loss for this example to the results of the other three computation methods in the next three sections demonstrates how poorly the Bullington method computes the loss as 46.6 dB. The Epstein-Peterson, Deygout, and Giovaneli methods compute the loss for the same edge scenario as: 95.9, 99.87, and 94.6 dB, respectively. The Vogler prediction method results in a loss prediction of 97.21 dB for this scenario. The reader is cautioned here that the Bullington method typically predicts a much lower loss than the other alternative methods and as a result a much stronger signal level.

3.3.2 The Epstein-Peterson Method

For the Epstein-Peterson method [4], it is assumed that each knife edge is illuminated by the transmitter or the diffracted energy from the top of the preceding knife edge. The attenuation due to diffraction is computed sequentially for each knife edge in turn, and the attenuations for all knife edges are summed together in decibels. The diffraction loss computation for n knife edges using this method requires the determination of the effective height of each knife edge, and the distances d_T and d_R of the knife edge from the transmitter (or previous knife edge) and from the receiver (or next knife edge), respectively.

Figure 9 shows how the effective height of a knife edge is determined graphically by drawing a reference line from the preceding knife-edge peak or transmitter to the next knife-edge peak or receiver. The distances between knife edges and knife-edge heights with respect to a transmitter to receiver baseline are an essential part of the input data and can be used to determine the effective heights of each knife edge. The effective height is the vertical distance between this reference line and the knife-edge peak. The original Epstein-Peterson method does not address sub-path knife edges explicitly [4], [5], [16], but the modified Epstein-Peterson All Knife-Edges Method discussed in this paper (Epstein-Peterson method with all knife edges corrected and uncorrected) does address sub-path knife edges to assess the effects of their inclusion on diffraction loss.

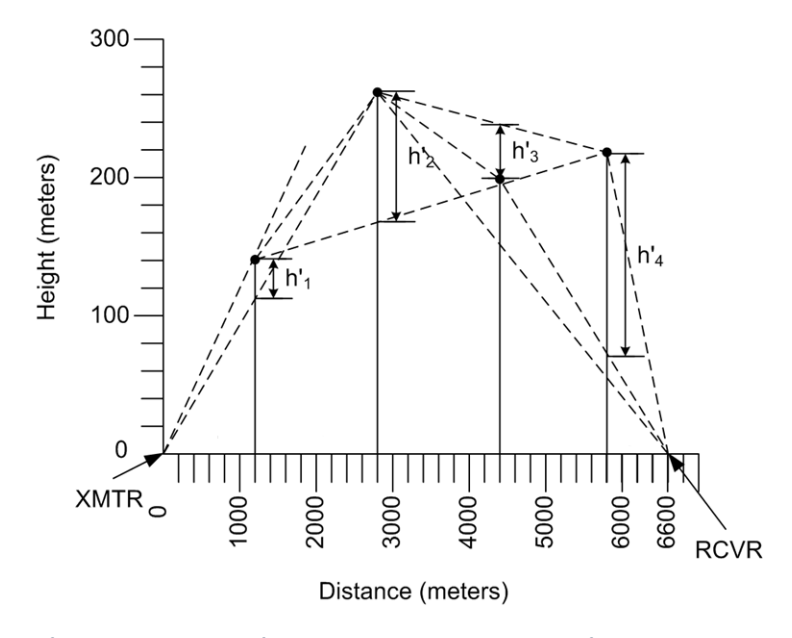


Figure 9: A four-knife-edge example for the graphical approach for the Epstein-Peterson method.

Figure 9 is an example of the graphical approach to the Epstein-Peterson method for four knife edges. The frequency is 1500 MHz. The effective height of the first knife edge is the vertical distance from the first knife-edge peak to the point where this baseline intersects the line representing the first knife edge. This can be determined by drawing a baseline from the transmitter, or it can be determined algebraically using (B-1) and (B-2) in Appendix B. The effective height of the second knife edge is the vertical distance from the second knife-edge peak to the point where this baseline intersects the line representing the second knife edge. The effective height of the third knife edge is the vertical distance from this knife-edge peak up to this baseline, and it is negative since it is a sub-path knife edge. The effective height of

the fourth knife edge is the vertical distance from this baseline to the knife-edge peak of the fourth knife edge.

The effective heights h' and distances d_T and d_R were used to calculate the Fresnel-Kirchhoff diffraction parameter ν from (10) and the diffraction loss in decibels for each knife edge using the $J(\nu)$ approximation (9). The knife-edge heights h_i and distances d_T and d_R used to compute the effective knife-edge heights and diffraction parameter ν are shown in Table 1 for each knife edge. The total diffraction loss is the sum of the individual losses for each knife edge and is (24.0 + 32.9 + 0.0 + 39.0) = 95.9 dB.

Knife-Edge Number/ Distance from XMTR (m)	Knife- Edge Height $oldsymbol{h}_i$ (m)	Effective Knife-Edge Height h ' (m)	Knife-Edge Computation Interval Distance d_T (m)	Knife-Edge Computation Interval Distance d_R (m)	Diffraction Parameter ν	Diffraction Loss <i>L</i> (dB)
1/1200	140	30	1200	1600	3.6	24.0
2/2800	260	90	1600	1600	10.1	32.9
3/4400	200	-40	1600	1400	-4.6	0.0
4/5800	220	145	1400	800	20.3	39.0

Table 1: Parameters and computation results for Epstein-Peterson example of Figure 9.

In addition to the Epstein-Peterson All Knife-Edges Method, other variations of the Epstein-Peterson method were also compared to the Vogler method. One variation used only the major three knife edges (the Epstein-Peterson Major Three Knife-Edges Method) and one deleted the sub-path knife edges (the Epstein-Peterson No Sub-Path Knife-Edges Method). Each of these three Epstein-Peterson Methods were also modified with the correction based on the GTD described in Beyer [7]. These three additional variations of the Epstein-Peterson method were designated as the Epstein-Peterson All Knife-Edges Method corrected, the Epstein-Peterson Major Three Knife-Edges Method corrected, and the Epstein-Peterson No Sub-Path Knife-Edges Method corrected.

3.3.3 The Deygout Method

For the Deygout method [5], it is assumed that each knife edge is illuminated by either the transmitter or diffracted energy from the top of the preceding knife edge. This is similar to the Epstein-Peterson method, but Deygout uses a different method of computing effective height for each knife edge. The knife edges are classified in terms of the magnitude of their Fresnel-Kirchhoff diffraction parameter ν . Figure 10 is an example of the Deygout method for four knife edges.

The procedure starts with computing the Fresnel-Kirchhoff diffraction parameters for all of the knife edges using the effective knife-edge heights above the transmitter-to-receiver baseline as if the other knife edges were absent using equations from Appendix C. The distances for each knife edge in the computation of ν are the distances from the transmitter to subject knife edge d_T and from the subject knife edge to the receiver, d_R . The knife edge with the largest Fresnel-Kirchhoff diffraction parameter is the primary knife edge for the Deygout method. This is also the knife edge with the largest loss. The solid lines extending to the top of knife edge 4 in Figure 10 illustrate the geometry of the computation to determine the Fresnel-Kirchhoff diffraction parameter for knife edge 4. After computation of the Fresnel-

Kirchhoff diffraction parameters for the other remaining knife edges, knife edge 4 has the maximum value for this parameter and is the primary knife edge.

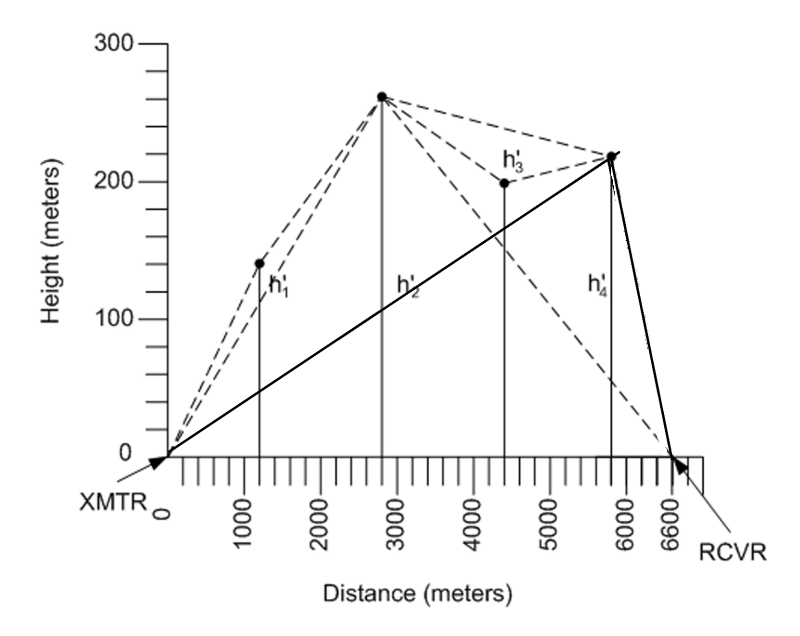


Figure 10: A four-knife-edge example for the graphical approach to the Deygout method.

The diffraction parameter ν is used as an indicator instead of the loss, so that the diffraction loss does not need to be computed for all knife edges in this interim procedure. The primary loss is computed using the effective height and diffraction parameter for only the primary knife edge. Subsequent losses, for the remaining knife edges, are computed in a sequence of steps with different effective knife-edge heights. In this example, the frequency is 1500 MHz. The Fresnel-Kirchhoff diffraction parameters in Table 2 for knife edges 1, 2, 3, and 4 are 14.13, 20.48, 16.51, and 26.24, respectively, so the fourth knife edge is the primary knife edge, and the diffraction loss is 41.27 dB for the primary knife edge.

As illustrated in Figure 10, the primary knife edge, 4, divides the path into two separate regions and the computation of the diffraction parameter is repeated over each region separately to determine a secondary knife edge using an effective knife-edge height with respect to baselines drawn between the transmitter antenna and the primary knife edge 4 for one region and the primary knife edge 4 and the receiver antenna for the other region, using graphical methods or the algorithms in Appendix C. Notice only the region to the left of primary knife edge 4 has knife edges, and the region to the right of knife edge 4 has no knife edges. Since the main (primary) knife edge is knife edge 4, all of the remaining knife edges are in a region to the left of knife edge 4.

Knife-Edge	Knife-	Effective	Knife-Edge	Knife-Edge	Diffractio	
Number/	Edge	Knife-Edge	Computation	Computation	n	Diffraction
Distance from	Height	Height $m{h}'$	Interval	Interval	Parameter	Loss <i>L</i> (dB)
XMTR (m)	h_i (m)	(m)	Distance $oldsymbol{d}_T$ (m)	Distance $d_{\scriptscriptstyle R}$ (m)	ν	
	Parame	ters and comp	outations for determ	ining the primary kr	nife edges	
1/1200	140	140	1200	1600 + 1600 + 1400 + 800 = 5400	14.13	Secondary knife edge
2/2800	260	260	1200 +1600 = 2800	1600 +1400 + 800 = 3800	20.48	Secondary knife edge
3/4400	200	200	1200 +1600 +1600 = 4400	1400 +1800 = 2200	16.51	Secondary knife edge
4/5800	220	220	1200 +1600 +1600 +1400 = 5800	800	26.24	Primary knife edge 41.27
	Paramete	ers and compu	ıtations for determiı	ning the secondary l	knife edges	
1/1200	140	94.48	1200	1600 + 1600 +1400 = 4600	9.69	Third-level knife edge
2/2800	260	153.79	1200 + 1600 = 2800	1600 + 1400 = 3000	12.78	Secondary knife edge 34.99
3/4400	200	33.10	1200 + 1600 + 1600 = 4400	1400	3.21	Third-level knife edge
	Paramete	ers and compu	tations for determin	ning the third-level I	knife edges	
3/4400	200	-38.67	1600	1400	-4.48	0.0

Table 2: Parameters and computation results for Deygout example of Figure 10.

The second part of Table 2 shows the process of determining the secondary knife edge for the region to the left of primary knife edge 4. The effective knife-edge height for determining the secondary knife edge is the distance from this new baseline to the respective knife-edge peaks in the region, determined using graphical methods or the algebraic algorithms in Appendix C. The secondary knife edge is the knife edge with the maximum value of diffraction parameter over the secondary region to the left of the primary knife edge. Using the new baseline, the diffraction parameter is computed only for three potential secondary knife edges 1, 2, and 3 using new effective heights. Since knife edge 2 has the maximum value for the diffraction parameter ν , it is the secondary knife edge for this example; the loss for this knife edge is shown in the second part of Table 2 as 34.99.

1200

1600

3.45

23.6

1/1200

140

28.57

This is a recursive algorithm where the method repeatedly divides the edge scenario into different regions that are subsets of the original region and subregions until the diffraction losses have been computed for all edges. This is demonstrated by the equations given in Appendix C. The diffraction parameter ν for all remaining knife edges is computed using the equations in Appendix C and the distances and knife-edge heights shown in Table 2. The diffraction parameters for knife edges 1 and 3 are less than that of knife edge 2, so knife edges 1 and 3 are the third level knife edges for this region.

A new baseline for calculating the effective height of third-level knife edge 1 is established by drawing a line from the transmitter to secondary knife edge 2. A new baseline for determining the effective height of the third-level knife edge 3 is established by a line

extending from the peak of secondary knife edge 2 to the peak of primary knife edge 4. Since this knife edge 3 is below this new baseline established by knife edges 2 and 4, it has a negative effective height. The diffraction parameter ν is negative and less than a value of -0.78, so the equation for $I(\nu)$ cannot be used to calculate the diffraction loss.

From a curve in ITU-R P.526 [8], the value of diffraction loss is less than 1.0 dB for values of ν less than -0.78. The value of ν computed for knife edge 3 is -4.48 and from the P.526 curve the loss is 0.0 dB.

The results of the computation for third-level knife edges 1 and 3 are shown in the third part of Table 2. The total diffraction loss using the Deygout method is the sum of these individual diffraction losses in dB for knife edges 1, 2, 3, and 4 as 23.61 + 34.99 + 0.0 + 41.27 respectively, which is equal to 99.87 dB.

Several variations of the Deygout method were also used in the comparison: using only the major three diffraction knife edges (the Deygout Major Three Knife-Edges Method) and ignoring the sub-path knife edges (the Deygout No Sub-Path Knife-Edges Method).

3.3.4 The Giovaneli Method

Giovaneli's method [6] agrees with Vogler's more rigorous multiple knife-edge diffraction methods [1], [2] for more than two knife edges. The Giovaneli method uses a different approach for computing the diffraction losses with a geometry that uses the diffraction angles that better represent the ray paths across the knife edges. This method is an improvement over the Deygout method and the Epstein-Peterson method when the number of knife edges is greater than three.

The history of the development of the four alternative diffraction computation methods spans many years. The Bullington, Epstein-Peterson, Deygout, and Giovaneli methods were published in 1947, 1953, 1966, and 1984, respectively. Each was an improvement over the previous method, but in many cases each method has an advantage in how it avoids the incident shadow boundary, because the ray angles are treated differently in the three later methods. In Section 5, it will be shown that for the many different scenarios that can exist, one method may be more suitable than another due to the different ray paths and their relationship with the incident shadow boundaries.

Figure 11 is an example of the graphical approach to the Giovaneli method for four diffraction knife edges. The frequency is 1500 MHz. For the Giovaneli method [6], the primary knife edge over the entire transmitter-to-receiver interval is the tallest knife edge with respect to the transmitter-to-receiver baseline, which is unlike the other methods. Its effective height can be determined by a graphical construction as shown in Figure 11, or the mathematics of Appendix D.

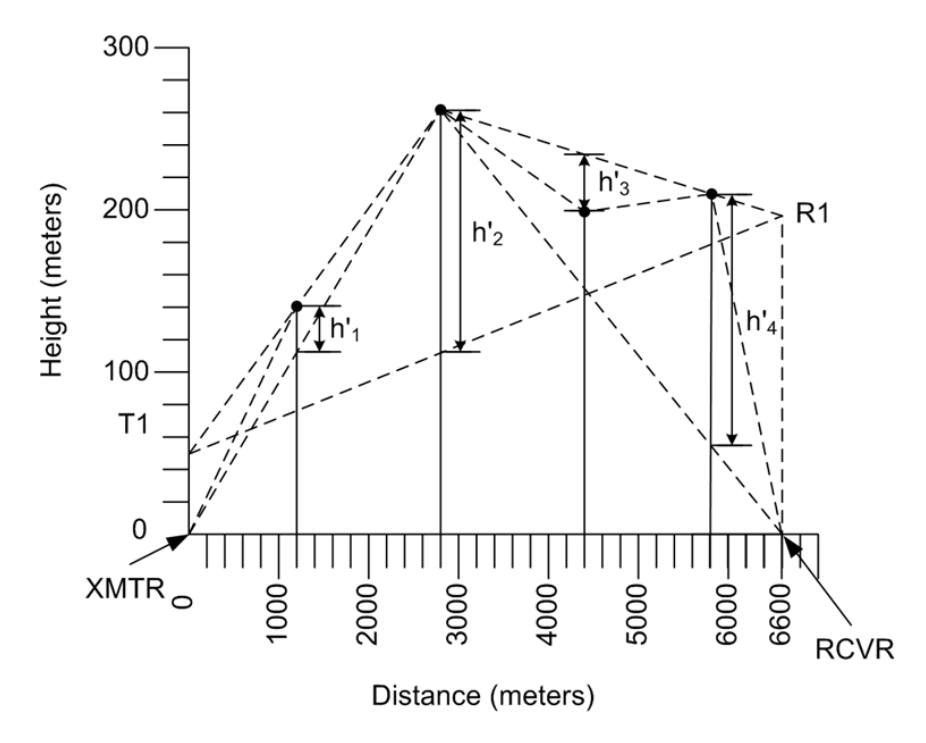


Figure 11: A four-knife-edge example for the graphical approach to the Giovaneli method.

If there are two tallest knife edges with equal heights, then the Fresnel-Kirchhoff parameter ν is computed for both knife edges. The primary or tallest knife edge is the knife edge with the largest value of ν . The graphical construction starts with extending two vertical lines in an upward direction, one from the transmitter and one from the receiver. Separate lines are then drawn from the main knife edge (knife edge 2 peak) through the preceding (knife edge 1 peak) and the next knife edge (knife edge 4 peak) that are not sub-path knife edges and have the minimum absolute value of slope with respect to the primary knife edge.

These lines are then extended beyond these knife-edge peaks to intersect the vertical lines that have been drawn vertically from the transmitter and receiver at points T1 and R1, respectively. This creates observation points for the diffraction over the primary knife edge (knife edge 2) from the preceding knife edge 1 and to the next knife edge 4 that are not subpath knife edges. A line connecting the points of intersection of these separate lines with the vertical lines serves as the baseline for determining the knife-edge effective height of primary knife edge 2. The effective height is the distance between this baseline and the knife edge 2 peak. This height can be determined graphically or algebraically from the equations in Appendix D.

Table 3 contains the knife-edge separation distances, knife-edge heights, effective antenna height, diffraction parameter, and diffraction loss. The sub-path knife-edge peaks are skipped at this point in the procedure. They are included after the completion of the computation loss for the knife edges that are not sub-path knife edges.

Knife-Edge Number/ Distance from XMTR (m)	Knife- Edge Height $oldsymbol{h}_i$ (m)	Effective Knife-Edge Height <i>h'</i> (m)	Knife-Edge Computation Interval Distance d_T (m)	Knife-Edge Computation Interval Distance d_R (m)	Diffraction Parameter ν	Diffraction Loss <i>L</i> (dB)
1/1200	140	28.57	1200	1600	3.0	22.5
2/2800	260	142.8	1200 + 1600 = 2800	1600 + 1400 + 800 = 3800	11.4	34.0
3/4400	200	-38.67	1600	1400	-3.5	0.0
4/5800	220	165.26	1600 +1400 = 3000	800	18.2	38.1

Table 3: Parameters and computation results for Giovaneli example of Figure 11.

This process is repeated as follows for the next largest knife edge, establishing new observation points for the diffraction over the knife edges 1, 3, and 4. For knife edge 1 a line is drawn through the primary knife edge 2 peak from the peak of knife edge 1, since the energy diffracted from knife edge 1 must diffract over knife edge 2. Another line is drawn from the transmitter antenna to knife edge 1 since this is the source for the diffraction at knife edge 1. The new baseline for the effective height of knife edge 1 is a line connecting the transmitter antenna and the peak of knife edge 2. The effective height of knife edge 1 is the difference between the knife edge 1 peak and this baseline, which can be determined graphically or algebraically from the equations in Appendix D. The knife-edge separation distances, knife-edge heights, effective knife-edge heights, diffraction parameter, and diffraction loss are contained in Table 3 for knife edge 1.

Knife edge 4 is the next knife edge that is not a sub-path knife edge on the right side of the primary knife edge. For knife edge 4 a line is drawn through the primary knife edge 2 peak from the peak of knife edge 4 since the energy diffracted from knife edge 2 must diffract over knife edge 4. Another line is drawn from the receiver antenna to knife edge 4, since this is the receptor for the energy diffracted from the fourth knife edge 4. The new baseline for the effective height of knife edge 4 is a line connecting the receiver antenna and the peak of knife edge 2. The effective height of knife edge 4 is the difference between the knife edge 4 peak and this new baseline. The knife-edge separation distances, knife-edge heights, effective knife-edge heights, diffraction parameter and loss are contained in Table 3 for knife edge 4.

The last knife edge (knife edge 3) in Figure 11 is a sub-path knife edge and the baseline for computing its effective height is a line extending from the peak of knife edge 2 to the peak of knife edge 4. The effective height of knife edge 3 is the distance between this baseline and the peak of knife edge 3. This height can be determined graphically or with the equations from Appendix D. The total diffraction loss is equal to (34.0 + 22.5 + 38.1 + 0.0) = 94.6 dB. The total diffraction loss for the Giovaneli method is obtained by summing the losses of all knife edges in decibels.

Two variations of the Giovaneli method were used in the comparison: using only the major three knife edges (the Giovaneli Major Three Knife-Edges Method) and deleting the sub-path knife-edges (the No Sub-Path Knife-Edges Method).

3.3.5 Summary Comments on the Alternative Methods

Computations made with all of the alternative methods except Bullington [3] tend to agree with measured data. The Bullington method does have its place for use when the actual terrain is so complicated that it is difficult to decide which terrain features are significant and allow the two major knife edges to be selected as the most prominent diffraction edges. Computations made with Bullington for the long path on 63rd Street, mentioned later in Section 6.2, were on average within 12 dB of measured data, whereas the other three alternative methods were on average within 4 dB of measured data. The 12 dB loss predicted with the Bullington method is less than that predicted with the more precise alternative methods. This results in a 12 dB increase in predicted signal level. The 12 dB lower loss is better than the results shown in Section 3.3.1 where Bullington predicts 46.3 dB and the Three alternative methods of Epstein-Peterson, Deygout, and Giovaneli predict 95.9, 99.87, and 94.6 dB, respectively.

When comparing the Epstein-Peterson method to the Deygout method, [22] and [19] demonstrated that the Deygout method was more theoretically correct, because of its relationship to the rigorous spectral theory of diffraction as described in [19]. The accuracy of the Deygout approach is highest when there is one dominant diffraction knife edge. When there are two comparable obstacles, a correction can be applied using a spacing parameter for the Deygout method [22]. The Deygout method is more difficult to implement than the others described.

Giovaneli [6] claims that his method agrees well with GTD outside of the transition regions, and for two or more knife edges the method agrees with the Vogler method [22], [19]. Giovaneli also mentions that as the number of knife edges increases, the Deygout method incurs a larger error; it is usually terminated after computing the loss for the major three knife edges [22], [16]. In general, the Deygout method shows very good agreement (±3 dB) with the rigorous multiple knife-edge approach of Vogler [1], but it becomes pessimistic (predicting larger diffraction losses than the actual loss or the loss computed with the rigorous multi knife-edge approach) when there are multiple obstacles and/or the knife edges are close together [22]. In this case, the difference between the diffraction loss computed by Deygout and that by Giovaneli increases [17]. The difference can vary with different scenarios.

Results presented later in Section 5.1 (Figures Figure 29 and Figure 30) demonstrate that the 50 scenarios introduced in Section 4 get better results than the original Epstein-Peterson method when compared to the Epstein-Peterson method that contains the GTD-based correction cited in [7].

The Bullington and Epstein-Peterson methods tend to underestimate the diffraction loss and the Deygout method tends to overestimate the diffraction loss when compared to the Vogler method. This is demonstrated later in Tables 17 and 18 in Section 5.2. The diffraction angle of the knife edge used by the Deygout method for computation of the primary (main) knife-edge diffraction tends to be larger than the diffraction angle actually required for the ray from the previous knife edge to pass over the knife edge in question to the next knife edge. Thus, a larger value is used for the Fresnel-Kirchhoff parameter ν and the diffraction loss for the primary knife edge is overstated. The Deygout-computed loss diverges more from the

actual loss when the diffraction knife edges have similar losses and when they are spaced close together [17].

The Giovaneli method is not reciprocal in general, and it is most important to define the primary knife edge for the diffraction analysis before the other minor knife edges are selected. If the primary knife edge is not correctly defined, then only a small error occurs in the prediction of diffraction loss with this method [6]. This method corrects the Deygout method's error in diffraction angle because it uses a diffraction angle that more closely coincides with that used for the GTD method [6].

Since the Epstein-Peterson method predicts a lower loss than the GTD method, and the Deygout method predicts a greater loss than the GTD method, it is expected that the Giovaneli method will predict a loss that will more closely agree with the GTD method and be bounded from below by the Epstein-Peterson method and above by the Deygout method [6]. When a grazing incidence for an intermediate knife edge occurs between two knife edges, the intermediate knife-edge height equals zero with respect to the line between the transmitter antenna or previous knife edge and the receiver antenna or next knife edge); or a sub-path obstacle (negative knife-edge height) occurs, then the Deygout and Giovaneli methods for treating sub-path obstacles are equivalent [22].

Preliminary results of this analysis show where each of the alternative multiple knife-edge methods investigated can be used in place of the rigorous Vogler diffraction method to reduce computation time while maintaining suitable accuracy. It was shown that no single alternative method can cover all scenario variations. Which alternative diffraction method works best in a given scenario depends on how a method treats sub-path obstacles and the alignment of the ray path from one knife edge to the next knife edge with the shadow boundaries at the knife edges.

3.3.6 The Vogler Method

The four knife-edge scenario used in Figures 8 through 11 (Case 13 of Table 12) was also computed with the Vogler method. The Vogler method uses the diffraction angles for each knife edge that are defined in Figure 2 in addition to the effective heights and distances between knife edges to compute a diffraction parameter as described in Section 3.1. The result for the total diffraction loss was 97.21 dB for the four-knife-edge scenario. (See Case 13 in Table 17.)

3.4 Examples of Alternative Computation Methods with Six Knife Edges

This section demonstrates how complex the computations get when up to six knife edges are present in a diffraction scenario. The discussion of each of the methods in this section shows the different computation procedure and graphical construction. All edges are included in the computations. These examples with six edges are different than the 50 cases of Section 4. For comparison purposes the total diffraction loss computed in this section for the Bullington, Epstein-Peterson, Deygout, and Giovaneli methods are 9.767 dB, 38.038 dB, 39.421 dB, and 38.161 dB, respectively. The Vogler prediction for this scenario is 38.91 dB.

3.4.1 Six Knife-Edge Example for the Bullington Method

The Bullington method finds the point of two intersecting horizon rays and ascribes the total loss to that of a single equivalent knife edge. The procedure first determines the diffraction knife edges that represent the horizons using (A-1) and (A-2). Table 4 contains the results of applying these equations. Figure 12 illustrates the knife-edge configuration and graphical construction for this method. Knife edge M_1 is the horizon from the transmitter antenna and M_5 is the horizon from the receiver antenna. The knife-edge computation intervals from Figure 10 are $d_T = 3.438$ km and $d_R = 2.962$ km.

Table 4: Horizon	parameter	determination	for the six	diffraction	knite edges.

	M_1	M_2	M_3	M_4	M_5	M_6
Tangent of angle in mrad from Transmitter Antenna	1.6	1.0	1.133	0.714	0.520	0.283
Tangent of angle in mrad from Receiver Antenna	0.296	0.524	1.0	1.364	1.857	1.700
Distance of edge from XMTR (km)	1.0	2.2	3.0	4.2	5.0	5.4

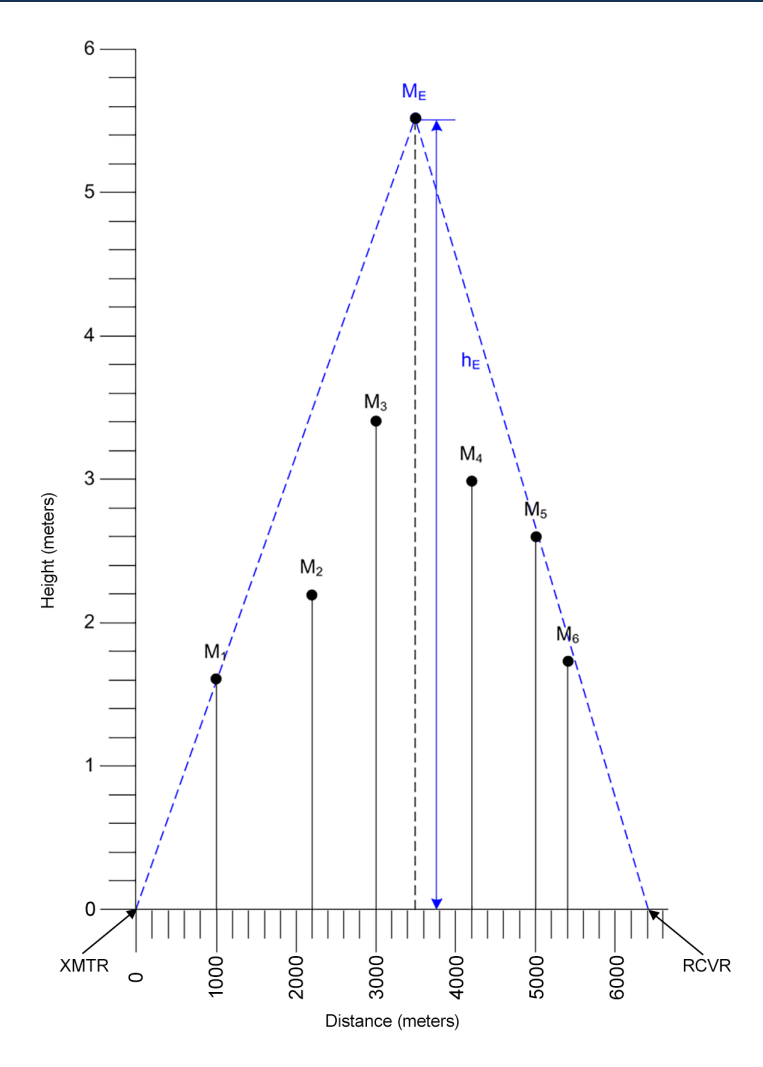


Figure 12: Six knife-edge diffraction example for Bullington method with sub-path knife edges M_2 and M_6 .

The heights and distances for knife edge M_1 in (A-3) and knife edge M_5 in (A-4) are used to represent the equations of the two lines along the horizon from the transmitter and receiver antennas, respectively. These equations are solved simultaneously to determine the distance, d_T , of 3.438 km from the transmitter of the single knife edge that represents the effective height for the Bullington method. Equation (A-5) is used to calculate the distance d_R of this knife edge from the receiver as 2.962 km and (A-6) is used to calculate the effective height of the knife edge as 5.501 meters. The diffraction parameter $\nu=0.4361$ and the total diffraction loss is 9.767 dB.

3.4.2 Six Knife-Edge Example for the Epstein-Peterson Method

The example for the Epstein-Peterson method is best illustrated by referring to Figure 13 and the results of Table 5. The single knife-edge diffraction losses are computed over the knife edges in order from transmitter to receiver antenna terminals over the convex hull of the ray between terminals (similar to a stretched string that passes over all of the intervening knife edges). The total diffraction loss is the sum of the six diffraction losses (38.04 dB) in Table 5.

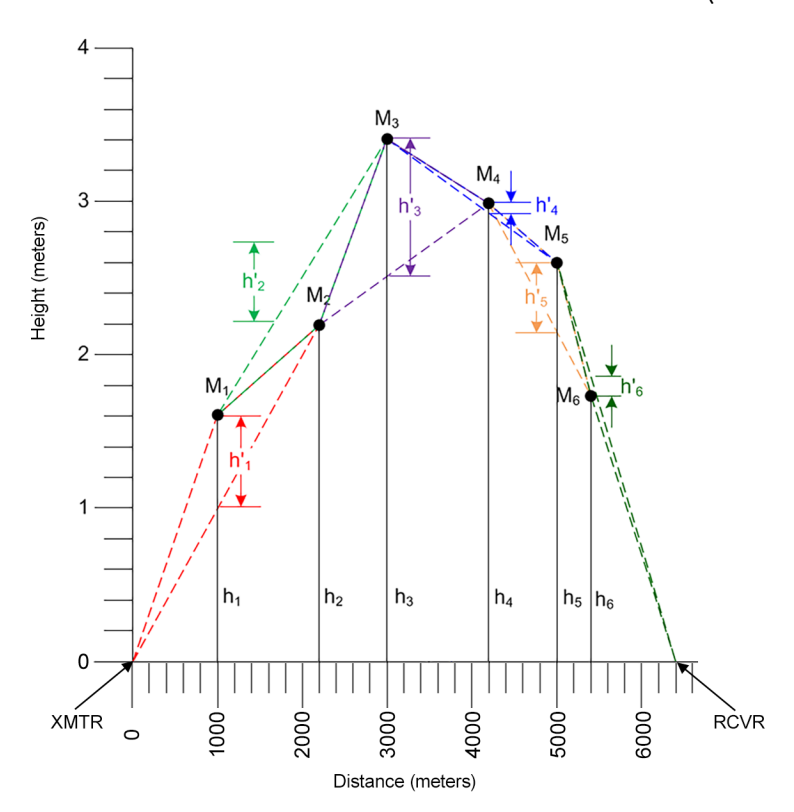


Figure 13: Six knife-edge diffraction example for Epstein-Peterson method with sub-path knife edges M_2 and M_6 .

T	1. (. 1	1 1	r . i	E D .	. 1 1
Table 5. Resi	ults tar si	IX KNITA-A	dae exampl	es tor the	Epstein-Peters	son method
Table J. Nesi	uito iti si	N NIIIIE-EU	iue exambi	C3 101 111C	LUSICIII-I CICI.	3011 11161

Parameter	M_1	M_2	M_3	M_4	M_5	M_6
$d_T(km)$	1.0	1.2	0.8	1.2	0.8	0.4
d_R (km)	1.2	0.8	1.2	0.8	0.4	1.0
h_i (m)	1.6	2.2	3.4	3.0	2.6	1.7
h_i' (m)	0.600	-0.480	0.880	0.080	0.467	-0.157

Parameter	M_1	M_2	M_3	M_4	M_5	M_6
Edge Distance from XMTR (km)	1.0	2.2	3.0	4.2	5.0	5.4
ν	0.0812	-0.0693	0.127	0.012	0.090	-0.029
<i>L</i> (dB)	6.737	5.437	7.135	6.133	6.817	5.779

3.4.3 Six Knife-Edge Example for the Deygout Method

Figure 14 is a graphical illustration of the Deygout method. The method begins with using (C-1) through (C-5) to compute the Fresnel-Kirchhoff diffraction parameter ν and the diffraction loss for all knife edges separately as if the other knife edges were absent. The actual heights with respect to the transmitter to receiver baseline are used for the effective heights in this initial calculation for determining the primary knife edge. Table 6 shows the results of this calculation. Knife edge M_2 is the primary knife edge, since it has the largest value of ν and the largest diffraction loss. This is the final loss for knife edge M_3 . The final losses for the other knife edges are determined using other reference baselines.

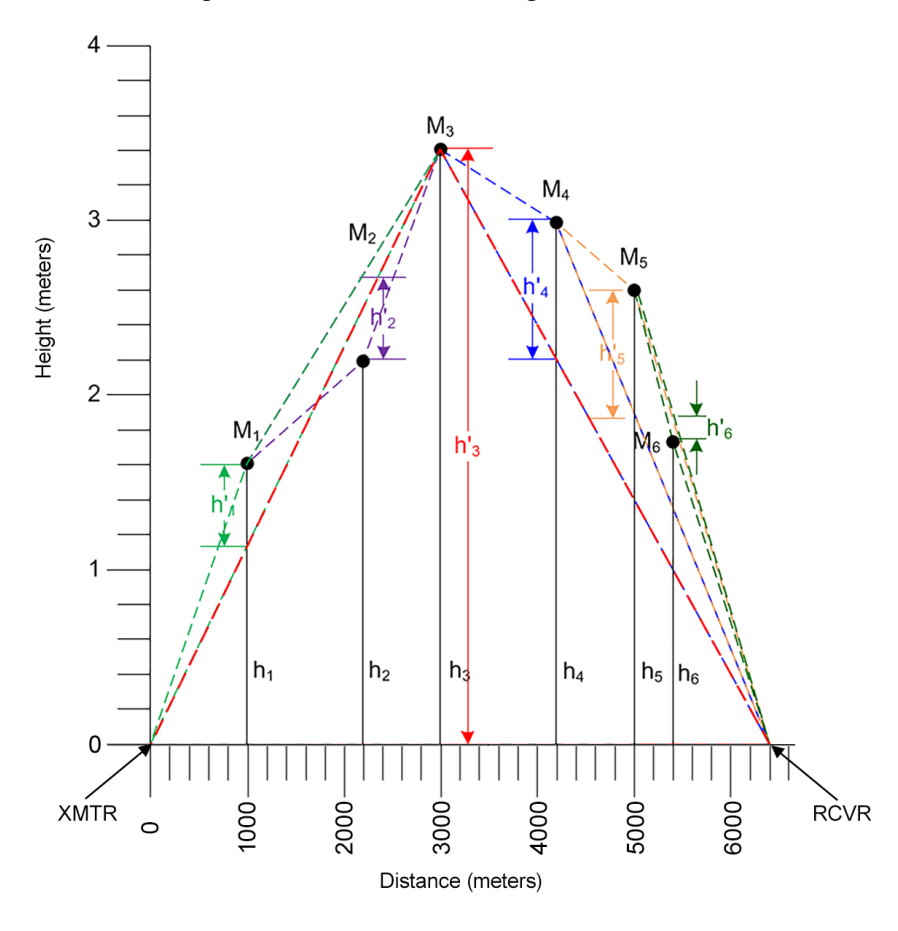


Figure 14: Six-knife-edge diffraction example for Deygout method with sub-path knife edges M_2 and M_6 .

Table 6: Computation of Fresnel-Kirchhoff diffraction parameter ν and diffraction loss to determine the
primary knife edge.

Parameter	M_1	M_2	M_3	M_4	M_5	M_6
$d_T(km)$	1.0	2.2	3.0	4.2	5.0	5.4
d_R (km)	5.4	4.2	3.4	2.2	1.4	1.0
h_i (m)	1.6	2.2	3.4	3.0	2.6	1.7
h_i' (m)	1.6	2.2	3.4	3.0	2.6	1.7
Edge Distance from XMTR (km)	1.0	2.2	3.0	4.2	5.0	5.4
ν	0.174	0.183	0.269	0.250	0.249	0.185
L (dB)	7.544	7.621	8.364	8.195	8.186	7.638

Knife edge M_3 divides the path into two regions. Equations (C-1) and (C-5) through (C-9) are used to compute the effective heights, diffraction parameter, and diffraction loss for all knife edges located to the left of the primary knife edge using a new baseline to determine the secondary knife edge in this region. Table 7 shows the results of these calculations. Knife edge M_1 is the secondary knife edge to the left of the primary knife edge, since it has the next largest diffraction parameter and diffraction loss. This is the final loss for knife edge M_1 but not for knife edge M_2 .

Table 7: Computation of Fresnel-Kirchhoff diffraction parameter ν and diffraction loss to determine the secondary knife edge on the left side of the primary knife edge.

Parameter	M_1	M_2
$d_T(km)$	1.0	2.2
d_R (km)	2.0	0.8
$h_i(m)$	1.6	2.2
h_i' (m)	0.467	-0.293
ν	0.057	-0.038
<i>L</i> (dB)	6.528	5.703

Knife edge M_2 is the only third-level knife edge remaining on the left side of the primary knife edge, and it is located on the right side of the secondary knife edge M_1 , so (C-1) and (C-17) through (C-19) are used to compute the effective heights, distances, and diffraction parameter. Equation (C-5) is used to compute the diffraction loss. The results are presented in Table 8. This is the final loss for knife edge M_2 .

Table 8. Computation of Fresnel-Kirchhoff diffraction parameter ν and diffraction loss for the third-level knife edge on the left side of the primary knife edge and the right side of the secondary knife edge M_1 .

Parameter	M_2
$d_T(km)$	1.2
d_R (km)	0.8
h_i (m)	2.2
h_i' (m)	-0.480
ν	-0.069
<i>L</i> (dB)	5.437

Equations (C-1) and (C-10) through (C-13) are used to compute the effective heights and diffraction parameter, and (C-5) is used to compute the diffraction loss for all knife edges

located to the right of the primary knife edge using a new baseline to determine the secondary knife edge for this region. Table 9 shows the results of these calculations. Knife edge M_5 is the secondary knife edge to the right of the primary knife edge, since it has the largest diffraction parameter and diffraction loss. This is the final loss for the knife edge M_5 .

Table 9. Computation of Fresnel-Kirchhoff diffraction parameter ν and diffraction loss for three edges to determine the secondary knife edge on the right side of the primary knife edge.

Parameter	M_4	M_5	M_6
$d_T(km)$	1.2	2.0	2.4
d_R (km)	2.2	1.4	1.0
h_i (m)	3.0	2.6	1.7
h_i' (m)	0.80	1.20	0.70
ν	0.091	0.132	0.083
<i>L</i> (dB)	6.820	7.180	6.755

Knife edges M_4 and M_6 are the two remaining third-level knife edges of the right side of the primary knife edge. Knife edge M_4 is on the left side of secondary knife edge M_5 , so (C-20) through (C-22) are used to compute the effective heights and distances, (C-1) is used to compute the diffraction parameter, and (C-5) is used to compute the diffraction loss. Knife edge M_6 is on the right side of secondary knife edge M_5 , so (C-23) through (C-25) are used to compute the effective heights and distances, (C-1) is used to compute the diffraction parameter, and (C-5) is used to compute the diffraction loss. The results are shown in Table 10. These are the final losses for knife edges M_4 and M_6 .

Table 10. Computation of the Fresnel-Kirchhoff diffraction parameter ν and diffraction loss for the third-level knife edges M_4 and M_6 on the right side of the primary knife edge and each side of the secondary knife edge M_5 .

Parameter	M_4	M_6
$d_T(km)$	1.2	0.4
d_R (km)	0.8	1.0
h_i (m)	3.0	1.7
$h_i'\left(m ight)$	0.080	-0.157
ν	0.012	-0.029
<i>L</i> (dB)	6.133	5.779

The total diffraction loss is 40.12 dB, which is the sum of the decibel losses for knife edges M_1 through M_6 from Tables 6 through 10.

3.4.4 Six Knife-Edge Example for the Giovaneli Method

Figure 15 is a graphical illustration of the Giovaneli method. The primary knife edge is the tallest knife edge M_3 . The procedure starts with determining the effective height of the primary knife edge using the secondary knife edges. The slopes of lines drawn from the primary knife edge to each of the other knife edges are calculated to determine which knife edges have the minimum slope on each side of the primary knife edge. The minimum slope is associated with the secondary knife edge M_1 on the left side of the primary knife edge. To determine the equation of the line that passes through the knife-edge peaks of knife edges M_3 and M_1 , (D-4) is solved for the y intercept, b_L , at the vertical line from the transmitter using

the fact that it is equal to the height h_m at the distance location of the primary knife edge M_3 . The minimum slope is associated with the secondary knife edge M_4 on the right side of the primary knife edge. The equation of a line that passes through the peaks of knife edges M_3 and M_4 is determined using (D-5).

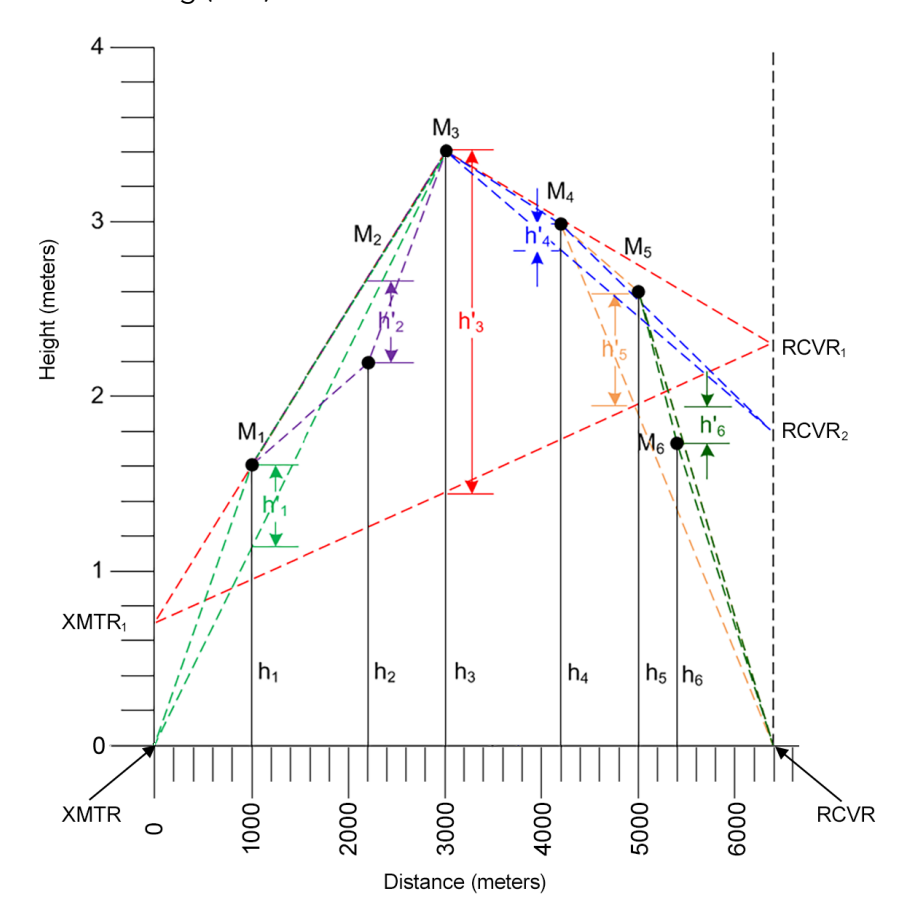


Figure 15. Six knife-edge diffraction examples for Giovaneli method with sub-path knife edges M_2 and M_6 .

The reference baseline given by (D-6) is then used to connect the points where (D-4) and (D-5) intersect the vertical lines at the transmitter and receiver, respectively. Equation (D-6) is used to determine the baseline for the effective height of the primary knife edge and (D-7) and (D-8) are used for calculating the distances. Equation (D-9) is used for calculating the diffraction parameter ν and (D-10) is used to calculate the diffraction loss.

For determination of the effective heights of the secondary knife edges, the secondary knife edges are used as the main knife edges and their effective heights calculated with a similar computation to that used for the primary knife edge. For the left side of the primary knife edge, since knife edge M_1 has a minimum slope and is not a sub-path knife edge, use (D-15) through (D-17) and (D-23) to determine effective heights and distances, and (D-9) and (D-10) for the diffraction parameter and diffraction loss. Since knife edge M_2 has a maximum slope and is a sub-path knife edge, use (D-19) through (D-23) to determine the effective heights and distances, and (D-9) and (D-10) for the diffraction parameter and diffraction loss. The results are presented in Table 11.

For the right side of the primary knife edge, since knife edges M_4 and M_5 are not sub-path knife edges, use (D-11) through (D-14) to determine the effective heights and distances, (D-23) for the diffraction parameter ν , and (D-10) for the diffraction loss. Since knife edge M_6 is a sub-path knife edge, use (D-19) through (D-23) to determine the effective heights, distances, and diffraction parameter ν , and calculate the diffraction loss with (D-10). The results are presented in Table 11. The total diffraction loss is 38.161 dB, which is the sum of the decibel losses for all knife edges in Table 11.

Table 11. Computation of the Fresnel-Kirchhoff diffraction parameter v and diffraction loss for the Giovaneli method.

Parameter	M_1	M_2	M_3	M_4	M_5	M_6
$d_T(km)$	1.0	1.2	3.0	1.2	0.8	0.4
d_R (km)	2.0	0.8	3.4	2.2	1.4	1.0
h_i (m)	1.6	2.2	3.4	3.0	2.6	1.7
h_i' (m)	0.467	-0.480	1.966	0.130	0.691	-0.157
Edge distance from XMTR (km)	1.0	2.2	3.0	4.2	5.0	5.4
ν	0.057	-0.069	0.156	0.015	0.097	-0.029
<i>L</i> (dB)	6.528	5.437	7.384	6.160	6.873	5.779

4. Description of the 50 Multiple Knife-Edge Diffraction Scenarios Considered for the Analysis

Fifty different diffraction scenarios were tested against the alternative methods for an initial attempt at simulation of many possible actual diffraction configurations, including some with sub-path and grazing incidence knife edges. The test scenarios listed in Tables 12 and 13 included many variations of distances between knife edges, heights, and height-to-distance ratios between knife edges chosen to explore the accuracies and computation limits of the alternative methods. The frequency for all scenarios is 1500 MHz. All heights and distances are in meters or kilometers. The diffraction knife-edge heights for all figures in this discussion are graphically exaggerated for clarity. Due to the actual ratios of the heights to the distances in many of the scenarios, the magnitudes of the slant distances are approximately equal to the horizontal distances.

Figures 16 through 25 show the diffraction scenarios described in Tables 12 and 13; the last column in Tables 12 and 13 indicates the corresponding figure. Figures 16 through 25 are for Cases 3, 8, 13, 18, 23, 28, 33, 38, 43, and 48, respectively. For example, Figure 16 corresponds to Case 3, Figure 17 corresponds to Case 8, Figure 18 corresponds to Case 13, etc. These figure numbers are listed in the last column of the Tables 12 and 13. If there is no corresponding figure for a row, then it is indicated by a (-) entry in that row. $Td_i = Td_1$, Td_2 , Td_3 , ..., Td_7 are the distances of the edges from the transmitter shown in Tables 12 and 13. The last edge entry of the row in the Tables is the receiver location.

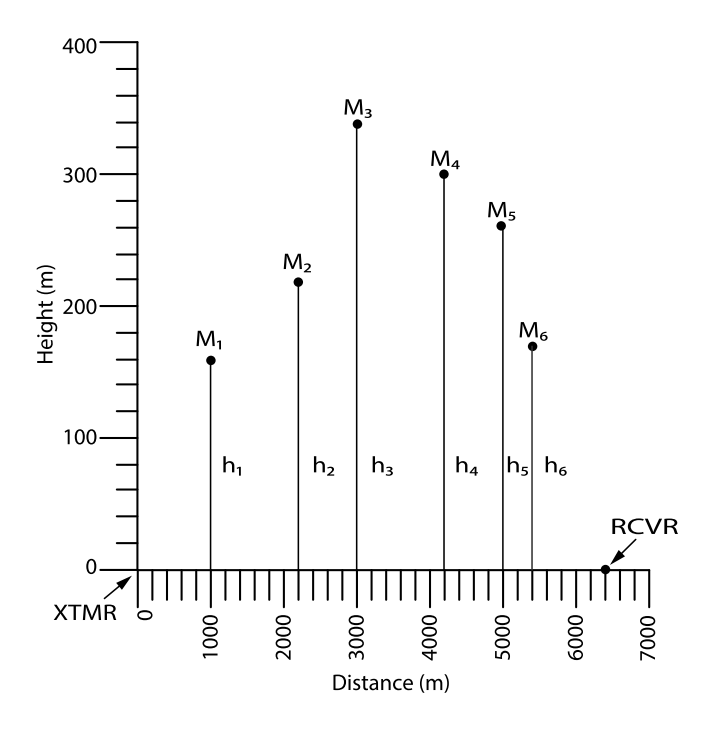


Figure 16: Six knife-edge diffraction scenario (Case 3) with two sub-path knife edges, M_2 and M_6 .

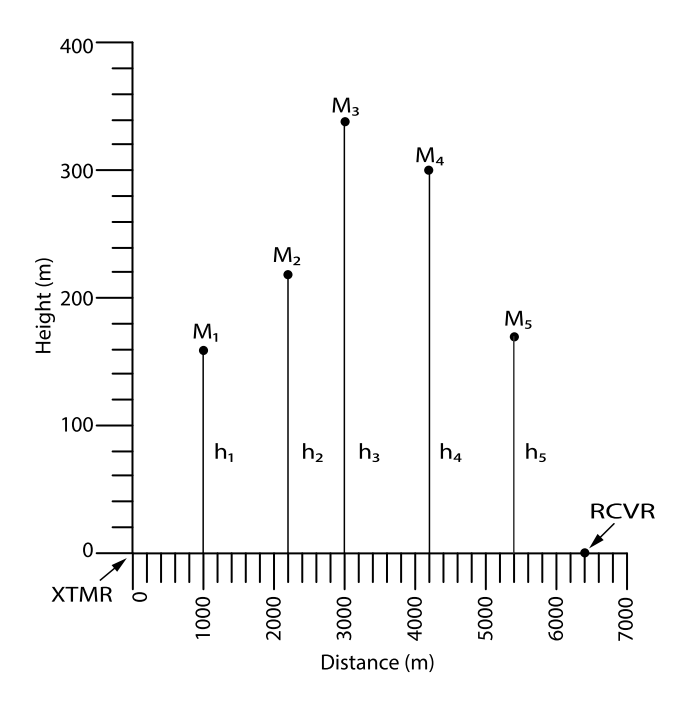


Figure 17: Five-knife-edge diffraction scenario (Case 8) with one sub-path knife edge, M_2 .

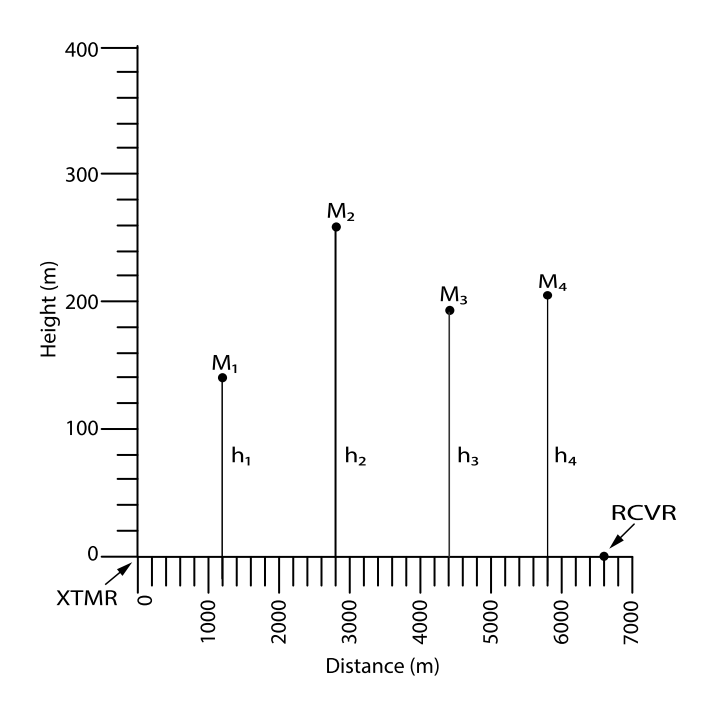


Figure 18: Four-knife-edge diffraction scenario (Case 13) with one sub-path knife edge, M_3 .

The 50 scenarios in Tables 12 and 13 all have transmitter and receiver antenna heights of zero for simplification of the computation and graphical presentation. There is no loss of validity for the analysis if these antenna heights are set to zero for these scenarios. Nonzero antenna heights for the transmitter or receiver translate each of the knife-edge heights in the

scenario. Equation (3) can be used to perform the translation for situations where the antenna heights are not zero by subtracting the appropriate Δh_i from each knife-edge height h_t .

Table 12 contains parameters for scenario Cases 1 through 25 with 6, 5, 4, 3, and 2 diffraction knife edges. Table 13 contains parameters for scenario Cases 26 through 50 for a variety of scenarios, all with six diffraction knife edges. The first 20 scenario cases (26 through 45) of Table 13 demonstrate reciprocity of the methods. Here, the term reciprocity means that the predicted path loss is invariant when the transmitter and receiver terminals are interchanged. Cases 26 through 30 are reciprocal to Cases 31 through 35, respectively, and Cases 36 through 40 are reciprocal to Cases 41 through 45, respectively.

Table 13 shows cases that agree with each other for the diffraction computations, because their height-to-distance ratios for each knife edge are the same and hence yield the same diffraction parameter and diffraction loss, even though the heights and distances are different. Cases that have the same height-to-distance ratios in Table 13 are Cases 28 and 29, Cases 33 and 34, Cases 38 and 39, Cases 43 and 44, and Cases 48 and 49. All of these cases do not contain the additional propagation loss in free space. The total losses for these cases will be different when free space loss is added to the diffraction loss because the distances between knife edges are different even though the height-to-distance ratios are the same. Longer distances will have larger free space losses for the cases in Tables 12 and 13.

Table 12: Height and distance parameters for Cases 1 through 25.

0 "	Td₁(m)	Td₂(m)	Td₃(m)	Td ₄ (m)	Td₅(m)	Td ₆ (m)	Td ₇ (m)	F: . "
Case #	h_1 (m)	h_2 (m)	h_3 (m)	$oldsymbol{h_4}$ (m)	$oldsymbol{h}_5$ (m)	$oldsymbol{h}_6$ (m)	h_7 (m)	Figure #
1	500	1100	1500	2100	2500	2700	3200	
1	1.6	2.2	3.4	3.0	2.6	1.7	0	-
2	100	220	300	420	500	540	640	
	1.6	2.2	3.4	3.0	2.6	1.7	0	-
3	1000	2200	3000	4200	5000	5400	6400	Eiguro 14
3	160	220	340	300	260	170	0	Figure 16
4	10	22	30	42	50	54	64	
4	1.6	2.2	3.4	3.0	2.6	1.7	0	-
5	20	44	60	84	100	108	128	
5	0.8	1.1	1.7	1.5	1.3	0.85	0	-
6	500	1100	1500	2100	2700	3200		-
0	1.6	2.2	3.4	3.0	1.7	0		
7	100	220	300	420	540	640		
/	1.6	2.2	3.4	3.0	1.7	0		-
8	1000	2200	3000	4200	5400	6400		Figure 17
0	160	220	340	300	170	0		Figure 17
9	10	22	30	42	54	64		
7	1.6	2.2	3.4	3.0	1.7	0		-
10	20	44	60	84	108	128		
10	0.8	1.1	1.7	1.5	0.85	0		-
11	600	1400	2200	2900	3300			
11	1.4	2.6	2.0	2.2	0			-
12	120	280	440	580	660			
12	1.4	2.6	2.0	2.2	0			-
13	1200	2800	4400	5800	6600			Eiguro 10
13	140	260	200	220	0			Figure 18

	Td₁(m)	Td₂(m)	Td₃ (m)	Td₄(m)	Td₅ (m)	Td₀(m)	Td ₇ (m)	
Case #	h_1 (m)	h_2 (m)	h ₃ (m)	h_4 (m)	h_5 (m)	h ₆ (m)	h ₇ (m)	Figure #
1.4	12	28	44	58	66			
14	1.4	2.6	2.0	2.2	0			-
1 5	24	56	88	116	132			
15	0.7	1.3	1.0	1.1	0			-
16	600	1400	2300	2900				
10	1.8	2.4	2.2	0				
17	120	280	460	580				
17	1.8	2.4	2.2	0				-
18	1200	2800	4600	5800				Eigura 10
10	180	240	220	0				Figure 19
19	12	28	46	58				-
17	1.8	2.4	2.2	0				
20	24	56	92	116				
20	0.9	1.2	1.1	0				-
21	800	2000	2800					
21	2.4	2.0	0					-
22	160	400	560					
	2.4	2.0	0					-
23	1600	4000	5600					Figure 20
23	240	200	0					Figure 20
24	16	40	56					
24	2.4	2.0	0					
25	32	80	112					
25	1.2	1.0	0					-

Table 13: Height and distance parameters for Cases 26 through 50

0 "	Td₁(m)	Td ₂ (m)	Td₃(m)	Td₄(m)	Td₅(m)	Td ₆ (m)	Td ₇ (m)	F: //
Case #	h_1 (m)	h_2 (m)	h_3 (m)	h_4 (m)	h_5 (m)	h_6 (m)	h_7 (m)	Figure #
26	500	1000	1500	2000	2500	3000	3500	
20	1.4	2.8	3.4	3.75	3.9	4.3	0	-
27	100	200	300	400	500	600	700	
27	1.4	2.8	3.4	3.75	3.9	4.3	0	-
28	1000	2000	3000	4000	5000	6000	7000	Figure 21
20	14.0	28.0	34.0	37.5	39.0	43.0	0	Figure 21
29	10	20	30	40	50	60	70	
27	1.4	2.8	3.4	3.75	3.9	4.3	0	-
30	20	40	60	80	100	120	140	
30	0.7	1.4	1.7	1.875	1.95	2.15	0	-
31	500	1000	1500	2000	2500	3000	3500	
31	4.3	3.9	3.75	3.4	2.8	1.4	0	-
32	100	200	300	400	500	600	700	
32	4.3	3.9	3.75	3.4	2.8	1.4	0	-
33	1000	2000	3000	4000	5000	6000	7000	Figure 22
33	43.0	39.0	37.5	34.0	28.0	14.0	0	rigure 22
34	10	20	30	40	50	60	70	
34	4.3	3.9	3.75	3.4	2.8	1.4	0	-
35	20	40	60	80	100	120	140	
33	2.15	1.95	1.875	1.7	1.4	0.7	0	-

0 "	Td₁(m)	Td₂(m)	Td₃(m)	Td₄(m)	Td₅(m)	Td ₆ (m)	Td ₇ (m)	F: . "
Case #	h_1 (m)	h_2 (m)	h_3 (m)	h_4 (m)	h_5 (m)	h_6 (m)	h_7 (m)	Figure #
27	500	1000	1500	2000	2500	3000	3500	
36	1.7	1.8	2.5	3.7	4.1	4.3	0	_
37	100	200	300	400	500	600	700	
37	1.7	1.8	2.5	3.7	4.1	4.3	0	-
38	1000	2000	3000	4000	5000	6000	7000	Eiguro 22
30	17.0	18.0	25.0	37.0	41.0	43.0	0	Figure 23
39	10	20	30	40	50	60	70	
37	1.7	1.8	2.5	3.7	4.1	4.3	0	_
40	20	40	60	80	100	120	140	
40	0.85	0.9	1.25	1.85	2.05	2.15	0	-
41	500	1000	1500	2000	2500	3000	3500	
41	4.3	4.1	3.7	2.5	1.8	1.7	0	_
42	100	200	300	400	500	600	700	_
42	4.3	4.1	3.7	2.5	1.8	1.7	0	
43	1000	2000	3000	4000	5000	6000	7000	Figure 24
43	43.0	41.0	37.0	25.0	18.0	17.0	0	Figure 24
44	10	20	30	40	50	60	70	
44	4.3	4.1	3.7	2.5	1.8	1.7	0	-
45	20	40	60	80	100	120	140	
43	2.15	2.05	1.85	1.25	0.9	0.85	0	-
46	500	1000	1500	2000	2500	3000	3500	
40	2.0	3.3	4.0	3.7	2.7	1.5	0	-
47	100	200	300	400	500	600	700	
47	2.0	3.3	4.0	3.7	2.7	1.5	0	-
48	1000	2000	3000	4000	5000	6000	7000	Figure 25
40	20.0	33.0	40.0	37.0	27.0	15.0	0	Figure 23
49	10	20	30	40	50	60	70	
47	2.0	3.3	4.0	3.7	2.7	1.5	0	_
50	20	40	60	80	100	120	140	
30	1.0	1.65	2.0	1.85	1.35	0.75	0	_

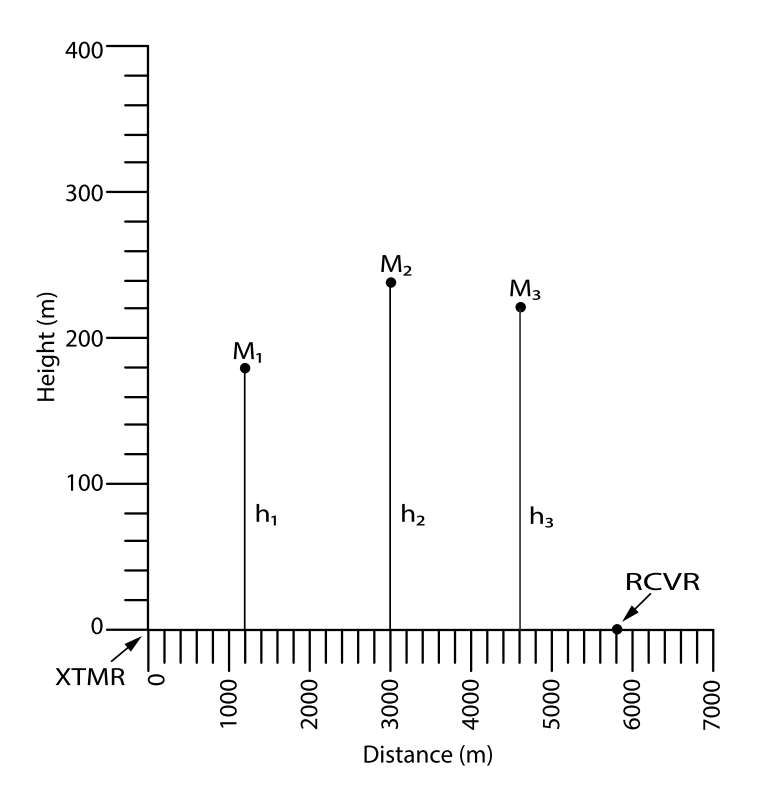


Figure 19: Three-knife-edge diffraction scenario (Case 18) with no sub-path knife edges.

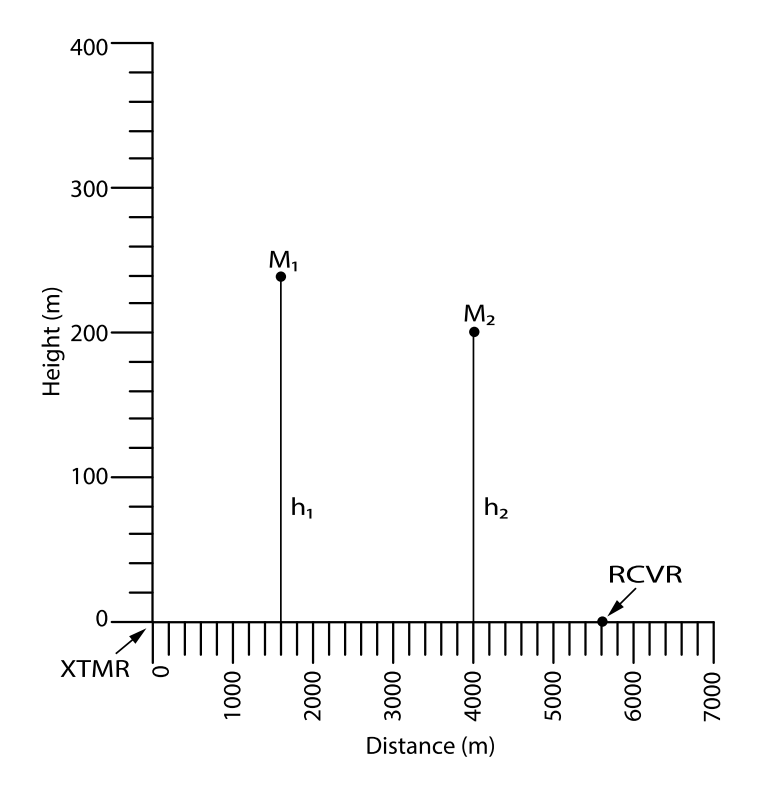


Figure 20: Two-knife-edge diffraction scenario (Case 23) with no sub-path knife edges.

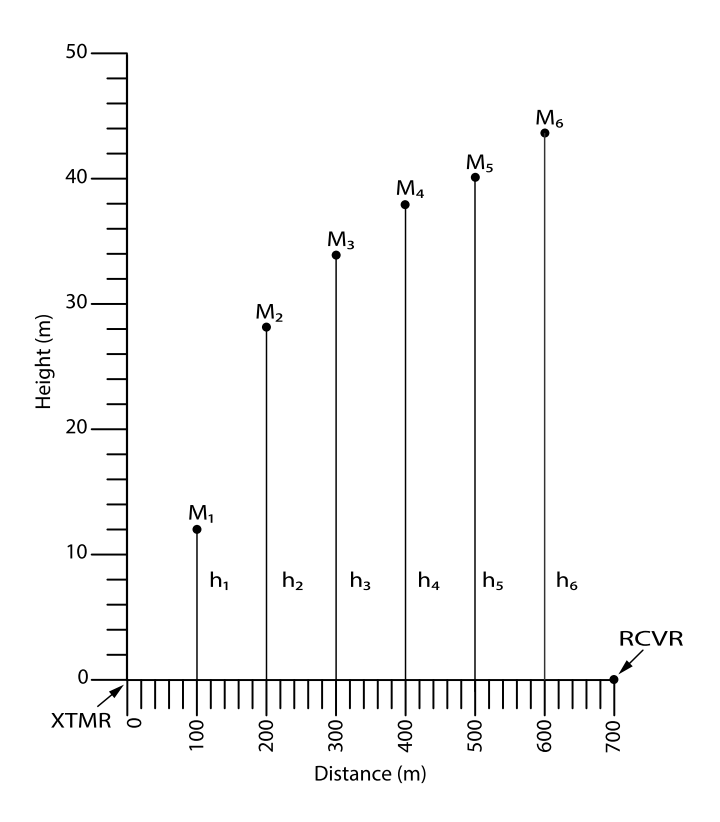


Figure 21: Six-knife-edge ascending scenario (Case 28) with one sub-path knife edge, M_5 , and one grazing knife edge, M_1 .

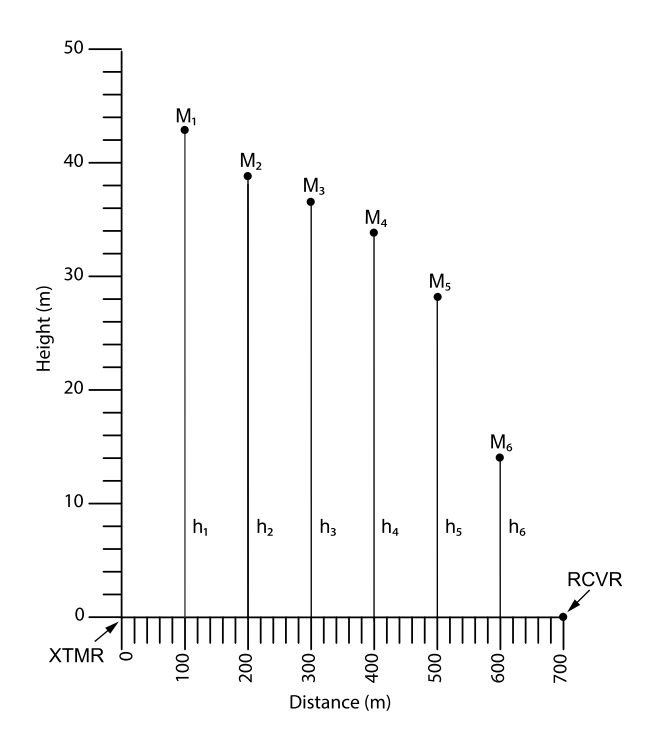


Figure 22: Six-knife-edge descending scenario (Case 33) with one sub-path knife edge, M_2 , and one grazing knife edge, M_6 .

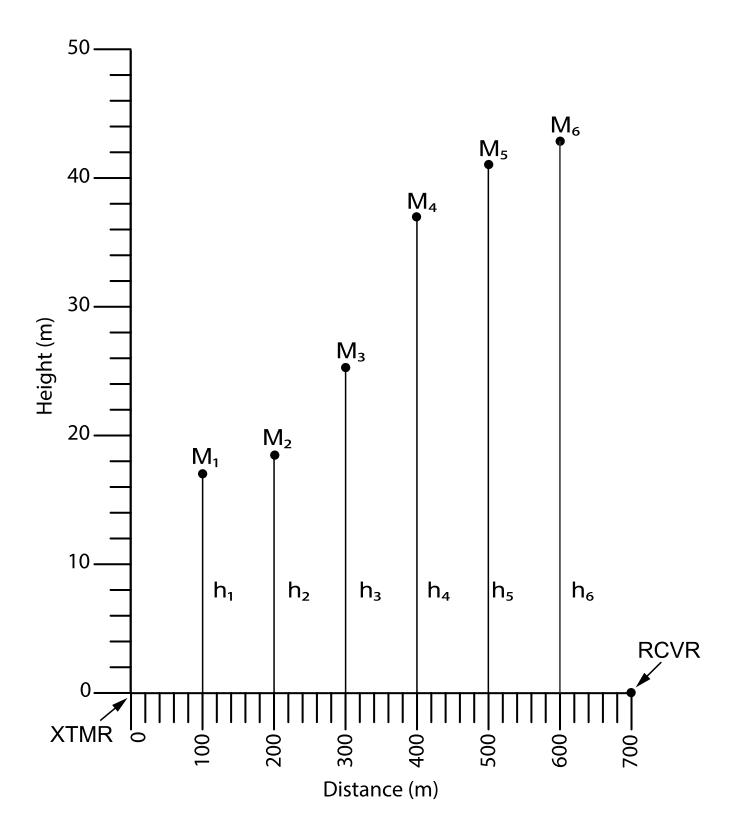


Figure 23: Six-knife-edge ascending scenario (Case 38) with two sub-path knife edges: M_2 and M_3 .

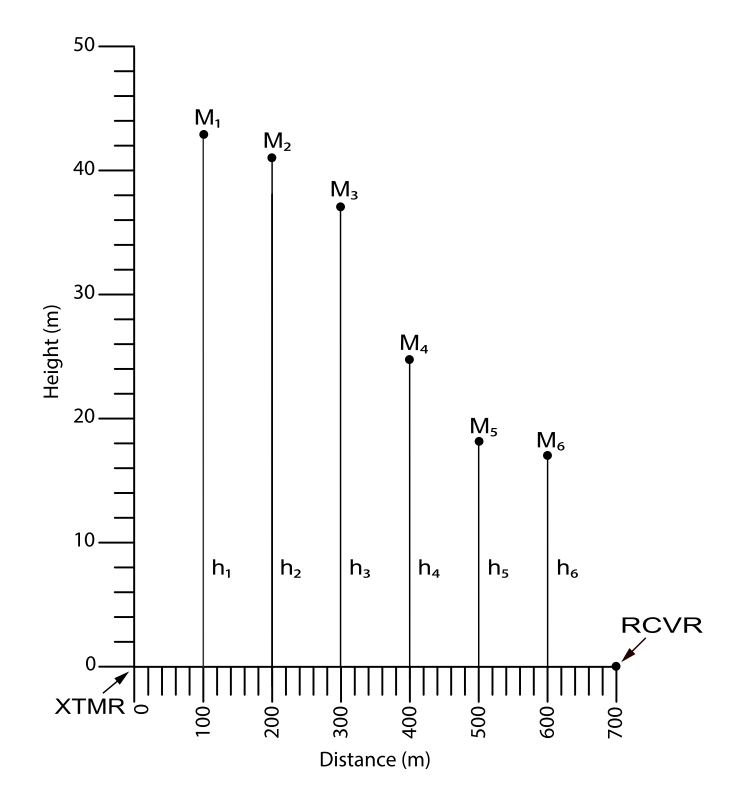


Figure 24: Six-knife-edge descending scenario (Case 43) with two sub-path knife edges: M_4 and M_5 .

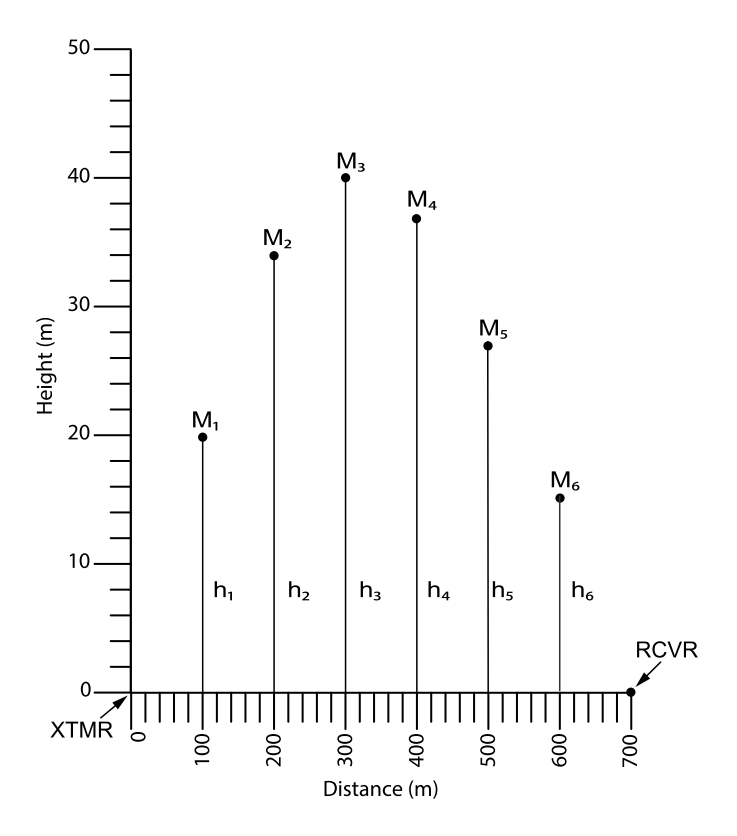


Figure 25: Six-knife-edge ascending and descending scenario (Case 48) with no sub-path knife edges.

5. Comparison of Alternative Computation Methods with the Vogler Method

5.1 Comparisons of Loss Predictions for the Vogler Method and the Alternative Methods

The results of the loss computations for the knife-edge scenarios in Figures 16 through 25 discussed in Section 4 are presented in Figures 26 through 34. Figures 26 through 34 compare the losses predicted with each of the methods to those predicted with the Vogler method. These results are based on the scenarios of Figures 16 through 25 and Tables 12 and 13. The attenuation ratios are plotted versus the case number from Tables 12 and 13. The attenuation ratios are computed by subtracting the loss computed by the Vogler method from the loss computed by the alternative computation method.

Figure 26 is a comparison of the four main methods for all 50 cases from Tables 12 and 13. The diffraction computations were made with all of the diffraction knife edges included. Because the Bullington method has a much larger error than the other methods, the scale on the figure had to be expanded; this figure demonstrates the magnitude of error achieved with the Bullington method and why the Bullington method was not considered to be a major contender for an alternative diffraction computation method. Figure 27 is Figure 26 with the Bullington method removed so that the vertical scale could be magnified to show better resolution of the attenuation ratio versus case number for the three other alternative methods.

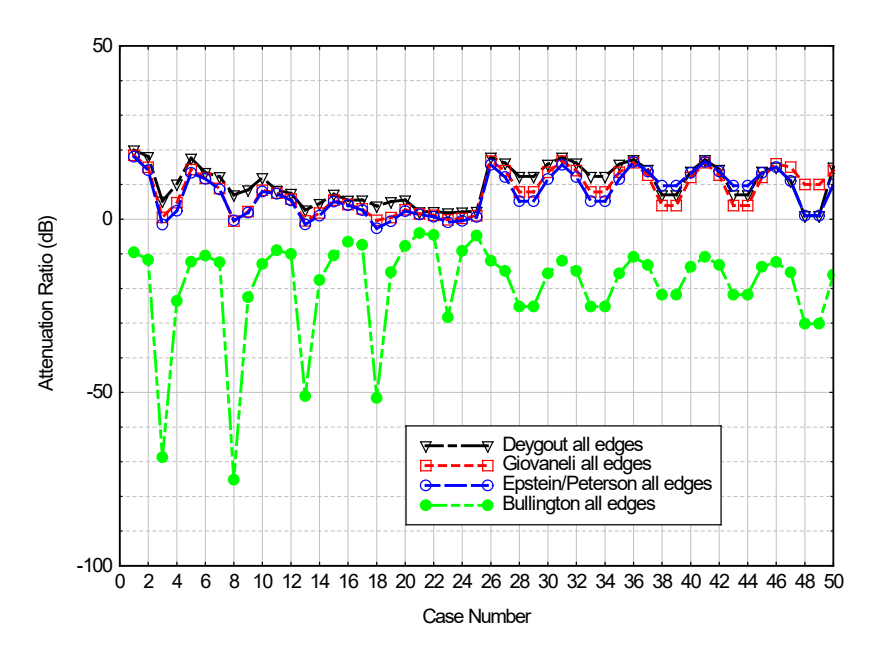


Figure 26: Attenuation ratio comparison to Vogler method for four alternative methods with all knife edges. Attenuation ratio (dB) = alternative method (dB) – Vogler method (dB).

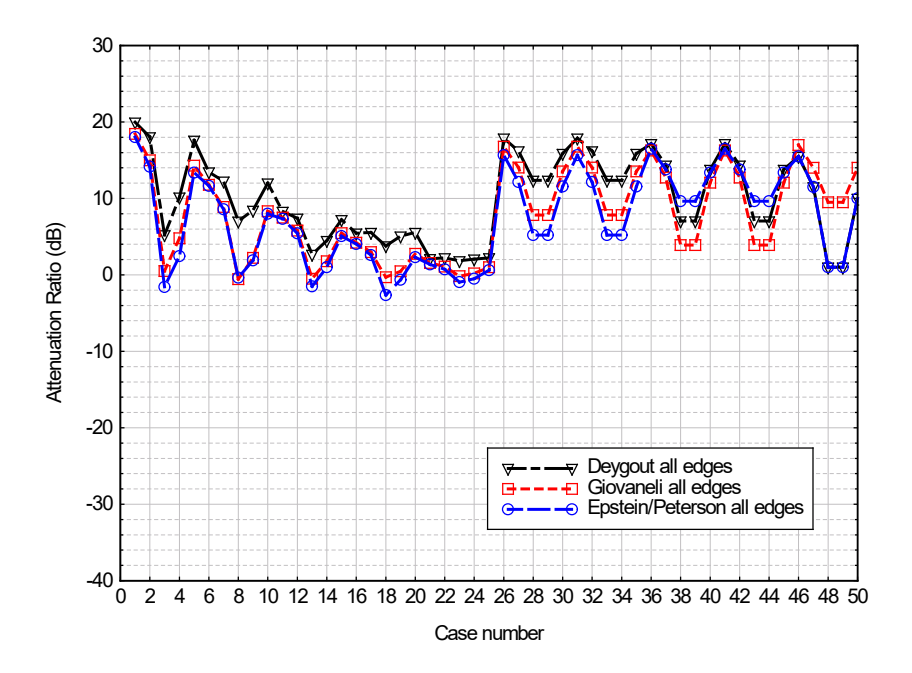


Figure 27: Attenuation ratio comparison to the Vogler method for three alternative methods with all knife edges. Attenuation ratio (dB) = alternative method (dB) - Vogler method (dB).

Each method takes all the diffraction knife edges into consideration. The attenuation ratios for Cases 11 through 15 (four knife edges), 16 through 20 (three knife edges), and 21 through 25 (two knife edges) are much lower than the rest of the cases. The attenuation ratio is shown to increase with the number of knife edges. The prediction gets worse with respect to Vogler as the number of edges increases.

Among the three methods the Epstein-Peterson method usually predicts the lowest diffraction loss. The Deygout method predicts the highest diffraction loss, and the Giovaneli method predicts a diffraction loss that is between the highest and lowest diffraction loss. None of the three methods have acceptable attenuation ratios (less than 3 dB) for the cases with five or six diffraction knife edges, so it is necessary to look at modifications of the three methods to see if the attenuation ratio can be minimized below 3 dB.

More edges in a scenario will result in a larger attenuation ratio, where the attenuation ratio is defined as the alternative method prediction minus the Vogler prediction. As the number of edges increases the cumulative computation error increases. In his paper [5], Deygout states that the major three knife edges are those with the largest Fresnel diffraction parameter ν . He then uses only those three edges to make his prediction. This approach will minimize the cumulative error in the diffraction loss computation. Deygout recommends using not more than three or four diffraction edges for a multiple edge diffraction computation. Deygout used graphical methods for computation. If many edges are used in the graphical computation procedure, cumulative error would occur for four or more edges. The mathematical algorithms in the appendices of this report would be more accurate and may allow more edges when implemented in a computer program.

Figure 28 shows the attenuation ratio for the three alternative methods when only the major three knife edges of each case are used in the computation. In general, these are those with the largest Fresnel-Kirchhoff diffraction parameter for the Epstein-Peterson and the Devgout

methods. For the Giovaneli method the major edges are the tallest edge and the two edges for which a line drawn between the peak of the tallest edge and the peak of that edge has a minimum slope. The cases with 4, 3, or 2 diffraction knife edges (11-15, 16-20, and 21-25, respectively) do have reasonably low attenuation ratios, but the rest of the cases with five and six diffraction knife edges are not within a 3 dB limit.

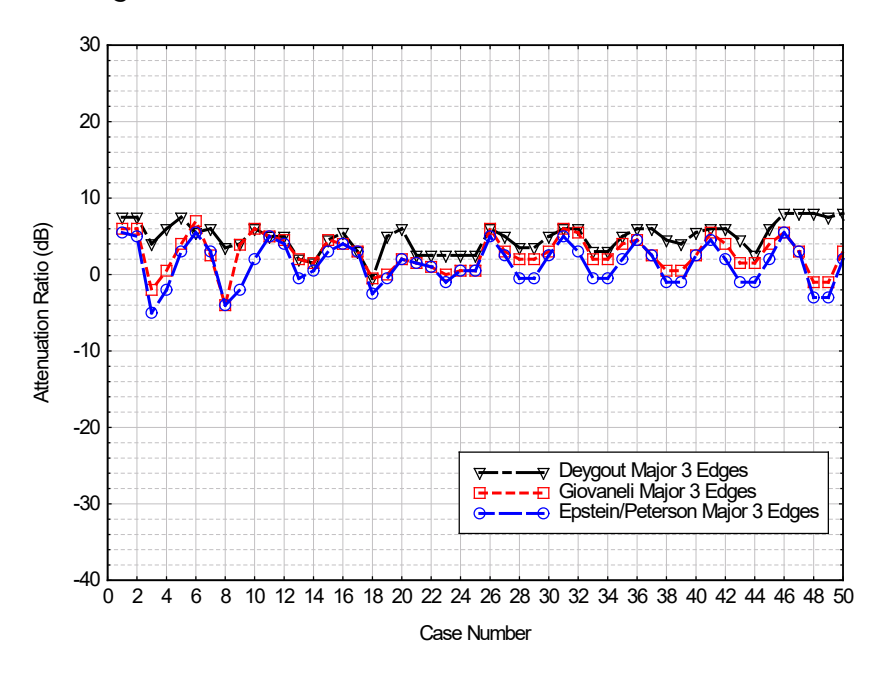


Figure 28: Attenuation ratio comparison to the Vogler method for three alternative methods with major three knife edges. Attenuation ratio (dB) = alternative method (dB) – Vogler method (dB).

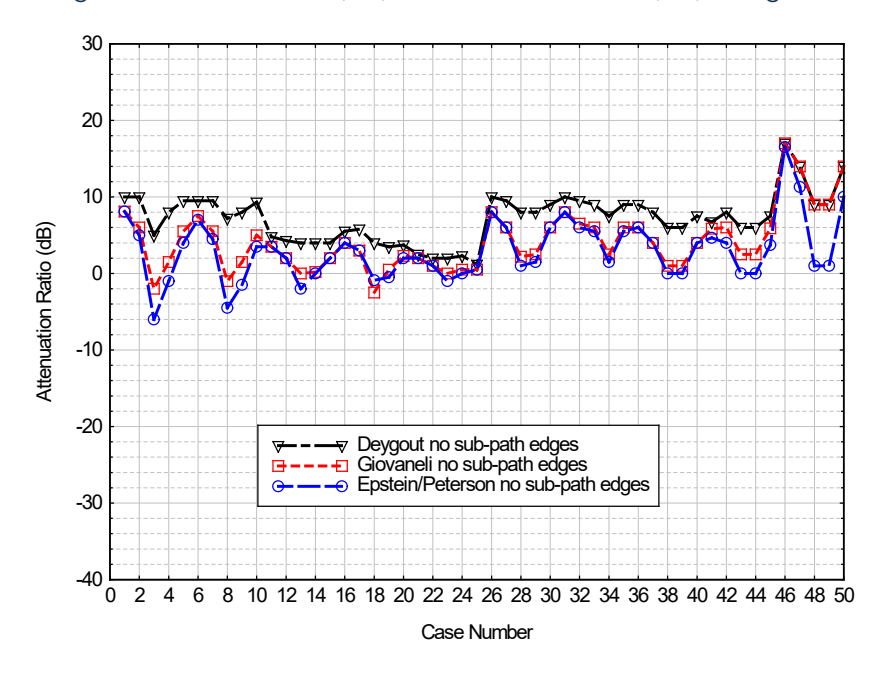


Figure 29: Attenuation ratio comparison to the Vogler method for three alternative methods with no sub-path knife edges. Attenuation ratio (dB) = alternative method (dB) – Vogler method (dB).

Figure 29 shows the attenuation ratio for the three alternative methods when the sub-path knife edges have been deleted from the diffraction loss computation. Deleting the sub-path knife edges from the diffraction loss computation adds considerable improvement (compared to the all knife edge and major three knife edge variations of Figures 27 and 28, respectively) in reducing the attenuation ratio except for Cases 46 through 50, which have no sub-path knife edges. Cases 46, 47, and 50 have a scenario geometry that aligns the ray path from one knife edge to the next with the incident shadow boundary, causing the large attenuation ratio. This phenomenon was discussed previously in Section 3.3, where methods to reduce the error in diffraction loss prediction were described. Again, the Epstein-Peterson method has the lowest overall attenuation ratio and the Giovaneli method has the second lowest attenuation ratio.

Figure 30 shows the attenuation ratio for the previously described variations of the Deygout method: the Deygout All-Knife-Edges Method, Deygout Major Three Knife-Edges Method, and Deygout No Sub-Path Knife-Edges Method. The attenuation ratios are shown for Cases 26 through 50, each of which has six knife edges and uses the Deygout No Sub-Path Knife-Edges Method.

The Deygout No Sub-Path Knife-Edges Method has the best performance (i.e., minimum overall attenuation ratio) of the four Deygout method variations. The Deygout method is more complicated than the other methods, and, as stated above, he recommends computing diffraction loss and limiting the number of edges to four or fewer with his method. This is a result of the logic Deygout uses, as described in the previous two paragraphs, which limits the number of edges to reduce the cumulative mathematical error when performing the computations graphically—the only way they could be performed in 1966.

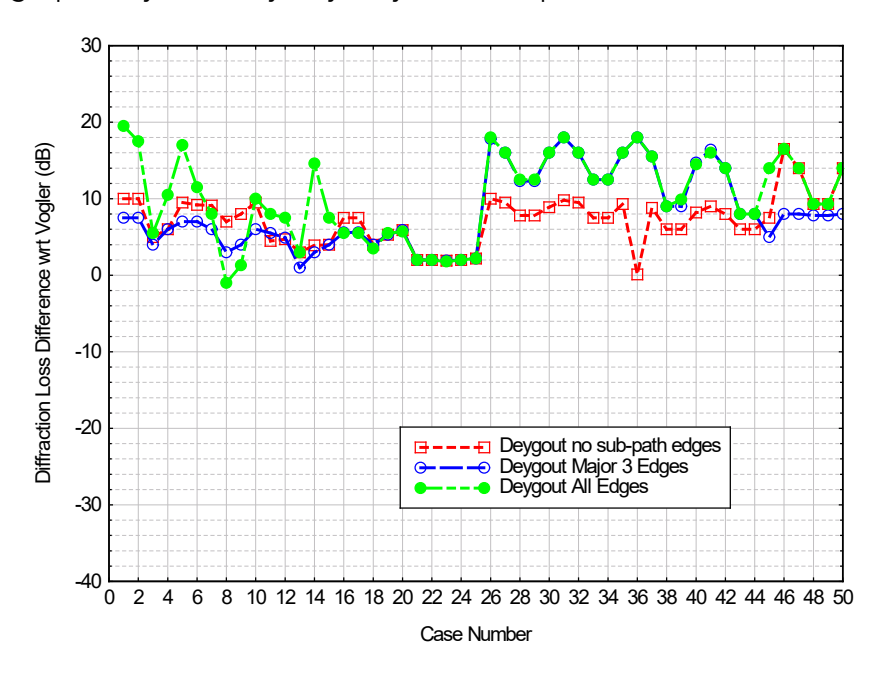


Figure 30: Attenuation ratio comparison to Vogler method for three variations of the Deygout method. Attenuation ratio (dB) = Deygout method (dB) - Vogler method (dB).

Figure 31 shows the attenuation ratio versus case number for six variations of the Epstein-Peterson method. Three of these variations apply the correction from [7] to the original

variations of all knife edges, no sub-path knife edges, and major three knife edges. The correction provides a significant improvement to all the knife-edge methods but causes an increase in the attenuation ratio for the Major Three Knife Edges Method and the No Sub-Path Knife-Edges Method.

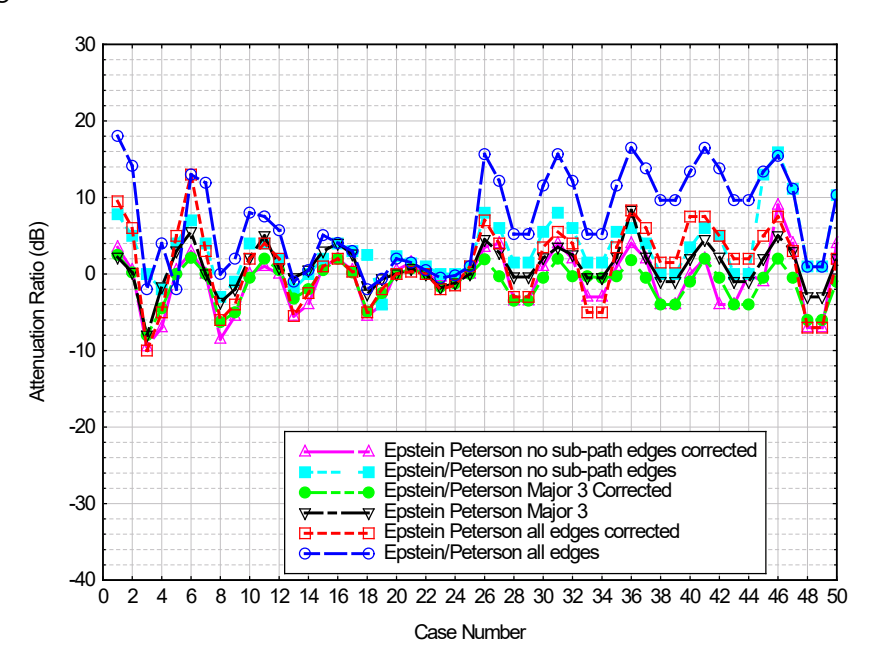


Figure 31: Attenuation ratio comparison to Vogler method for six variations of the Epstein-Peterson method. Attenuation ratio (dB) = Epstein-Peterson method (dB) – Vogler method (dB).

Figure 32 is Figure 31 with the deletion of the two worst methods involving the major three knife edges.

Figure 32 shows that the Epstein-Peterson cases with all knife edges corrected using the correction technique in [7] reduces the attenuation ratio significantly when compared to all knife edges variation uncorrected. Also shown is the significant increase in attenuation ratio for the Epstein-Peterson No Sub-Path Knife-Edges corrected method when compared to the Epstein-Peterson No Sub-Path Knife-Edges uncorrected method.

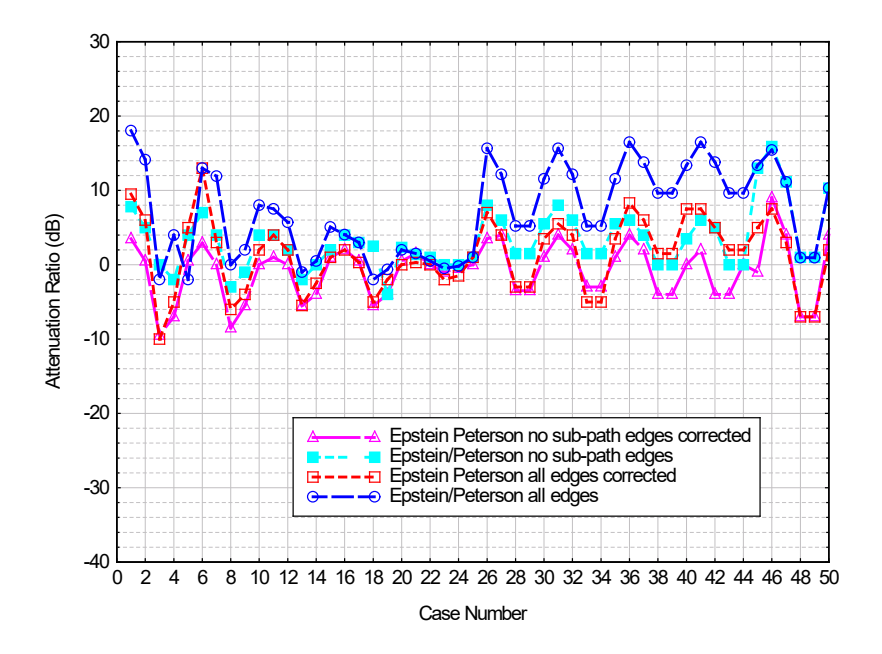


Figure 32: Attenuation ratio comparison to the Vogler method for four variations of the Epstein-Peterson method (two curves with largest errors removed for clarity). Attenuation ratio (dB) = Epstein-Peterson method (dB) - Vogler method (dB).

Figure 33 shows the comparison of attenuation ratio versus case number for three variations of the Giovaneli method. The variation containing no sub-path knife edges appears to provide the best performance except for cases 46, 47, and 50, which are situations where the ray path aligns with the incident shadow boundary causing a large attenuation ratio.

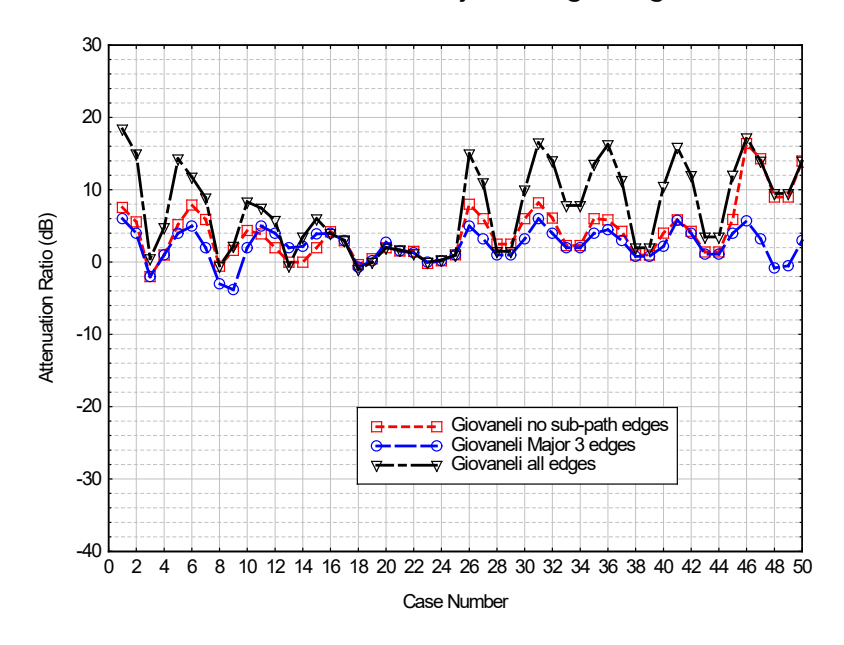


Figure 33: Attenuation ratio comparison to Vogler method for three variations of the Giovaneli method. Attenuation ratio (dB) = Giovaneli method (dB) - Vogler method (dB).

Figure 34 shows the comparison of the four best methods based on the previous analysis of attenuation ratio versus case number. This figure demonstrates that no one method can be

used exclusively for the diffraction loss computations, but a combination of methods is required to provide a suitable diffraction loss for all of the analyses. A technique for choosing a particular method is described in Section 3.3, which requires computation of the *FTFP* to select the method with the least attenuation ratio.

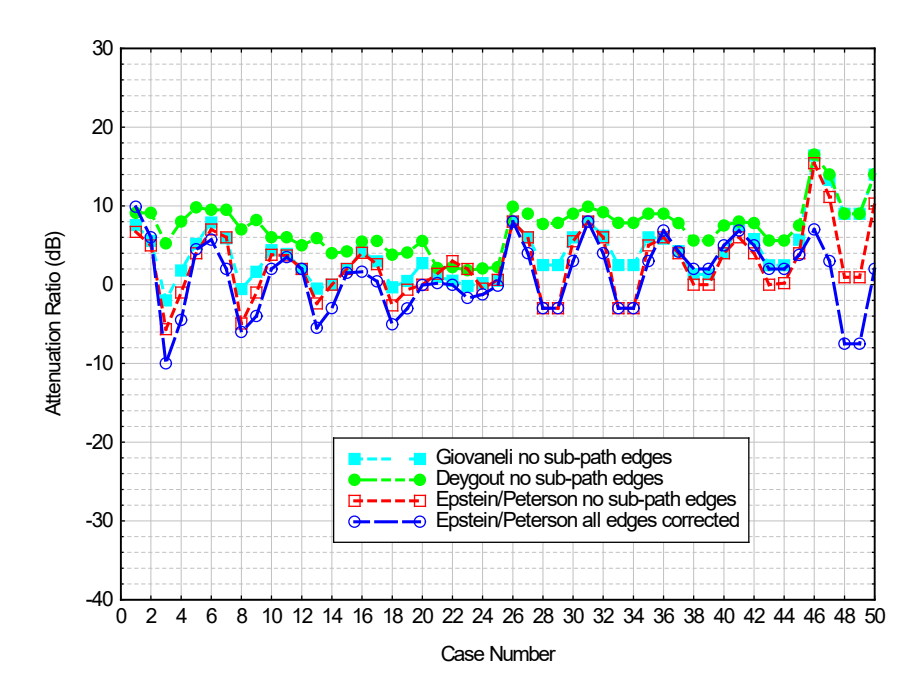


Figure 34: Attenuation ratio comparison to Vogler method of the alternative methods that result in the lowest attenuation ratio. Attenuation ratio (dB) = alternative method (dB) – Vogler method (dB).

For example, the Deygout No Sub-Path Knife-Edges Method has a small attenuation ratio for cases 15 to 25 of less than +6 dB. The Epstein-Peterson method with all knife edges corrected method also does well (±6 dB) for most cases. The Giovaneli method can provide low attenuation ratios for cases 28, 29, 33, and 34, where other methods cannot. The cases that demonstrate poor agreement in these figures are those where Vogler shows in [2] that there should be a large deviation between his method and the four alternative methods that were investigated.

Preliminary results of this analysis show where each of the alternative multiple knife-edge methods investigated can be used in place of the rigorous Vogler diffraction method to reduce computation time while maintaining suitable accuracy. It was shown that no one alternative method can cover all scenario variations. Which alternative diffraction method works best in a given scenario depends on how a method treats sub-path obstacles and the alignment of the ray path from one knife edge to the next knife edge with the shadow boundaries at the knife edges.

The best method implies a larger angle between the ray path and the incident shadow boundary and as a result avoidance of the incident shadow boundary. A step-by-step procedure for determining the best alternative diffraction loss computation was described in Section 3.3. There the argument x in F(x) is described as being related to this angular separation between the incident shadow boundary and the ray path and the function F(x) is the multiplicative magnitude needed to keep the loss prediction mathematically finite. A

large value of F(x) (close to 1.0) results in a small attenuation ratio. A small attenuation ratio indicates agreement with the Vogler computation of diffraction loss.

Figures 35 through Figure 38 plot attenuation ratio on the same graph as the FTFP(x) to demonstrate how the candidate methods can be used to provide an accurate diffraction loss prediction. Figure 35 shows the attenuation ratio and FTFP(x) versus case number for the Epstein-Peterson with all knife edges included. The attenuation ratio is minimized when the FTFP(x) approaches unity. Figure 36 shows the FTFP(x) plotted with the attenuation ratio versus case number for the Epstein-Peterson method with no sub-path knife edges. The attenuation ratio is small when the FTFP(x) is significantly greater than zero. Examinations of Figures Figure 33 through Figure 36 show that a maximum value of FTFP(x) = 1.0 corresponds to a minimum or zero value of attenuation ratio, which is indicative of agreement with the Vogler computation of diffraction loss. Values of FTFP(x) that are less than 1.0 corresponds to larger attenuation ratios, which implies a lesser agreement with the Vogler diffraction loss prediction. The disagreement with the Vogler method increases as the FTFP(x) approaches zero.

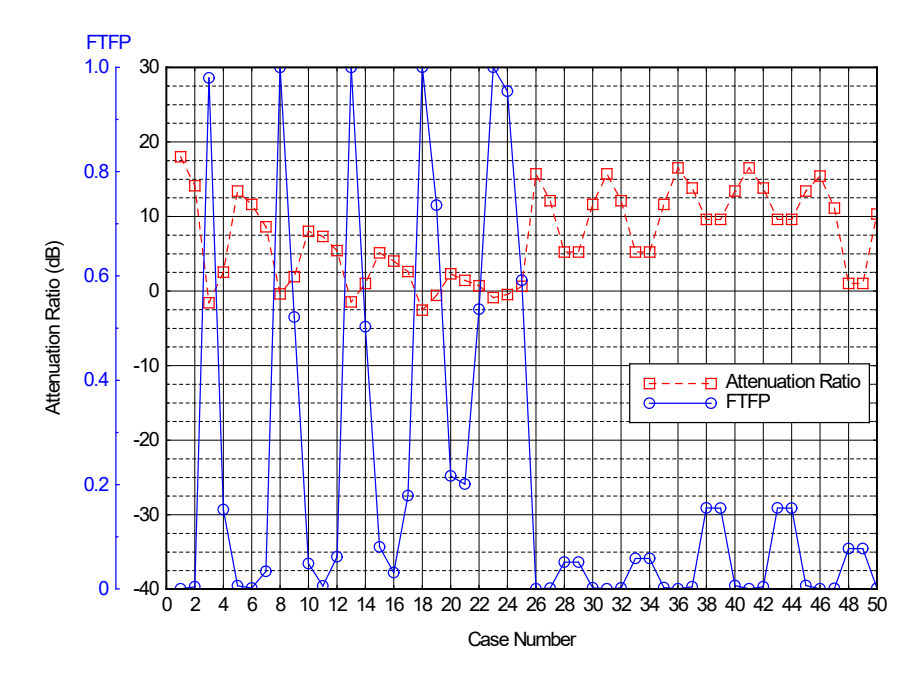


Figure 35: Attenuation ratio and Fresnel transition function product versus case number for Epstein-Peterson method with all knife edges. Attenuation ratio (dB) = Epstein-Peterson method (dB) – Vogler method (dB).

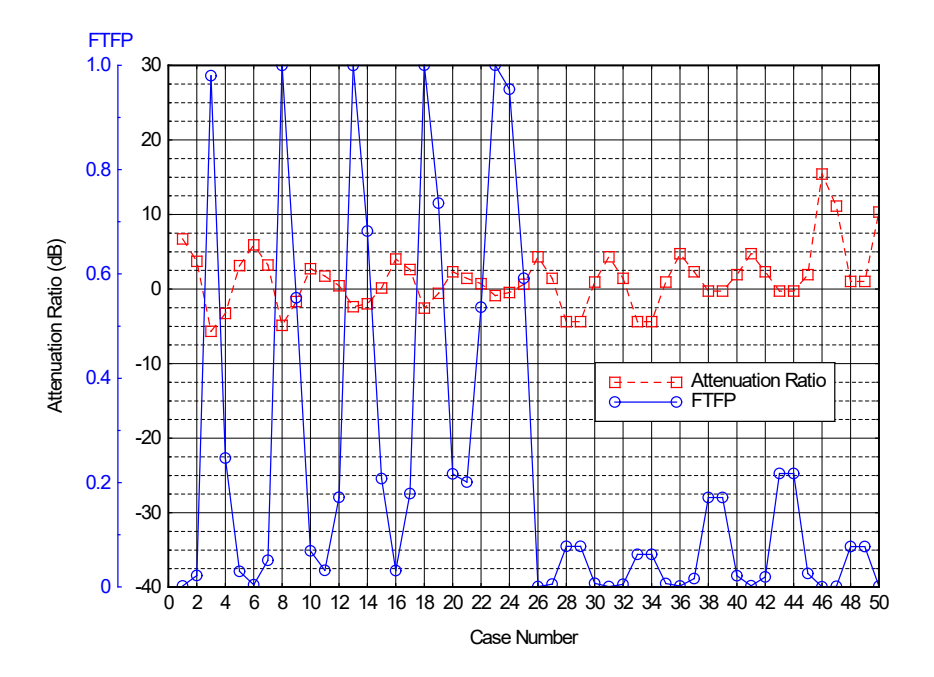


Figure 36: Attenuation ratio and Fresnel transition-function product versus case number for Epstein-Peterson method with no sub-path knife edges. Attenuation ratio (dB) = Epstein-Peterson method (dB) - Vogler method (dB).

Figure 37 shows the *FTFP* plotted with the attenuation ratio versus case number for the Giovaneli method with no sub-path knife edges. This figure also shows that the attenuation ratio is small when the *FTFP* is significantly greater than zero. As the *FTFP* approaches 1.0, the diffraction loss error is reduced even further.

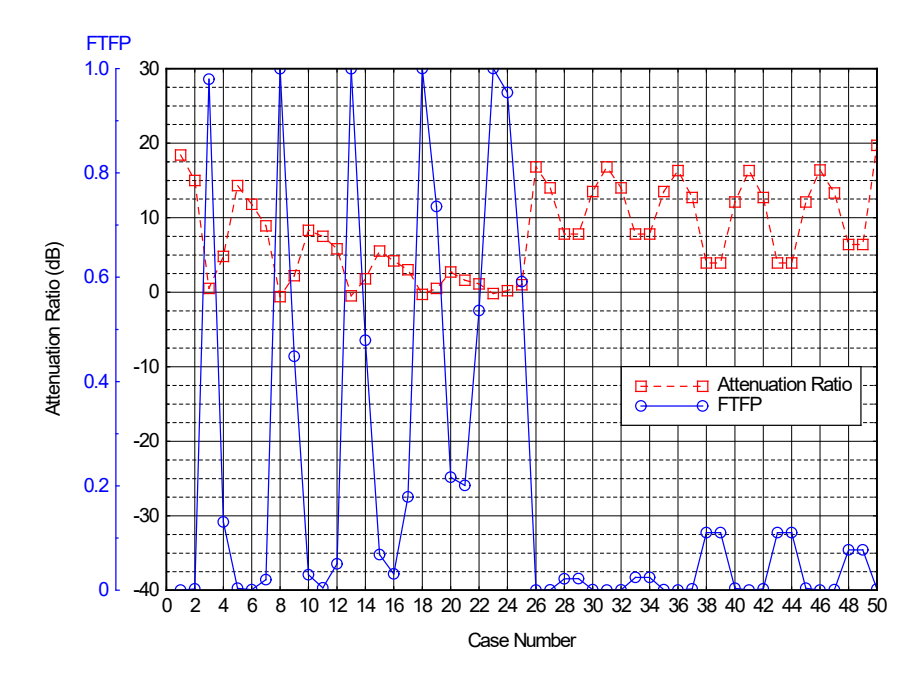


Figure 37: Attenuation ratio and Fresnel transition function product versus case number for Giovaneli method with no sub-path knife edges. Attenuation ratio (dB) = Giovaneli method (dB) – Vogler method (dB).

Figure 38 shows the *FTFP* plotted with the attenuation ratio versus case number for the Deygout method with no sub-path knife edges. This figure shows that the attenuation ratio is small when the *FTFP* is significantly greater than zero. As the *FTFP* approaches 1.0, the attenuation ratio decreases.

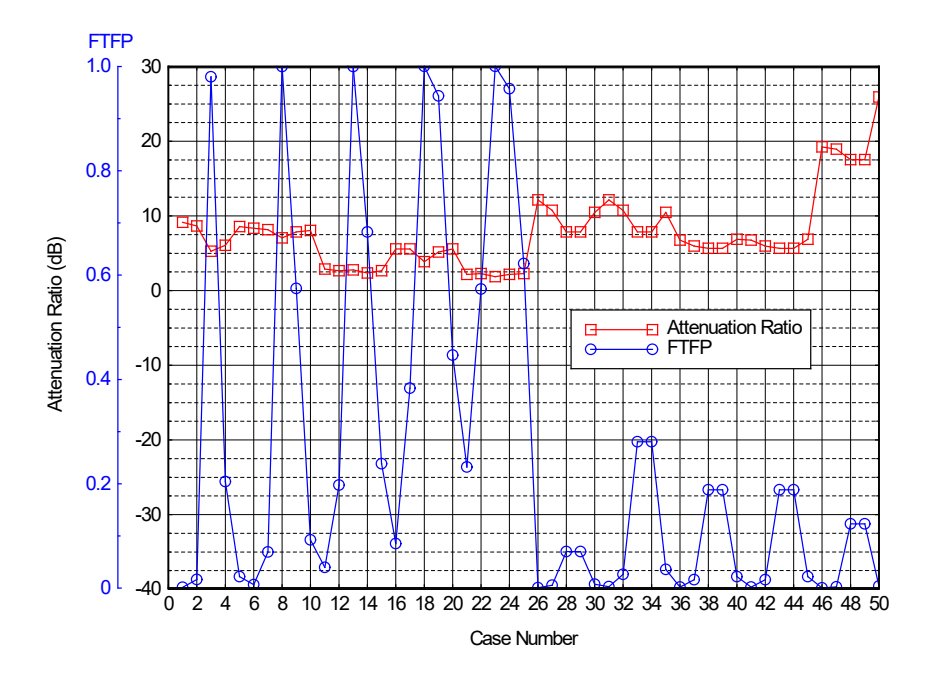


Figure 38: Attenuation ratio and Fresnel transition function product versus case number for the Deygout method with no sub-path knife edges. Attenuation ratio (dB) = Deygout method (dB) – Vogler method (dB).

Comparisons of the alternative multiple knife-edge diffraction methods show a ±3 dB agreement (Look at figures between the Vogler results and both the Epstein-Peterson and Giovaneli results for a variety of cases. Some differences depend on whether the sub-path knife edges (obstacles) are included in the diffraction loss computation for the different methods. It was found by comparative computations that removing the sub-path obstacles improves agreement between the Deygout method and the Vogler method. The Epstein-Peterson method's agreement with the Vogler method also improves when the sub-path knife edges are removed, but if this method with no sub-path knife edges is corrected with the ITU method in [8], then the agreement degrades. This agrees with Deygout when he mentions in his paper [5] that accuracy improves when the number of edges are limited to three or four edges. However, the Epstein-Peterson method with all knife-edges included and corrected by the Beyer method [7] improves agreement with the Vogler method.

The Giovaneli method with no sub-path knife edges agrees well with the Vogler method. This can be demonstrated in Tables 17 and 18 for many of the cases. This agreement varies from as small as 2 dB up to about 6 dB. The diffraction scenarios of Tables 12 and 13 were created to challenge the alternative models, but still represent realizable scenarios that could exist in nature. But since they do not exist, they could not be measured. These terrain paths could exist if a search were made for paths that contain measured data and were similar in peaks to the examples.

5.2 Comparisons of Execution Times and Path Loss Predictions for the Vogler Method and the Alternative Methods.

Comparisons of execution times with up to six knife edges between the Vogler method and the alternative methods of Bullington, Epstein-Peterson, Deygout, and Giovaneli resulted in run times that were more than three orders of magnitude (up to 1000:1) greater than the alternative methods. Figure 39 compares the run time results of the 50 different scenarios (cases) from Tables 12 and 13 of this section. Table 14 lists the parameters of the personal computer used to perform execution time comparisons for the 50 cases from Tables 12 and 13. Tables 15 and 16 list execution times in milliseconds for the cases in Tables 12 and 13, respectively.

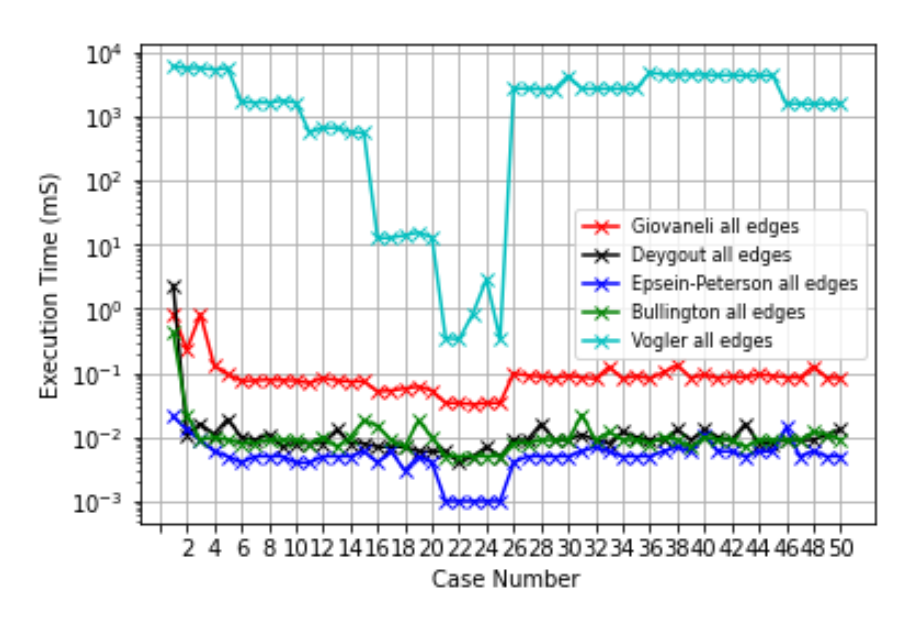


Figure 39. Comparison of execution times of the four alternative methods to the Vogler method for 50 different cases.

Table 14. Parameters of the computer used to perform the comparisons of execution times of the four alternative methods to the Vogler method for 50 different cases.

Parameter Item Name	Parameter Value		
Operating System	Microsoft Windows 10 Professional		
Version	10.0.19042 Build 19042		
System Manufacturer	Dell Inc.		
System Model	Latitude 7490 Laptop		
System Type	X64-based PC		
Processor	Intel(R)Core™ i7-8650UCPU@1.9 GHz 2112		
Hard Disk	220 Gbytes		
BIOS Version/Date, SM BIOS Version	Dell Inc. 1.13.1, 11/8/2019 3.1		
Embedded Controller	255.255		
BIOS Mode	UEFI		
Hardware Abstraction	Version = "10.019041.1151"		

Table 15. Execution times in milliseconds for the Vogler method and the four alternative loss prediction methods for Cases 1 through 25 of Table 12.

Test Case	Vogler	Giovaneli	Deygout	Epstein- Peterson	Bullington
1	5404.182	0.170	0.043	0.006	0.032
2	5413.140	0.134	0.014	0.006	0.014
3	5503.007	0.258	0.017	0.009	0.014
4	5383.887	0.099	0.014	0.007	0.011
5	5351.338	0.095	0.010	0.006	0.009
6	2034.857	0.094	0.009	0.007	0.010
7	1906.591	0.089	0.009	0.006	0.011
8	1885.911	0.094	0.016	0.006	0.010
9	2009.927	0.083	0.011	0.005	0.010
10	1885.705	0.086	0.008	0.007	0.013
11	650.246	0.077	0.011	0.006	0.010
12	619.995	0.078	0.015	0.011	0.014
13	665.417	0.079	0.009	0.005	0.008
14	628.114	0.082	0.099	0.004	0.010
15	629.208	0.076	0.008	0.006	0.009
16	14.752	0.059	0.008	0.004	0.009
17	14.497	0.060	0.007	0.006	0.020
18	15.810	0.068	0.008	0.005	0.009
19	18.666	0.097	0.007	0.005	0.014
20	15.360	0.099	0.007	0.005	0.016
21	0.485	0.040	0.008	0.002	0.006
22	0.384	0.039	0.006	0.001	0.006
23	1.008	0.037	0.005	0.001	0.006
24	3.332	0.041	0.007	0.002	0.007
25	0.617	0.044	0.011	0.002	0.006

Table 16. Execution times in milliseconds for the Vogler method and the four alternative loss prediction methods for Cases 26 through 50 of Table 13.

Test Case	Vogler	Giovaneli	Deygout	Epstein- Peterson	Bullington
26	3503.589	0.415	0.013	0.013	0.051
27	3259.990	0.122	0.098	0.007	0.011
28	3250.047	0.112	0.014	0.006	0.010
29	3051.458	0.127	0.021	0.007	0.013
30	5025.433	0.106	0.012	0.010	0.010
31	3190.233	0.147	0.026	0.007	0.016
32	3296.204	0.095	0.011	0.006	0.010
33	3096.530	0.093	0.013	0.005	0.010
34	3292.862	0.090	0.011	0.005	0.010
35	3849.522	0.106	0.022	0.007	0.015
36	6188.151	0.155	0.017	0.007	0.013
37	5481.165	0.113	0.012	0.055	0.010
38	5507.022	0.100	0.010	0.006	0.008
39	5632.101	0.159	0.010	0.008	0.013
40	6554.998	0.103	0.013	0.015	0.012

Test Case	Vogler	Giovaneli	Deygout	Epstein- Peterson	Bullington
41	5569.170	0.148	0.013	0.006	0.014
42	5273.096	0.103	0.011	0.007	0.010
43	5464.709	0.107	0.024	0.007	0.010
44	5791.748	0.117	0.011	0.007	0.009
45	5708.579	0.198	0.010	0.009	0.022
46	2030.612	0.170	0.042	0.032	0.043
47	2032.883	0.100	0.011	0.007	0.011
48	1966.461	0.152	0.011	0.007	0.011
49	1982.297	0.106	0.011	0.012	0.014
50	1966.449	0.105	0.018	0.006	0.012

Tables 17 and 18 list the path loss predictions in decibels (dB) greater than free space for the Vogler method and the four alternative loss prediction methods for Tables 12 and 13, respectively. These loss predictions correspond to the execution times in Tables 15 and 16 for the cases in Tables 12 and 13, which were obtained from running computer code developed by ITS. Although there are faster ways to evaluate the Fresnel Integral in the Vogler method, there would still be a large computation time difference between Vogler and the alternative diffraction methods. An example of a typical area coverage loss prediction over multiple radials from a transmitter using the execution times from Tables Table 15 and Table 16. If we choose 36000 radials for 0.01-degree increments in angle from the transmitter for an adequate number of sample points for area coverage at a 7 km distance. For Case 28 in Table 16, with a 7 km path distance with six knife edges, the Vogler method would take 3250 milliseconds (3.25 seconds) to compute one radial, whereas the slowest alternative method would require 0.112 milliseconds, which is a reduction in time ratio of 3.45E-5. The Vogler method would then require 32.5 hours to compute the area coverage with 36000 radials, whereas the slowest alternative diffraction method would require 0.00112 hours. Even if a way to evaluate the Fresnel integral were a thousand times faster, then a faster integral method implemented in the Vogler method would require 0.0325 hours to compute.

The free space loss will be different for different cases, since the distances are different for the cases. These total distances can be obtained by adding the distances from Tables 12 and 13 for each case. The free space losses are then computed from these total distances. The total loss is computed by adding the corresponding free-space loss to the losses shown in Tables 17 and 18.

Table 17. Path loss predictions in decibels (dB) greater than free space for the Vogler method and the four alternative loss prediction methods for Cases 1 through 25 of Table 12.

Test Case	Vogler	Giovaneli	Deygout	Epstein- Peterson	Bullington
1	21.234	38.765	40.738	38.802	11.147
2	28.257	41.919	45.911	42.002	16.136
3	114.433	111.857	119.665	112.855	45.748
4	49.024	52.126	59.394	52.688	25.754
5	29.672	42.567	46.913	42.671	16.994
6	21.516	33.128	33.006	33.149	10.942
7	28.239	36.768	36.520	36.824	15.805
8	120.471	119.462	119.434	120.119	45.364

Test Case	Vogler	Giovaneli	Deygout	Epstein- Peterson	Bullington
9	47.757	49.128	49.048	49.662	25.371
10	29.587	37.523	37.263	37.597	16.651
11	20.446	28.211	28.772	27.769	11.406
12	26.631	33.030	34.086	32.069	16.546
13	97.205	99.327	99.884	95.706	46.215
14	43.636	46.993	48.253	44.632	26.219
15	27.857	33.998	35.122	32.934	17.418
16	17.543	21.741	22.999	21.583	10.746
17	23.227	26.169	28.767	25.823	15.483
18	96.896	95.992	100.966	94.262	44.984
19	40.549	40.880	45.625	39.930	24.992
20	24.380	27.087	29.924	26.705	16.315
21	13.991	15.513	16.111	15.370	9.901
22	18.626	19.630	20.846	19.351	14.027
23	71.448	71.448	73.292	70.517	43.168
24	32.244	32.409	34.308	31.757	23.188
25	19.558	20.471	21.789	20.167	14.786

Table 18. Path loss predictions in decibels (dB) greater than free space for the Vogler method and the four alternative loss prediction methods for Cases 26 through 50 of Table 13.

Test Case	Vogler	Giovaneli	Deygout	Epstein- Peterson	Bullington
26	25.412	40.370	43.312	41.078	13.321
27	34.207	44.904	50.412	46.359	19.310
28	54.283	55.362	66.642	59.490	29.204
29	54.283	55.362	66.642	59.489	29.204
30	35.797	45.744	51.681	47.346	20.244
31	25.412	41.883	31.387	41.078	13.321
32	34.207	47.736	38.661	46.359	19.310
33	54.283	60.869	66.642	59.489	29.204
34	54.283	60.869	66.642	59.489	29.204
35	35.797	48.787	51.680	47.346	20.244
36	24.410	39.984	42.358	41.354	13.942
37	32.937	44.114	48.315	47.047	20.122
38	51.770	53.717	60.724	61.357	30.047
39	51.770	53.717	60.724	61.357	30.047
40	34.466	44.879	49.346	48.125	21.065
41	25.580	40.939	42.149	41.354	13.942
42	33.774	45.677	47.846	47.047	20.122
43	51.717	55.050	59.275	61.357	30.047
44	51.717	55.050	59.275	61.357	30.047
45	35.232	46.497	48.822	48.125	21.065
46	23.810	40.764	40.586	39.231	11.385
47	31.856	46.354	45.991	42.986	16.514
48	56.239	65.316	65.419	57.196	26.183
49	56.239	65.316	65.419	57.196	26.183
50	33.476	47.515	47.133	43.785	17.385

6. Comparisons of Alternative Computation Methods with Measured Data

This section contains comparisons of analytical computations of diffraction loss to measured diffraction loss for actual paths existing in nature. Measured data was available from four sources and used for comparison with analytical predictions using the alternative methods described previously and the Vogler method. One source of measured data was Deygout's original paper [5], which gave data for 10 paths over both hilly and mountainous terrain at multiple frequencies. The figures of actual terrain for those 10 paths are contained in Deygout's original 1966 paper. The fidelity of the terrain figures in Deygout's report is poor. The other three measurements were performed by ITS at multiple frequencies over three separate paths containing multiple diffraction knife edges.

ITS measured data are presented for three propagation paths. Two of these are located along 63rd Street in Boulder, CO. The first path is heading north along a straight section of 63rd Street located between the Ryssby Church and Nelson Road ("short path"). The second path is heading south along 63rd Street from Ryssby Church to Highway 119 ("long path"). The 63rd Street terrain paths are illustrated in Section 6.2. The third path is along Plateau Road at the Table Mountain Field Site and Radio Quiet Zone, which is 15 km north of the Department of Commerce Boulder Laboratories campus. The Plateau Road path is shown in Section 6.3.

The 63rd Street paths are illustrated in Section 6.2 with the edges that were used in the Tables of Section 6.2. The Plateau Road path is shown in Section 6.3. The computation examples for the 63rd Street paths are limited to six knife edges, which is within the limit for the alternative computation methods. The authors used the alternative computation methods using only six edges to compare to the measurements made on the 63rd Street paths. As can be seen from the results in Section 6.2, the alternative methods also demonstrated a ± 2.5 dB agreement with the loss predictions for the 63rd Street paths when compared to the loss predictions when using the Vogler method. In addition, the alternative methods agreed with measured data within ± 1.5 dB for the short path and ± 2.5 dB for the long path.

6.1 Comparisons to Measured Data from Devgout's Original Paper

Table 1 from Deygout's original paper [5] describes 10 paths over hilly and mountainous terrain. In this table he compares the measured propagation loss data to loss predictions made with his own method and the Epstein-Peterson method [4]. In Deygout's classic paper, the method takes all knife edges into consideration for the computation of diffraction loss. The Epstein-Peterson method implemented by Deygout considered sub-path knife edges if they interfered with the first Fresnel zone, except for his path 5 where he did not include them even if they interfered with the first Fresnel zone. The original Epstein-Peterson method does not address sub-path knife edges explicitly [4], [5], [19] but the Epstein-Peterson All

Knife-Edges Method used for comparison to measured data in this section will take sub-path knife edges into consideration.

Table 19 describes the 10 paths in Deygout's paper. The alternative methods of Epstein-Peterson, Deygout, and Giovaneli described previously, which include all knife edges and their variations of no sub-path edges, and the major three edges were compared to the measured data of all 10 paths of Deygout's paper. In this table, he compares the measured propagation loss data to loss predictions made with his own method and the Epstein-Peterson method [4]. Path 5 appears to be the most challenging path to all three methods. Figures 40 through 42 demonstrate the results of the prediction accuracy for the alternative methods of Epstein-Peterson, Deygout, and Giovaneli.

Path Number	F (MHz)	Total Path Length (km)	Knife-Edge Number	Actual Knife-Edge Height (m)	Knife Edge Distance from XMTR (km)	
1	1850	44	$M_1 M_2$	60 38	17 21.5	
2	1800	58	M_1 M_2	77.7 136	12 21	
3	1800	41	M_1 M_2	53 70	22 27	
4	1850	44	M ₁ M ₂ M ₃	38.75 75 64	6 24 28	
5	1800	52	M ₁ M ₂ M ₃ M ₄ M ₅	0.5 29.07 46.43 50 4.5	6.5 23 26 28 46	
6	160	89	$M_1 M_2$	560 364.29	40 65	
7	2450	64.5	M_1 M_2	435.74 500	43 50.5	
8	2450	22	M_1 M_2	393.57 450	11 14	
9	2450	85	M_1 M_2	1120 1067.08	40.5 43	
10	2450	40.5	M_1	650	11.5	

Table 19. Descriptions of the 10 paths from Deygout's original paper.

Figure 40 plots the results of the comparisons of the Epstein-Peterson method for all the knife edges, no sub-path knife edges, and major three knife edges to the measured data for each of the 10 paths. The prediction in Figure 40 for the case where the sub-path knife edges were included shows better agreement with measured data than the case where the sub-path knife edges were not included. Figure 38 shows that the deviation from measured data for the Epstein-Peterson method can be as much as -8.5 dB in Path 9, but as small as -2 dB for Path 3. Figure 40 does not include the correction by Beyer mentioned previously, because Deygout did not correct his computations in his 1966 paper [5], since it predated the report by Beyer [7]. Figure 41 plots the results of the comparisons of the Deygout method for all the knife edges, no sub-path knife edges, and major three knife edges to the measured data for

662.76

each of the 10 paths. This resulted in the most accurate loss prediction for his own method. In his paper, Deygout only computed the cases with all knife edges [5].

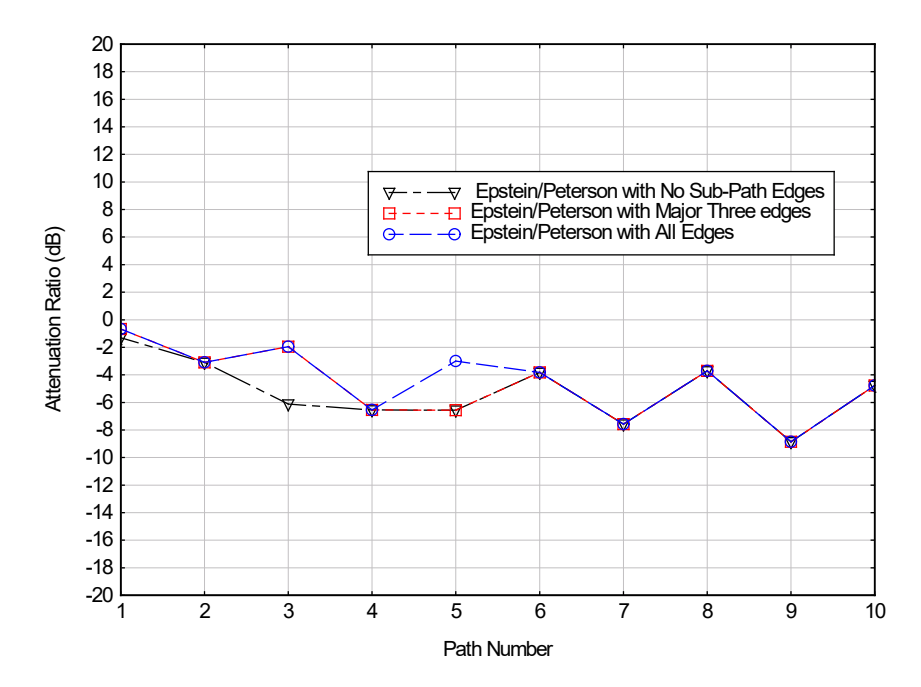


Figure 40: Epstein-Peterson loss prediction compared to measured data for the 10 paths in Deygout's original paper. Attenuation ratio (dB) = Epstein-Peterson method (dB) – measured data (dB).

Figure 41 shows that the deviation for the Deygout method can be as large as 6 dB for Path 5 but can be as small as 1 dB for some paths. Figure 42 plots the results of the comparisons of the Giovaneli method for all of the knife edges, no sub-path knife edges, and major three knife edges to the measured data for each of the 10 paths. Figure 42 shows that the deviation for the Giovaneli method can be as much as 7 dB for Path 5, but for the other paths it can be as small as 1 dB. The Giovaneli method provides a similar prediction error to the Deygout method of diffraction loss for some methods but can have a prediction that is much less than the Epstein-Peterson and Deygout methods. Comparison of the results of Figures 40 through 42 demonstrate this.

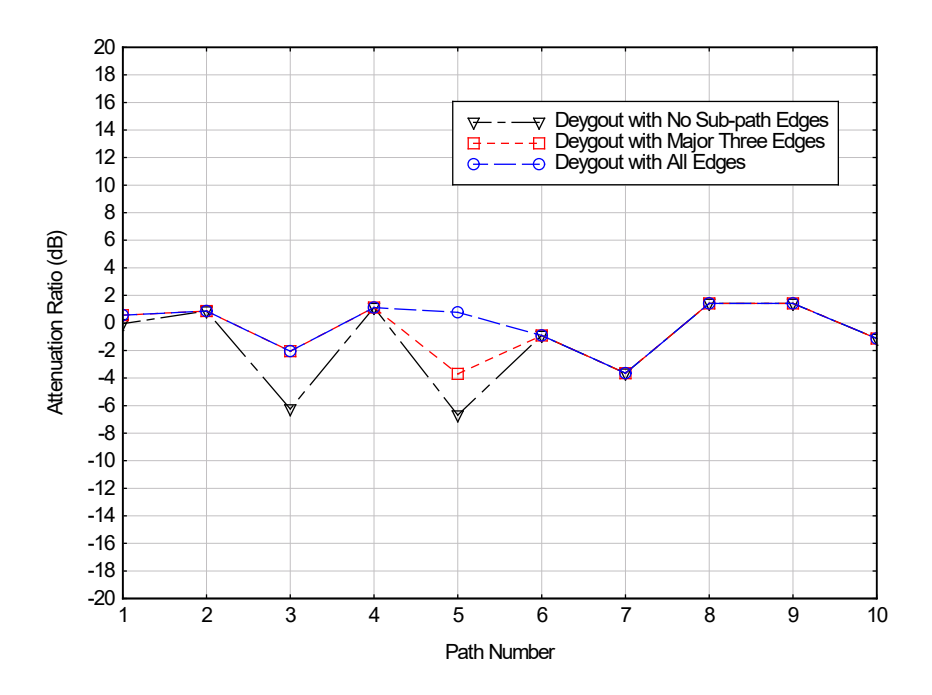


Figure 41: Deygout loss prediction compared to measured data for the 10 paths in Deygout's original paper. Attenuation ratio (dB) = Deygout method (dB) - measured data (dB).

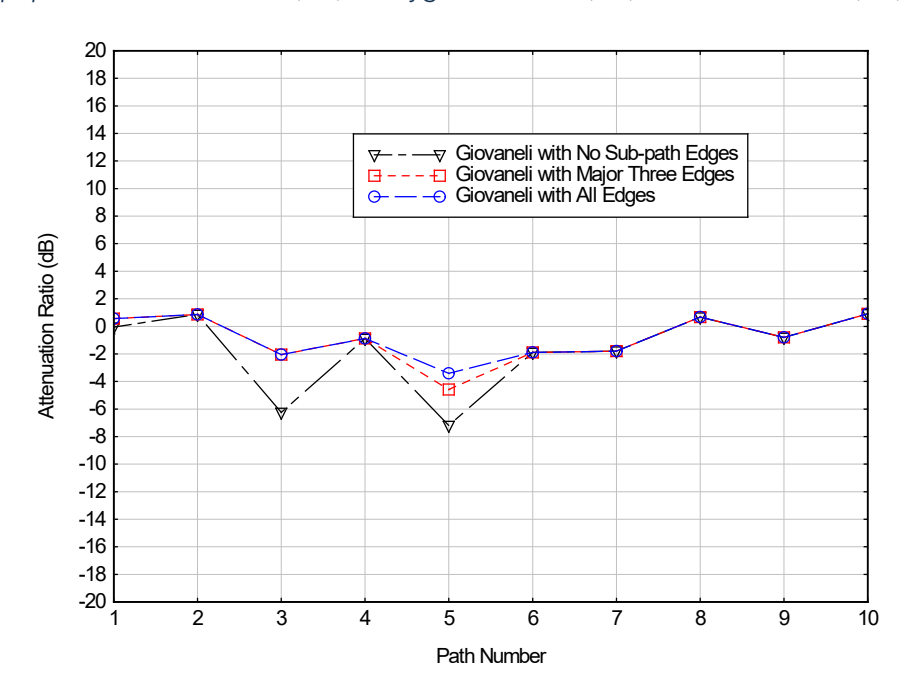


Figure 42: Giovaneli loss prediction compared to measured data for the 10 paths in Deygout's original paper. Attenuation ratio (dB) = Giovaneli method (dB) – measured data (dB).

6.2 Comparisons of Predictions to Measured Data for the 63rd Street Paths

Table 20 lists terrain heights and distances of each diffraction edge from the transmitter along the 63rd Street short path that were selected from the terrain data for the diffraction edges for the diffraction analysis. The transmitter and receiver antenna heights and the distance of the receiver from the transmitter at the end of the path are also given in Table 20. The transmitter location is zero reference for these distances. Diffraction edge distance locations used for the diffraction loss computations are at 60, 360, 690, 990, 1260, and 1290 meters from the transmitter, as shown in Table 20 below. The heights of the diffraction edges that were used for the diffraction loss computations are also marked at their peaks with a dot in Figure 43.

Table 20. Diffraction knife-edge height and diffraction-edge distance description of each diffraction edge for the short path on 63rd Street.

Terrain Height (m)	Short Path Terrain Distance from Transmitter (m)
H ₁ =1578	60
H ₂ =1575	360
H ₃ =1582	690
H ₄ =1572	990
H ₅ =1567	1260
H ₆ =1566	1290
XMTR Antenna Height =1579.2	XMTR Antenna Distance = 0
RCVR Antenna Height =1563.2	RCVR Antenna Distance =1380

Figure 43 is a profile plot of the terrain contour for the short path. The terrain data was available at 30-meter intervals along the path with a 1-meter resolution in elevation with respect to sea level.

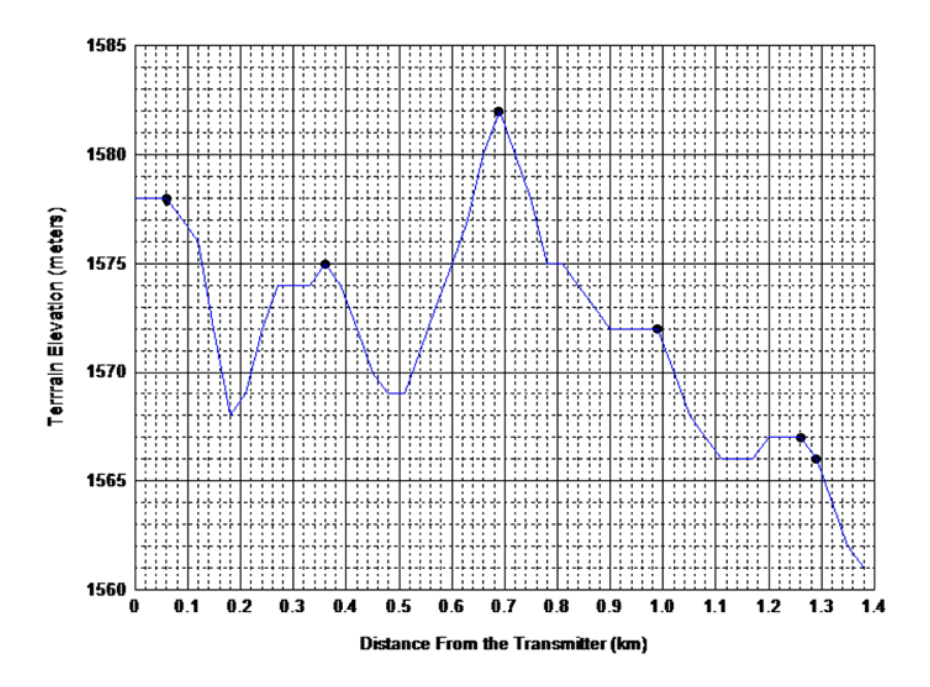


Figure 43: Terrain contour for the short (north) path along 63rd Street, 12 km northeast of city center, Boulder, CO.

Table 21 lists terrain heights and distances of each diffraction edge from the transmitter along the 63rd Street long path that were selected from the terrain data for the diffraction analysis. The transmitter and receiver antenna heights and the distance of the receiver from the transmitter at the end of the path are also given. The transmitter location is zero reference for these distances. Diffraction edge distance locations used for the diffraction loss computations are at 420, 2100, 4890, 5520, 6060, and 6930 meters from the transmitter and are listed in Table 21 below. The heights of the diffraction edges that were used for the diffraction loss computations are also marked at their peaks with a dot in Figure 44.

Table 21. Diffraction edge height and diffraction edge distance description of long path on 63rd Street.

Diffraction Edge Height (m)	Long Path Edge Distance from Transmitter (m)
$H_1 = 577$	420
$H_3 = 585$	2100
H ₅ = 583	4890
H ₆ = 583	5520
H ₇ =1582	6060
H ₈ =1582	6930
XMTR Antenna Height = 1579.2	XMTR Antenna Distance = 0
RCVR Antenna Height =1574.2	RCVR Antenna Distance = 7110

Figure 44 is a profile plot of the terrain contour for the long path. The terrain data were available at 30-meter intervals along the path with a 1-meter elevation resolution with respect to sea level. Figure 45 is a photo of part of the short path along 63rd Street that shows the transmitter van on location at the Ryssby Church.

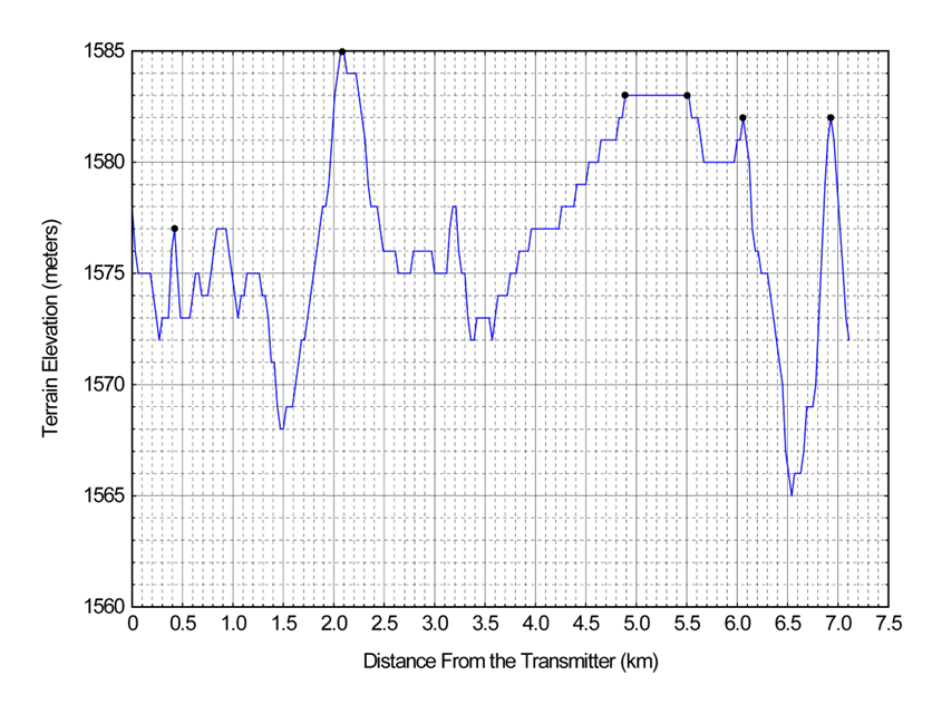


Figure 44: Terrain contour for the long (south) path along 63rd Street, 12 km northeast of city center, Boulder, CO.



Figure 45: Short propagation path and ITS transmitter van on 63rd Street.

The 63rd Street paths are considered rural environment: a two-lane road located at a constant longitude running directly north-south about 12 km north of the city center flanked by open fields and widely separated houses and farmland. Trees and some fences are sparse along this section of the road. There are overhead power lines along the entire length of the road. The transmitter was located at the Ryssby Church, and the receiver van was driven along paths in a north (short path) and south (long path) direction from the church. Data was recorded for both incoming and outgoing directions. There was minimal traffic along this road during the measurements.

The loss prediction of the alternative methods was first compared to the rigorous Vogler method. Figure 46 presents these results for both the short and long paths as a function of frequency at the maximum distances of 1.38 and 7.11 km for the short and long paths, respectively. The seven frequencies at which the loss comparisons to Vogler were made in Figure 46 were 183, 430, 915, 1350, 1602.5, 2260, and 5750 MHz. When the alternative methods were compared to the Vogler method, the maximum deviation was 3.7 dB. Figure 46 shows this agreement between the rigorous Vogler method and the alternative approximate methods.

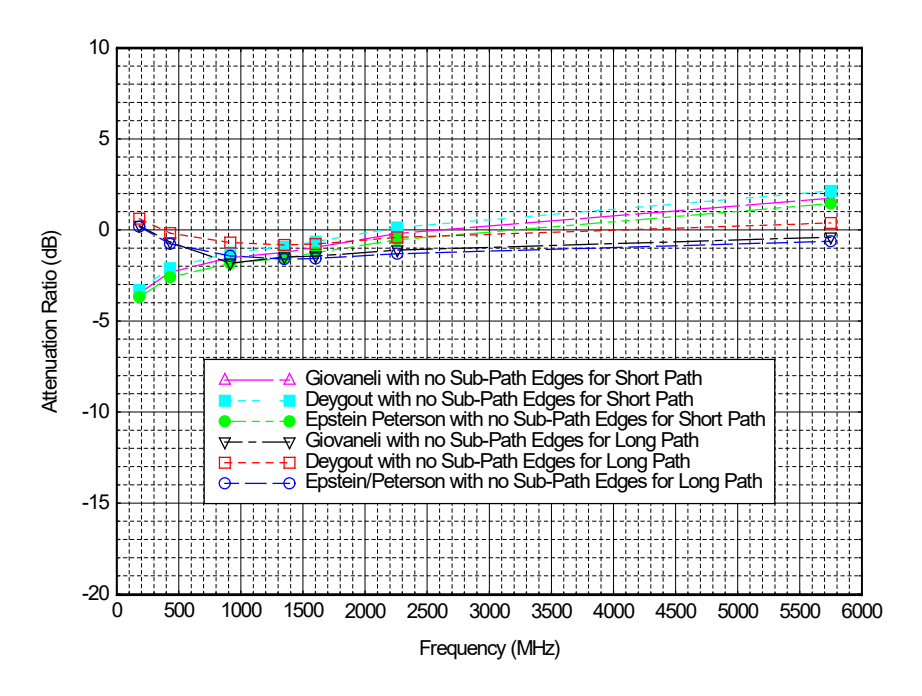


Figure 46. Loss prediction of alternative methods compared to Vogler loss prediction for short and long paths along 63rd Street. Attenuation ratio (dB) = alternative method (dB) – Vogler method (dB).

Figure 47 presents the results of comparisons of the three alternative methods to the measured data for the short path with the receiver located at 1.38 km from the transmitter. Figure 48 presents the results of comparisons of the three alternative methods to the measured data for the long path with the receiver located at 7.11 km from the transmitter. The measured data in Figures 47 and 48 was only available at five frequencies: 183, 430, 915, 1602.5, and 2260 MHz. The measured data is the average of the incoming and outgoing recorded data at the receiver location. Figures 47 and 48 demonstrate the agreement with measured data. The correction method for the Epstein-Peterson method described by Beyer [7] was not used here. The maximum deviation from measured data for the short path in Figure 47 is 4 dB, but most of the data for this path is within 2 dB. The maximum deviation from measured data for the long path in Figure 48 is 5 dB, but most of the data is within 3 dB.

The plots of Figures Figure 48 and Figure 49 are the results of a limited amount of measured data that can represent the capability of the alternative multiple-edge diffraction models to predict basic transmission loss and compare the prediction data to measured data. The measured data is from a limited number of distances and frequencies. An extensive comparison to measured data is beyond the scope of the study of this report. The computation and comparison of the Vogler model to measured data was also beyond the

scope of the current report. A future study could address a more comprehensive area for research using more extensive measured data.

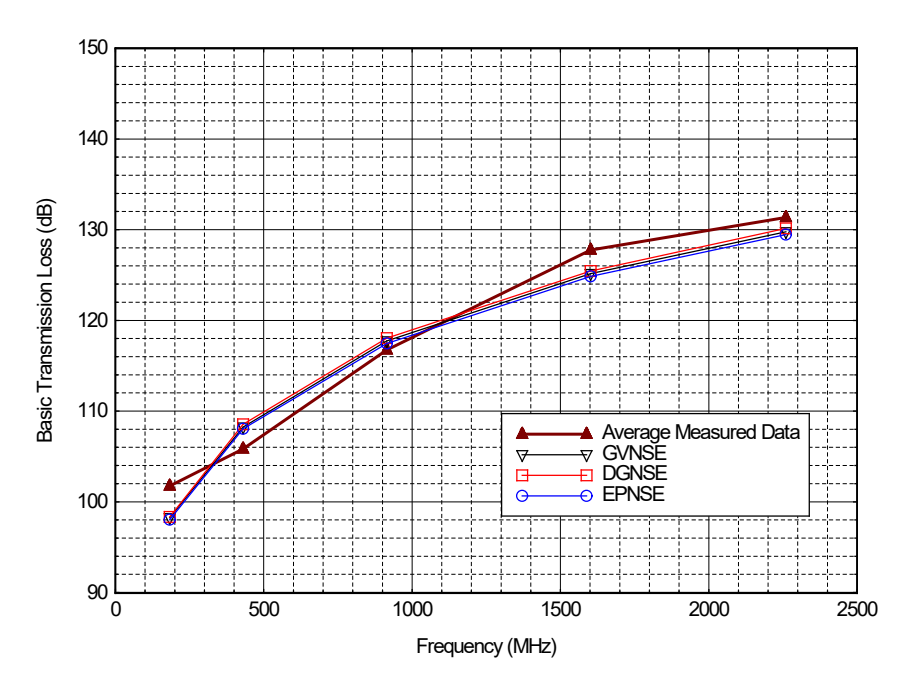


Figure 47. Prediction of basic transmission loss with Epstein-Peterson, Deygout, and Giovaneli loss prediction methods compared to measured data loss for the 63rd Street short path with receiver antenna at a distance of 1.38 km.

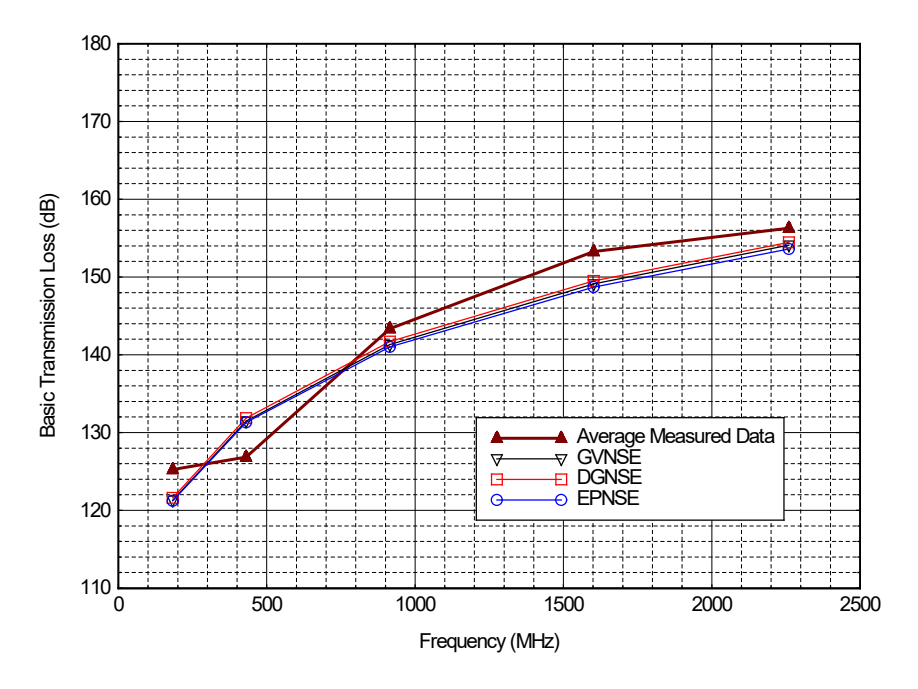


Figure 48: Prediction of basic transmission loss with Epstein-Peterson, Deygout, and Giovaneli loss prediction methods compared to measured data loss for the 63rd Street long path with receiver antenna at a distance of 7.11 km.

6.3 Comparisons of Predictions to Measured Data for the Table Mountain Field Site and Radio Quiet Zone

The third path is along Plateau Road, which runs through the center of the Table Mountain Field Site and Radio Quiet Zone and is itself located approximately 17 km north of the Department of Commerce Boulder Laboratories campus. Table Mountain is a rural environment and is a mesa elevated from the surrounding terrain. The diffraction path ran east-west along a straight section of Plateau Road.

Figure 49 shows a photograph of the path used in the measurements. Tables 22 and 23 contain the frequency, antenna heights, and antenna types for the Field Site diffraction path measurements for the first and second set of data taken along Plateau Road.



Figure 49: The Table Mountain Field Site Plateau Road diffraction path.

Table 22. Frequency, antenna type, and antenna height data for the Table Mountain Field Site Plateau Road diffraction path measurements for first set of data for Figure 51.

F (MHz)	(MHz) XMTR Antenna RCVR Antenna Height (m) Height (m)		XMTR Antenna Type	RCVR Antenna Type on Van
183	1.81	2.2	Discone	Monopole
430	1.81	2.2	Collinear	Monopole
915	0.62	2.2	Collinear	Monopole
1350	0.89	2.2	Collinear	Monopole
1602.5	0.64	2.7	Collinear	Discone
2260	0.79	2.7	Collinear	Discone
5750	0.70	2.7	Collinear	Discone

Table 23. Frequency, antenna type, and	antenna height data for the Table Mountain Field Site Plateau
Road diffraction path me	asurements for second set of data for Figure 52.

F(MHz)	F(MHz) XMTR Antenna RCVR Antenna Height (m) Height (m)		XMTR Antenna Type	RCVR Antenna Type on Van
183	1.0	2.2	Discone	Monopole
430	1.0	2.2	Monopole/GP	Monopole
915	1.0	2.2	Monopole/GP	Monopole
1350	1.71	2.2	Collinear	Monopole
1602.5	1.71	2.7	Collinear	Discone
2260	1.61	2.7	Collinear	Discone
5750	1.52	2.7	Collinear	Discone

A different set of antenna heights was used in the first (Table 22) and second (Table 23) sets of data. Figure 50 is a plot of the terrain contour for the Table Mountain Field Site Plateau Road path. Table 24 contains the terrain elevations and distance locations for this path. The elevations are with respect to sea level, and the distances are with respect to the transmitter. The transmitter is located at reference distance of 0 m, and the receiver measurements were taken at a distance of 400 meters from the transmitter. There are four major diffraction edges in Figure 48 at distances of approximately 60, 210, 240, and 270 meters from the transmitter indicated by dots at the edge peaks. These four edges were used in the diffraction loss computation. The diffraction computation has been limited to the most significant knife edges that contribute to the total diffraction loss. The sub-path knife edges that contribute a negligible amount to the total diffraction loss were not included.

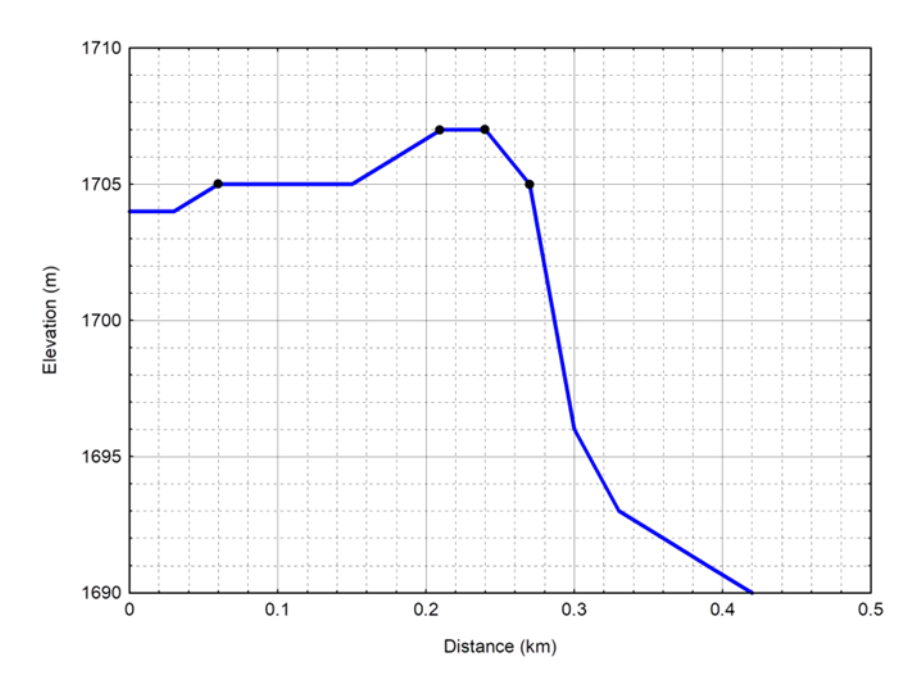


Figure 50. Terrain contour for the Table Mountain Field Site Plateau Road path.

	Table 24. T	errain data	for the Tab	ole Mountain	Field Site path.
--	-------------	-------------	-------------	--------------	------------------

Distance (m)	Elevation (m)
0.0 (Transmitter Antenna Location)	1704.0
30.0	1704.0
60.0	1705.0
90.0	1705.0
120.0	1705.0
150.0	1705.0
180.0	1706.0
210.0	1707.0
240.0	1707.0
270.0	1705.0
300.0	1696.0
330.0	1693.0
360.0	1692.0
390.0	1691.0
400.0 (Receiver Antenna Location)	1690.7

Figures 51 and 52 show the results of the two test conditions. They are the comparisons of predictions of basic transmission loss computed by the three alternative methods of Epstein-Peterson, Deygout, and Giovaneli to the measured data for the Table Mountain Field Site. Basic transmission loss includes the diffraction loss and the free space loss along the path.

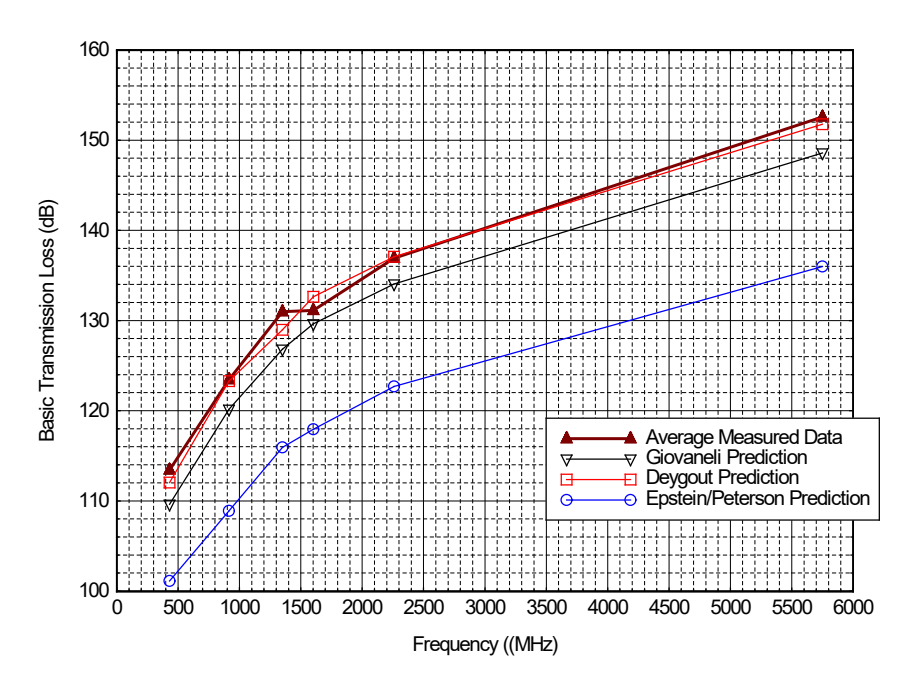


Figure 51: Comparisons of three prediction methods to data that was measured at the Table Mountain Field Site Plateau Road path at a distance 400 meters from the transmitter using Table 22 scenario data.

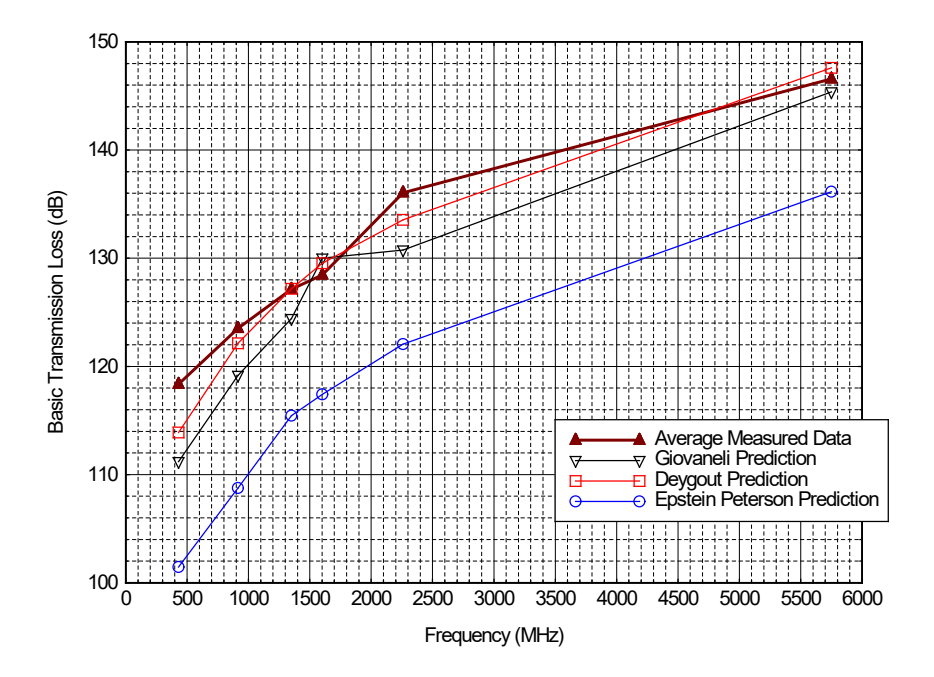


Figure 52: Comparisons of three prediction methods to data that was measured at the Table Mountain Field Site Plateau Road path at a distance of 400 meters from the transmitter using Table 23 scenario data.

The first and second sets of data show the diffraction effects of the different sets of antenna heights of the basic transmission loss computations of Figures 51 and 52. Notice that the propagation loss predicted with the Deygout and Giovaneli alternative methods agree with respect to measured data within ±2 dB, but the propagation loss predicted with the Epstein-Peterson alternative method does not and deviates as much as 14 dB with respect to measured data. In Figure 51 the agreement is within 4 dB at the low frequencies and most of the frequencies, but the agreement is within 2 to 3 dB at some frequencies for the Deygout and Giovaneli methods. In Figure 52 the agreement is within 6 dB at the lower frequencies, but at frequencies between 900 MHz and 1700 MHz the agreement is within 2 to 3 dB for the Deygout and Giovaneli methods. This is because the ray paths with the Epstein-Peterson alternative method align with the incident shadow boundaries. As discussed previously in this report, alignment of ray paths with the incident shadow boundaries can result in large prediction errors with some of the alternative methods, but not in the other alternative methods. This is due to the different procedures in establishing the ray paths for each of the alternative methods. The alternative methods of Deygout and Giovaneli do not have ray paths that align with the incident shadow boundaries for the above analysis.

7. Conclusions

This paper has described the results of a comparative analysis of four alternative multiple knife-edge diffraction methods and variations of these methods in place of a rigorous multiple knife-edge diffraction method to support radio wave propagation model development at ITS. The goal of this analysis was to investigate faster methods for computing knife-edge diffractions and a technique to select the best method. Section 3.3 describes this technique.

All of the alternative diffraction computation methods are approximations and are based on the Fresnel-Kirchhoff scalar theory of diffraction. The Kirchhoff boundary conditions are also approximate and only apply to scalars. This diffraction analysis is based on the classical approach of the Fresnel-Kirchhoff scalar theory of optics for a single knife edge. The assumption is made that the knife edge is a perfectly absorbing screen placed normal to the direction of propagation extending to infinity in both directions and vertically downwards. In a multiple knife-edge scenario, the losses for each edge will be combined using the alternative multiple knife-edge methods. There are a number of alternative methods for computing diffraction loss over multiple knife edges. Each method has its own unique procedure for computing diffraction loss.

The original motivation for this analysis effort was to determine which alternative diffraction computation method to use to compute diffraction loss over multiple knife edges based on criteria discussed in this report. The authors sought a selection technique to determine the optimum alternative diffraction computation method that is based on the relative geometric location of the incident shadow boundary and the ray path from one knife edge to the next.

Preliminary results of this analysis show where each of the alternative multiple knife-edge methods investigated can be used in place of the rigorous Vogler diffraction method to reduce computation time while maintaining suitable accuracy. It was shown that no one alternative method can cover all scenario variations. Which alternative diffraction method works best for a given scenario depends on how a method treats sub-path obstacles and the alignment of the ray path from one knife edge to the next knife edge with the incident shadow boundaries at the knife edges.

A method of selecting the best model in a particular situation was investigated and shows promise as a good indicator of which alternative method will predict the best estimate of diffraction loss. The procedure and order of computing knife-edge diffraction loss is different for each of the alternative methods investigated. As a result, for the same diffraction scenario, one method may avoid alignment of the ray path with the incident shadow boundary, while another may align the ray path with the incident shadow boundary. The method with the largest magnitude of the angular separation of the ray path and the incident shadow boundary that avoids this alignment will predict the diffraction loss with better accuracy.

The evaluation of the Fresnel transition function FTF(x) can be performed using (11), but it is easier to use Figure 6 with sufficient accuracy after using (12) to calculate x. A procedure for computing x, FTF(x), and the Fresnel transition function product FTFP(x) is listed below. The equations and figures referenced in the procedure below are in Section 3.3.

- Referring to Figure 4, compute the argument of FTF(x) using the parameters $\phi = \phi' + \pi$ and L as defined in (12), where ϕ is the incident shadow boundary and L is the distance from the diffraction knife edge to the observation point, which is the distance from the diffracting knife edge to the next knife edge.
- The angle, $\theta = \phi_{ray} \phi$ is the difference between the angle of the incident ray path for the next knife edge, ϕ_{ray} , and the angle of the incident shadow boundary ϕ .
- The wavelength λ is obtained from the operating frequency.
- Compute x from (12), compute $\log x$ from x, and then compute FTF(x) from Figure 6 using $\log x$.
- Repeat the four steps above for each diffraction edge.
- Compute the product of all diffraction edges, FTFP(x), by multiplying all the individual FTF(x) computations together.

The FTF(x) value of 1.0 indicates that for a single diffraction edge, the ray path to the next edge is far away from the incident shadow boundary and the computation of the diffraction loss will be better than an edge with an FTF(x) value of less than 1.0. It follows that the FTFP(x) for multiple edges with a value of 1.0 will be better than an alternative method that has an FTFP(x) less than 1.0 or less than the other alternative method.

The approach described above and in Section 3.3 can be used for selecting an alternative diffraction method that achieves better accuracy (minimum error). Accuracy is improved by using the method that has the largest angular deviation between the ray path from one knife edge to the next knife edge and the incident shadow boundary. The best indicator for finding what magnitude of angular separation would produce a minimal diffraction loss error was determined to be the *FTF* magnitude. The *FTFP* is the product of the magnitude of the individual *FTFs* for each of the edges. The *FTFP* magnitude for all edges is computed by multiplying together the magnitudes of the *FTFs* of all knife edges in the scenario for each alternative method. The alternative method with the maximum magnitude of the *FTFP* was the most suitable alternative prediction method with minimum diffraction loss error.

The Bullington method was found unsuitable due to inaccurate results of the diffraction computation even with only two knife edges. Tables Table 17 and 18 show more than 6 dB difference between the Vogler method and the Bullington method. In many cases the difference is decades of dB.

Comparisons in Tables 17 and 18 of Section 5.2 show the agreement between the Vogler results and both the Epstein-Peterson, Deygout, and Giovaneli results for a variety of cases. Some differences depend on whether the sub-path knife edges (obstacles) are included in the diffraction loss computation for the different methods.

It was found by comparative computations that removing the sub-path obstacles improves the agreement between the Deygout method and the Vogler method. The Epstein-Peterson method's agreement with the Vogler method also improves when the sub-path knife edges are removed. This is in agreement with a comment made by Deygout in his paper [5], about limiting the number of edges to 3 or 4 edges for a diffraction loss computation.

However, the Epstein-Peterson method with all knife edges included and corrected by the Beyer method [7] improves agreement with the Vogler method. This is because the Beyer method is designed to improve the loss prediction agreement when increasing the number of knife edges by including the sub-path knife edges.

The Vogler method is valid for many knife edges up to 10. By including the diffraction loss effects of the sub-path knife edges, improved agreement with the Vogler method is achieved, since both methods include all knife edges. This is valid for both the Epstein-Peterson and Vogler methods, since the knife edges for the Epstein-Peterson method are corrected with the Beyer method [7]. The Giovaneli method with no sub-path knife edges agrees with the Vogler method, as shown in Section 5.1.

Comparisons of the measured data were also performed with four separate sets of available data. One was measured data from the classic paper by Deygout [5]; the other three were from measurements performed by ITS. Two of these datasets were taken along medium length paths and the third along a much shorter diffraction path. Comparisons of measured data show the agreement with the Epstein-Peterson, Deygout, and Giovaneli methods in addition to the Vogler method, in Section 6. The clutter environment along the paths can cause some large deviations, since both the rigorous Vogler method and the alternative methods do not consider the reflections and multipath from trees, houses, power lines, and fences, etc. along the paths. The alternative multiple knife-edge diffraction methods are approximations, but, as shown in this report, they can provide the predictions of diffraction loss when care is exercised to avoid the alignment of the incident shadow boundaries with the ray paths between knife edges.

As stated above, the plots of Figures Figure 48 and Figure 49 are the results of a limited amount of measured data that can represent the capability of the alternative multiple-edge diffraction models to predict basic transmission loss and compare the prediction data to measured data. The measured data is from a limited number of distances and frequencies. An extensive comparison to measured data is beyond the scope of the study of this report. The computation and comparison of the Vogler model to measured data is also beyond the scope of the current report. A future study could address a more comprehensive area for research using more extensive measured data.

8. References

- [1] L. E. Vogler, "Further Investigations of the Multiple Knife-edge Diffraction," NTIA Technical Report 83-124, U.S. Department of Commerce, National Telecommunications and Information Administration, Institute for Telecommunication Sciences, May 1983. https://doi.org/10.70220/lk581prz.
- [2] L. E. Vogler, "The Attenuation of Electromagnetic Waves by Multiple Knife-edge Diffraction," NTIA Technical Report 81-86, U.S. Department of Commerce, National Telecommunications and Information Administration, Institute for Telecommunication Sciences, October 1981. https://doi.org/10.70220/k0xs4zfv.
- [3] K. Bullington, "Radio Propagation at Frequencies Above 30 Megacycles," *Proc. of the IRE*, vol. 35, no. 10, pp. 1122-1136, October 1947. https://doi.org/10.1109/JRPROC.1947.232600
- [4] J. Epstein and D. W. Peterson, "An Experimental Study of Wave Propagation at 850 MC," *Proc. of the IRE*, vol. 41, no. 5, pp. 595-611, May 1953. https://doi.org/10.1109/JRPROC.1953.274401
- J. Deygout, "Multiple Knife-Edge Diffraction of Microwaves," *IEEE Trans. Ant. Prop.*, vol. 14, no. 4, pp. 480-489, July 1966. https://doi.org/10.1109/TAP.1966.1138719
- [6] C. L. Giovaneli, "An Analysis of Simplified Solutions for Multiple Knife-edge Diffraction," *IEEE Trans. Ant. Prop.*, vol. 32, no. 3, pp. 297-301, March 1984. https://doi.org/10.1109/TAP.1984.1143299
- [7] J. Beyer, "A GTD-Based Correction of the Epstein-Peterson Method," *IEEE Trans. Ant. Prop.*, vol. 52, no. 3, pp. 888-891, March 2004. https://doi.org/10.1109/TAP.2004.825485
- [8] International Telecommunication Union-Radiocommunication Sector (ITU-R), Recommendation ITU-R P.526-15 (Oct. 2019), *Propagation by diffraction*, I TU, Geneva, Switzerland. https://www.itu.int/rec/r-rec-p.526/en
- [9] W. Gautschi, "Evaluation of the Repeated Integrals of the Coerror Function," ACM Trans. Math. Software vol. 3, no. 3, pp. 240-252, September 1977. https://doi.org/10.1145/355744.355748
- [10] K. Furutsu, "On the Theory of Radio-Wave Propagation Over Inhomogeneous Earth," J. Res. Natl. Bur. Stand., Sect. D., vol. 67D, pp. 39-62, January-February 1963. https://nvlpubs.nist.gov/nistpubs/jres/67D/jresv67Dn1p39_A1b.pdf
- [11] L. E. Vogler, "An Attenuation Function for Multiple Knife-edge Diffraction," *Radio Science*, vol. 18, no. 6, pp. 1541–1546, November-December 1982. https://doi.org/10.1029/RS017i006p01541

- [12] J. H. Whitteker, "Fresnel-Kirchhoff Theory Applied to Terrain Diffraction Problems," *Radio Science*, vol. 25, no. 5, pp. 837-851, September-October 1990. https://doi.org/10.1029/RS025i005p00837
- [13] M. Abramowitz and I. A. Stegun, eds., *Handbook of Mathematical Functions with Formulas, Graphs, and Mathematical Tables*, NBS Handbook, Applied Mathematics Series No. 55, U.S. Department of Commerce, National Bureau of Standards, Washington, D.C.: U.S. Government Printing Office, June 1964.
- [14] S. R. Saunders and A. A. Aragón-Zavala, *Antennas and Propagation for Wireless Communication Systems*, 2nd ed., Wiley, 2007.
- [15] L. Barclay, ed., *Propagation of Radiowaves*, *2nd Edition*, London, United Kingdom: The Institution of Engineering and Technology, April 2003.
- [16] R. J. Pogorzelski, "A Note on Some Common Diffraction Link Loss Models," *Radio Science*, vol. 17, no. 6, pp. 1536-1540, November-December 1982. https://doi.org/10.1029/RS017i006p01536
- [17] L. Boithias, Radio Wave Propagation, trans. David Beeson, McGraw Hill, 1987.
- [18] L. B. Felsen and N. Marcuvitz, Radiation and Scattering of Waves, Prentice Hall, 1973.
- [19] Y. Rahmat-Samii and R. Mittra, "Spectral Analysis of High-Frequency Diffraction of an Arbitrary Incident Field by a Half Plane–Comparison with Four Asymptotic Techniques," *Radio Science*, vol. 13, no. 1, pp. 31-48, January-February 1978. https://doi.org/10.1029/RS013i001p00031
- [20] R. G. Kouyoumjian and P. H. Pathak, "A Uniform Geometrical Theory of Diffraction for an Edge in a Perfectly Conducting Surface," *Proc. IEEE*, vol. 62, no. 11, pp. 1448–1461, November 1974. https://doi.org/10.1109/PROC.1974.9651
- [21] D. A. McNamara, C. W. I. Pistorius, and J. A. G. Malherbe, *Introduction to the Uniform Geometrical Theory of Diffraction*, Artech House, 1990.
- [22] J. D. Parsons, The Mobile Radio Propagation Channel, Pentech Press, 1992.
- [23] G. Millington, R. Hewitt, and F.S. Immirzi, "Double Knife-edge Diffraction in Field Strength Predictions," *Proc. of IEE, Part C: Monographs*, vol. 109, no. 16, pp. 419-429, September 1962. https://doi.org/10.1049/pi-c.1962.0059

Appendix A. The Bullington Mathematical Algorithm

The mathematical algorithm for the Bullington method begins with finding the knife edge with the maximum elevation angle from the transmitter antenna and another knife edge with the maximum elevation angle from the receiver antenna. These are the horizons from each antenna. This is equivalent to calculating the tangents of the angles for all n knife edges with respect to the transmitter antenna θ_{Ti} and the receiver antenna θ_{Ri} using:

$$\tan \theta_{Ti} = \frac{h_i}{\sum_{k=1}^{i} d_k} \tag{A-1}$$

$$\tan \theta_{Ri} = \frac{h_i}{\sum_{k=1}^{n+1} d_k - \sum_{k=1}^{i} d_k}$$
 (A-2)

The equation for a line from the transmitter antenna to the i^{th} knife edge of height h_i representing the horizon with respect to the transmitter antenna is:

$$y_T = \frac{h_i d}{\sum_{k=1}^i d_k} \tag{A-3}$$

where the distances d_k are defined in Figures 16 through 25, and d is the distance along the path. The equation for a line from the receiver antenna to the j^{th} knife edge of height h_i , representing the horizon with respect to the receiver antenna for n total knife edges is:

$$y_R = \frac{-h_j d}{\sum_{k=1}^{n+1} d_k - \sum_{k=1}^{j} d_k} + \frac{h_j \sum_{k=1}^{n+1} d_k}{\sum_{k=1}^{n+1} d_k - \sum_{k=1}^{j} d_k}$$
(A-4)

The effective height h' of the equivalent knife edge and the distance d_T from the transmitter are obtained by solving the above two equations for $d=d_T$ simultaneously where $y_T=y_R$ after entering all the numerical values for the knife edge heights and computing the summations in each of the equations. The distance d_R from the receiver is:

$$d_R = \left(\sum_{k=1}^{n+1} d_k\right) - d_T \tag{A-5}$$

The effective height is:

$$h' = y_T(d_T) = \frac{h_i d_T}{\sum_{k=1}^i d_k}$$
 (A-6)

The Fresnel-Kirchhoff diffraction parameter is then calculated as [8]:

$$\nu = h' \sqrt{\frac{2}{\lambda} \left(\frac{1}{d_T} + \frac{1}{d_R}\right)} \tag{A-7}$$

where $\lambda = \frac{c}{f}$ is the wavelength in meters, f is the frequency in Hertz, and c is the speed of light in meters per second. This diffraction coefficient is then used to calculate the diffraction loss using the equation for $J(\nu)$ [8]. For $\nu > -0.78$, the diffraction loss in dB is computed from [8]:

$$J(\nu) = 6.9 + 20\log\left(\sqrt{(\nu - 0.1)^2 + 1.0} + \nu - 0.1\right)$$
 (A-8)

Appendix B. The Epstein-Peterson Mathematical Algorithm

The mathematical algorithm for the Epstein-Peterson method begins with assuming that each knife edge is illuminated by the transmitter antenna or the diffracted energy from the top of the preceding knife edge. The attenuation due to diffraction is computed sequentially for each knife edge in dB, and the attenuations for all knife edges are summed together in dB. The diffraction loss computation for n knife edges using the Epstein-Peterson algorithm requires the determination of the effective height of each knife edge, and the distances d_T and d_R of each knife edge from the transmitter and receiver antenna, respectively. The effective height h_i' of the i^{th} knife edge with height h_i is given by:

$$h'_{i} = h_{i} - \frac{(h_{i+1} - h_{i-1})}{d_{i} + d_{i+1}} d_{i} - h_{i-1}$$
(B-1)

The distances d_T and d_R are: $d_T = d_i$ and $d_R = d_{i+1}$. This equation is used for sub-path knife edges and non-sub-path knife edges. The Fresnel-Kirchhoff diffraction parameter for the i^{th} knife edge is computed from [8]:

$$\nu_i = h_i' \sqrt{\frac{2}{\lambda} \left(\frac{1}{d_T} + \frac{1}{d_R}\right)}$$
 (B-2)

The diffraction loss for each knife edge is computed using (B-3) for J(v) [8]. The total diffraction loss is the sum of the individual diffraction losses for each knife edge.

$$J(\nu) = 6.9 + 20\log\left(\sqrt{(\nu - 0.1)^2 + 1.0} + \nu - 0.1\right)$$
 (B-3)

Appendix C. The Deygout Mathematical Method

C.1 Equations for the Primary Knife Edge

The diffraction loss computation algorithm for n knife edges using the Deygout method begins with computing the Fresnel-Kirchhoff diffraction parameter v_i using (C-1) for all knife edges as if the other knife edges were absent to determine the primary knife edge [8]. The primary knife edge has the highest value for v_i .

$$\nu_i = h_i' \sqrt{\frac{2}{\lambda} \left(\frac{1}{d_R} + \frac{1}{d_T}\right)} \tag{C-1}$$

The distances to the i^{th} knife edge for n knife edges are computed using the following equations:

$$d_T = \sum_{k=1}^{i} d_k \tag{C-2}$$

$$d_R = \sum_{k=i+1}^{n+1} d_k (C-3)$$

Note that equations (C-2) and (C-3) are equivalent to equations (1) and (2) with different symbols on the left-hand sides, respectively. For the i^{th} knife edge, h_i' is the effective height of the i^{th} knife edge with respect to the transmitter antenna to the receiver antenna baseline. These effective heights of the diffraction knife edges are used for the determination of the primary knife edge and are given by (C-4). The height h_i is the original height before normalization with respect to a baseline drawn between the transmitter antenna and the receiver antenna located at heights h_t and h_r , respectively.

$$h_i' = h_i - \left(h_t + \frac{(h_r - h_t)\sum_{k=1}^i d_k}{\sum_{k=1}^{n+1} d_k}\right)$$
 (C-4)

If the m^{th} knife edge has the largest v_i , then it is the primary knife edge and the diffraction loss J(v) of the m^{th} knife edge is computed using $h=h_m'$ for $v_i>-0.78$ with (C-1) through (C-5) [8].

$$J(\nu) = 6.9 + 20\log\left(\sqrt{(\nu - 0.1)^2 + 1.0} + \nu - 0.1\right)$$
 (C-5)

Only the loss for the m^{th} knife-edge (primary knife edge) can be computed using the above value of v_m . The losses for the remaining knife edges are computed using different values of v_i obtained from other procedures of computing effective heights with different and specific reference baselines for determination of the diffraction parameter v_i for the knife edges of secondary, third, fourth, and fifth levels. After the primary knife edge has been selected, new

baselines must be established for computing effective knife-edge heights and losses of the remaining knife edges. The effective heights h_i' computed above for the determination of the primary knife edge for nonzero receiver and transmitter antenna heights, will be used as the initial reference heights for the individual computation of the new effective heights h_i' with respect to the new baselines for the second-, third-, fourth-, and fifth-level knife edges. The diffraction losses for the primary knife edge and second-, third-, fourth-, and fifth-level knife edges are added together to obtain the total diffraction loss.

C.2 Determination of Effective Knife-Edge Heights and Distances for Secondary Knife Edges on Either Side of the Primary m^{th} Knife Edge

The m^{th} knife edge divides the transmitter to receiver distance region into two sub-path regions given by the distances d_T and d_R computed above for the primary knife edge. The transmitter source for the sub-path region to the left of the primary knife edge is located at the original transmitter antenna source, but the receiver antenna is located at the top of the primary knife edge. The transmitter antenna source for the sub-path region to the right of the primary knife edge is located at the top of the primary knife edge, and the receiver antenna is at the location of the original receiver antenna.

The new baselines are formed for computing effective heights h_i' for the secondary knife edges by drawing a line from the transmitter antenna to the primary knife edge, and from the primary knife edge to the receiver antenna. If the total number of knife edges is n and the primary knife edge height is h_m' , with index m, then the equation for the new baseline for knife edges located to the left of the primary knife edge is:

$$y_T = \frac{h_m' \sum_{k=1}^{i} d_i}{\sum_{k=1}^{m} d_k}$$
 (C-6)

The effective heights h'_i with respect to the new baseline of the i^{th} secondary knife edge h_i for knife edges to the left of the m^{th} primary knife edge are:

$$h'_{i} = h_{i} - \frac{h_{m} \sum_{k=1}^{i} d_{k}}{\sum_{k=1}^{m} d_{k}}$$
 (C-7)

where h_i is the reference height of the i^{th} knife edge with respect to the baseline between the transmitter and receiver antennas computed previously for the primary knife edge. The distances d_T and d_R for the i^{th} knife edge on the left side of the m^{th} knife edge are:

$$d_T = \sum_{k=1}^{i} d_k \tag{C-8}$$

$$d_R = \sum_{k=i+1}^m d_k \tag{C-9}$$

The equation for the new baseline for the secondary knife edges located to the right of the primary knife edge is:

$$y_R = \frac{-h_m}{\sum_{k=m+1}^{n+1} d_k} \left(\sum_{k=m+1}^{i} d_k \right) + h_m$$
 (C-10)

The effective heights, h'_i , with respect to the new baseline of the i^{th} secondary knife edge h_i for knife edges to the right of the m^{th} primary knife edge are:

$$h'_{i} = h_{i} + \frac{h'_{m} \sum_{k=m+1}^{i} d_{k}}{\sum_{k=m+1}^{n+1} d_{k}} - h_{m}$$
 (C-11)

where h'_i is the reference height of the i^{th} knife edge with respect to the line between the transmitter and receiver antennas. The distances d_T and d_R for the i^{th} knife edge on the right side of the m^{th} knife edge are:

$$d_T = \sum_{k=m+1}^{i} d_k \tag{C-12}$$

$$d_R = \sum_{k=i+1}^{n+1} d_k (C-13)$$

When there is more than one knife edge in the sub-path regions on each side of the primary knife edge, each knife edge must be evaluated to determine the secondary knife edge for each region. The values of v_i for all knife edges on each side of the primary (m^{th}) knife edge are computed using the appropriate values of h_i' , d_T and d_R to determine the knife edge with the largest value of v_i on each side of the primary m^{th} knife edge. These are the secondary knife edges.

These values of v_i can be used to compute the losses for only the two secondary knife edges that have the maximum value of v_i for that region on each side of the primary knife edge. These secondary knife edges subdivide the first two regions into two subregions, one on each side of the primary knife edge, for a total of four regions. To determine the losses for the third-level knife edges occurring in these regions, it is necessary to establish additional baselines that are lines from the previous primary knife edge, secondary knife edge, or transmitter to the next primary knife edge, secondary knife edge, or receiver antenna in their respective regions.

C.3 Equations for the Effective Height and Distances of the Third-Level i^{th} Knife Edges on the Left Side of the Primary Knife Edge h_m

For the left side of the secondary knife edge h_q :

$$h'_{i} = h_{i} - \frac{h_{q} \sum_{k=1}^{i} d_{k}}{\sum_{k=1}^{q} d_{k}}$$
 (C-14)

$$d_T = \sum_{k=1}^{i} d_k \tag{C-15}$$

$$d_R = \sum_{k=i+1}^q d_k \tag{C-16}$$

For the right side of the secondary knife edge h_q :

$$h'_{i} = h_{m} - \frac{(h_{m} - h_{q}) \sum_{k=q+1}^{i} d_{k}}{\sum_{k=q+1}^{m} d_{k}} - h_{q}$$
 (C-17)

$$d_T = \sum_{k=q+1}^i d_k \tag{C-18}$$

$$d_R = \sum_{k=i+1}^m d_k \tag{C-19}$$

All the values of v_i for the knife edges on the left side of the primary knife edge and each side of the secondary knife edge are then computed to determine the third-level knife edge for each side of the secondary knife edge. The largest values of v_i in these separate regions are then used to calculate the diffraction loss only for the third-level knife edges to the left side of the primary knife edge on each side of the secondary knife edge.

C.4 Equations for the Effective Height and Distances of the Third-Level i^{th} Knife Edges on the Right Side of the Primary Knife Edge h_m

For the left side of the secondary knife edge h_d :

$$h'_{i} = h_{i} + \frac{(h_{m} - h_{d}) \sum_{k=m+1}^{i} d_{k}}{\sum_{k=m+1}^{d} d_{k}} - h_{m}$$
 (C-20)

$$d_T = \sum_{k=m+1}^{i} d_k \tag{C-21}$$

$$d_R = \sum_{k=i+1}^d d_k \tag{C-22}$$

For the right side of the secondary knife edge h_d :

$$h'_{i} = h_{i} + \frac{h_{d} \sum_{k=d+1}^{i} d_{k}}{\sum_{k=d+1}^{n+1} d_{k}} - h_{d}$$
 (C-23)

$$d_T = \sum_{k=d+1}^{l} d_k \tag{C-24}$$

$$d_R = \sum_{k=i+1}^{n+1} d_k \tag{C-25}$$

All the values of v_i for the knife edges on the right side of the primary knife edge and each side of the secondary knife edge are then computed to determine the third-level knife edge on each side of the secondary knife edge. The largest values of v_i for the right side of the primary knife edge and each side of the secondary knife edge determine the third-level knife edge on each side of the secondary knife edge. The largest values of v_i are then used to calculate the diffraction loss only for the third-level knife edges to the right side of the primary knife edge on each side of the secondary knife edge.

The methods described previously for the primary, secondary, and third-level knife edges are then applied to the sub-path regions formed by the remaining knife edges to determine the effective heights, distances, Fresnel-Kirchhoff diffraction parameters, and diffraction loss for the fourth- and fifth-level knife edges.

C.5 Determination of Effective Knife-Edge Heights for Higher Order Knife Edges on Either Side of the Primary Knife Edge

After the third- and fourth-level knife edges have been determined and their losses computed, the remaining knife edges, if any, are fifth-level knife edges. For the fifth-level i^{th} knife edge, which is the highest level possible for n=6, the computation reduces to:

$$h_i' = h_i - \left[\frac{(h_{i+1} - h_{i-1})d_i}{\sum_{k=1}^{i+1} d_k - \sum_{k=1}^{i-1} d_k} + h_{i-1} \right]$$
 (C-26)

The distances for the fifth-level i^{th} knife edge are:

$$d_T = d_i \tag{C-27}$$

$$d_R = d_{i+1} \tag{C-28}$$

The losses are computed for the higher order knife edges using the distances and effective heights from the above equations in (C-1) for the diffraction parameter v_i , and then using this value of v_i in (C-5) for the loss J(v) [8]. When single or multiple consecutive knife edges with negative effective heights occur, then the computation of v_i and the diffraction loss for these knife edges are the last knife edge computations, and they are performed using the same equations as for the fifth-level knife edge, (C-26) through (C-28). The diffraction losses for all knife edges are added together for the total diffraction loss.

Appendix D. The Giovaneli Mathematical Algorithm

For this algorithm, as for the Deygout algorithm, the primary knife edge must be determined first. The primary knife edge for the Giovaneli algorithm is that with the maximum height. If there are two knife edges with equal maximum heights, then compute the Fresnel-Kirchhoff diffraction parameter v_i for each knife edge. The primary knife edge will be the knife edge with the largest value of v_i . It is possible for the primary knife edge to be the knife edge closest to the transmitter antenna, the knife edge closest to the receiver antenna, or a knife edge in between the transmitter and receiver antenna locations. When the primary knife edge is the knife edge closest to the transmitter antenna or receiver antenna, then the remaining knife edges are all on either the receiver antenna side or the transmitter side, respectively, of the primary knife edge. The total diffraction loss is the sum of the losses computed for all of the knife edges. The diffraction losses for the primary and remaining knife edges are computed using the procedure described in the next sections.

The Giovaneli method is an attempt to obtain more representative diffraction angles, so that the loss predictions will be less pessimistic than those produced by the Deygout method. The diffraction angles suggested by Giovaneli in his method are those that would be incurred by ray paths incident on the subject knife edge from the previous knife edge and by ray paths received at the next knife edge from the subject knife edge.

D.1 Effective Height and Distances for the Primary Knife Edge for the Giovaneli Algorithm

Using the primary knife edge h_m as the reference for the slope determination, calculate the absolute value of the slopes of lines drawn from the main knife edge to each of the secondary knife edges. The knife edge with the minimum slope on each side of the main knife edge is the secondary knife edge for that side of the primary knife edge and will be used to determine the effective height of the primary knife edge. These secondary knife edges are not sub-path knife edges. Procedures for sub-path knife edges are described in Section D.3. The distance of the i^{th} knife edge from the transmitter antenna is given by (D-1).

$$d_i = \sum_{k=1}^i d_k \tag{D-1}$$

The distance of the m^{th} knife edge from the transmitter antenna is calculated using (D-2).

$$d_m = \sum_{k=1}^m d_k \tag{D-2}$$

The receiver location from the transmitter for n total knife edges is calculated using (D-3).

$$d = \sum_{k=1}^{n+1} d_k$$
 (D-3)

The secondary knife edge on the left side of the primary knife edge is the reference source knife edge for the energy incident on the primary knife edge and the secondary knife edge on the right side of the primary knife edge is the receptor knife edge for energy diffracted over the primary knife edge. Computing the effective height of the primary knife edge requires the use of three equations of straight lines. This procedure begins when one vertical line is drawn at the transmitter antenna location d=0 and the other vertical line is drawn at the receiver antenna location. The first of these lines passes through the primary knife-edge peak and the secondary knife-edge peak on the left side of the primary knife edge continuing through that peak to intersect the vertical line at d=0. If L is the index of the secondary knife edge of height h_L on the left (transmitter) side of the main knife edge (index m) of height h_m , the equation for the line with minimum slope that connects the secondary knife edge to the primary knife edge and intersects the vertical line at the transmitter is given by (D-4).

$$y_{L} = \frac{(h_{m} - h_{L})d}{\sum_{k=L+1}^{m} d_{k}} + b_{L}$$
 (D-4)

At $d = \sum_{k=1}^{m} d_k$, $y_L = h_m$, the equation can be solved for b_L . If the primary knife edge is adjacent to the transmitter antenna at d = 0, then the index of the secondary knife edge is L = 0, and the heights are given by: $h_L = h_T$, and $h_L = h_T$.

The second line passes through the primary knife edge and secondary knife edge on the right side of the primary knife edge and the vertical line at the receiver location. If *P* is the index of the secondary knife edge on the right (receiver) side of the primary knife edge, the equation for the line with minimum slope that connects the secondary knife-edge peak to the primary knife-edge peak and intersects the vertical line at the receiver is given by (D-5).

$$y_P = \frac{-(h_m - h_P)(d - \sum_{k=1}^m d_k)}{\sum_{k=m+1}^p d_k} + h_m$$
 (D-5)

If the primary knife edge h_m is adjacent to the receiver, then $h_P = h_r$ (the receiver antenna height), and P = n + 1.

The lines of the equations for y_L and y_P are extended to intersect the vertical lines at d=0 and the receiver location distance. A third line is the baseline, which is drawn between the intersection points of the two lines given by y_L and y_P with the vertical lines at d=0 and the receiver location distance, respectively. The equation for this baseline is (D-6).

$$y_B = \frac{\left[y_P \left(d = \sum_{k=1}^{n+1} d_k - y_L(d=0)\right)\right] d}{\sum_{k=1}^{n+1} d_k} + b_B$$
 (D-6)

At d = 0, $(b_B = y_B = y_L = b_L)$.

The effective height for the primary knife edge is $h'_m = h_m - y_B(d = \sum_{k=1}^m d_k)$.

The distances for the computation of the diffraction parameter v_m for the primary knife edge are computed using (D-7) and (D-8).

$$d_T = \sum_{k=1}^m d_k \tag{D-7}$$

$$d_R = \sum_{k=m+1}^{n+1} d_k {(D-8)}$$

The diffraction loss for the primary knife edge is computed using this value of v_m (D-9) and (D-10) for J(v) [8].

$$\nu_m = h'_m \sqrt{\frac{2}{\lambda} \left(\frac{1}{d_T} + \frac{1}{d_R}\right)}$$
 (D-9)

$$J(\nu) = 6.9 + 20\log\left(\sqrt{(\nu - 0.1)^2 + 1.0} + \nu - 0.1\right)$$
 (D-10)

D.2 Effective Heights and Distances of the Secondary and Higher Order Knife Edges for the Giovaneli Algorithm

To determine the effective heights of the secondary knife edges, the secondary knife edges are used as the main knife edges and their effective heights calculated similarly to the primary knife edge. The computation procedures of the effective heights of the secondary and higher order knife edges depend on whether the knife edge is on the left (transmitter) or right (receiver) side of the primary knife edge. The computation procedure of effective heights and distances for third-level and higher-level knife edges is performed by extending the procedure for secondary knife edges.

For the right side (receiver side) of the primary knife edge, the effective knife-edge height of the i^{th} knife edge that is a not a sub-path knife edge is computed by determining the next q^{th} knife-edge peak (located to the right side of the i^{th} knife edge) that will serve as the receptor knife edge for the i^{th} knife edge. The primary (m^{th}) knife edge is the reference source knife edge for the i^{th} secondary knife edge. The receptor knife edge will be the q^{th} knife edge to the right of the secondary i^{th} knife-edge peak that is not a sub-path knife edge that has a minimum absolute value of slope of a line drawn from the primary m^{th} knife edge to the next q^{th} knife-edge peak. If the q^{th} knife edge does not exist, because the i^{th} knife edge is adjacent to the receiver antenna, then use the receiver antenna height h_r . If the next location is the receiver antenna, then q = n + 1, $h_q = h_r$. The equation of the line used for the baseline to calculate the effective height of the i^{th} knife edge is determined by finding the equation of the line that connects the previous knife edge m^{th} knife-edge peak of knife edge m^{th}

$$y_{PR} = \frac{-(h_m - h_q)(d - \sum_{k=1}^m d_k)}{\sum_{k=m+1}^{n+1} d_k} + h_m$$
 (D-11)

The effective height h'_i of the i^{th} knife edge is evaluated using y_{PR} at the i^{th} knife edge (D-12). The distances are calculated using (D-13) and (D-14).

$$h'_{i} = h_{i} - y_{PR} \left(d = \sum_{k=1}^{i} d_{k} \right)$$
 (D-12)

$$d_T = \sum_{k=m+1}^{i} d_k \tag{D-13}$$

$$d_R = \sum_{k=i+1}^{n+1} d_k {(D-14)}$$

This procedure is repeated sequentially to determine the effective heights and distances for all knife edges on the right side of the primary knife edge that are not sub-path knife edges until there are no knife edges left except the sub-path knife edges, which are treated separately in Section D.3.

For the left side (transmitter side) of the primary knife edge, the effective height of the i^{th} knife edge that is not a sub-path knife edge is computed by determining the previous x^{th} knife-edge peak (located to the left of the i^{th} knife-edge peak) that will serve as a reference source knife edge for the i^{th} knife edge on the left side of the primary knife edge. The reference source knife edge h_x will be the x^{th} knife edge that is not a sub-path knife edge that is located to the left of the secondary i^{th} knife edge that has a minimum absolute value of slope of a line drawn from the primary m^{th} knife-edge peak to the x^{th} knife-edge peak. For the i^{th} knife edge on the left side of the primary knife edge, the primary m^{th} knife edge is the receptor for the energy diffracted by the i^{th} knife edge. If the x^{th} knife edge does not exist, because the i^{th} knife edge is adjacent to the transmitter, then use the transmitter antenna height h_t for the knife-edge height. If the next location is the transmitter, then x=0 and $h_x=h_t$. The transmitter antenna will then serve as the reference source for the i^{th} secondary knife edge. The equation of a line for the baseline used to calculate the effective height of the i^{th} knife edge is the equation of a line that connects the m^{th} knife-edge peak to the x^{th} knife-edge peak of knife edge, given as (D-15).

$$y_{PL} = \frac{(h_m - h_x)d}{\sum_{k=1}^{m} d_k}$$
 (D-15)

The effective height h'_i of the i^{th} knife edge is evaluated using y_{PL} at the i^{th} knife edge (D-16). The distances are calculated using (D-17) and (D-18).

$$h'_{i} = h_{i} - y_{PL} \left(d = \sum_{k=1}^{i} d_{k} \right)$$
 (D-16)

$$d_T = \sum_{k=1}^{i} d_k \tag{D-17}$$

$$d_R = \sum_{k=i+1}^m d_k \tag{D-18}$$

This procedure is repeated sequentially for all knife edges on the left side of the primary knife edge that are not sub-path knife edges until there are no knife edges left except the sub-path knife edges, which are treated in the next section.

D.3 Effective Heights and Distances of the Sub-Path Knife Edges for the Giovaneli Algorithm

A sub-path knife edge is a knife edge between two knife edges whose peak is below a line drawn between the previous knife edge and the next knife edge. A sub-path knife edge can also occur between the transmitter antenna and the second knife edge, or the next-to-last knife edge and the receiver antenna. If the first knife edge or last knife-edge peak is below a ray represented by a line that is drawn between the transmitter antenna to the second knife-edge peak, or a line that is drawn from the next-to-last knife-edge peak and the receiver antenna, respectively, then the first or last knife-edge peak is a sub-path knife edge.

For knife edges on either side of the primary knife edge that are sub-path knife edges, the procedure involves using a baseline from the previous u^{th} knife-edge peak of knife edge h_u to the next z^{th} knife-edge peak of knife edge h_z that are not sub-path knife edges. The procedure shown here will also work for computing effective knife-edge heights of knife edges with zero effective height. The equation for the baseline for the effective height of the i^{th} knife-edge peak for a sub-path knife edge is.

$$y_N = \frac{(h_z - h_u)(d - \sum_{k=1}^u d_k)}{\sum_{k=u+1}^z d_k} + h_u$$
 (D-19)

where h_z is the height of the z^{th} knife-edge peak, and h_u is the height of the u^{th} knife edge. When the z^{th} knife edge does not exist, because the i^{th} knife edge is the last knife edge and the next location is at the receiver, then the baseline is a line between the u^{th} knife-edge peak and the receiver antenna at height h_r , the index z=n+1 and $h_z=h_r$. When the u^{th} knife edge does not exist, because the i^{th} knife edge is the first knife edge and the previous location is at the transmitter, then the baseline is a line between the z^{th} knife edge and the transmitter antenna height h_t , and the index u=0, and $h_u=h_t$. The effective height is the vertical distance from this baseline to the i^{th} knife-edge peak (D-20). The corresponding distances d_T and d_R for each knife edge are also computed (D-21), (D-22).

$$h_i' = h_i - y_N \left(d = \sum_{k=1}^i d_k \right) \tag{D-20}$$

$$d_T = \sum_{k=u+1}^{i} d_k \tag{D-21}$$

$$d_R = \sum_{k=i+1}^{Z} d_k \tag{D-22}$$

D.4 Final Summation of All Diffraction Losses

The losses for each knife edge are computed using the diffraction parameter v_i from (D-23) for each knife edge and (D-10) for J(v) [8]. The diffraction losses for all knife edges are added together for the total diffraction loss.

$$\nu_i = h_i \sqrt{\frac{2}{\lambda} \left(\frac{1}{d_T} + \frac{1}{d_R}\right)}$$
 (D-23)

	REPO	ORT DOCUME	NTATIO	N PA	GE		
4 DEDONT DATE		2000iiL				DED	
1. REPORT DATE October 2025		2. REPORT TYPE NTIA Technical Report			3. DATES COVERE START DATE		END DATE
4. TITLE AND SUBTITL A Comparative An	L E alysis of Multiple Knife	e-Edge Diffraction Me	ethods				<u> </u>
5a. CONTRACT NUME	BER	5b. GRANT NUMBER		5	c. PROGRA	M ELEM	ENT NUMBER
5d. PROJECT NUMBE 6130404 6. AUTHOR(S)		5e. TASK NUMBER 002			f. WORK UI		IBER
Nicholas DeMinco	, Paul M. McKenna, an	d Robert T. Johnk					
Institute for Teleco					REPOR	FORMIN T NUMB TR-26-5	
9. SPONSORING/MONITORING AGENCY NAME(S) AND ADDRESS(ES National Telecommunications and Information Administrat Herbert C. Hoover Building 1401 Constitution Ave., N.W. Washington, D.C. 20230			ACR	10. SPONSOR/MONITOR'S ACRONYM(S) NTIA			
	/AILABILITY STATEMENT lic release. Distribution	n is unlimited.					
13. SUPPLEMENTARY	NOTES						
diffraction are pres diffraction loss is ri model that prediction graphical prediction orders of magnitude terrain for many ra proposed. Graphic	prough comparative as sented and compared gorous and verified w as area coverage over on methods for diffract de faster. This is import dial directions from the cal techniques and ma methods are included.	to the method devel ith measured data, b irregular terrain. Math tion paths with up to tant for use in propa- e transmitter. A technatical algorithm	oped by Vog ut too comp nematical alg six knife edg gation mode nique for selo s are also de	gler. Thoutation gorithm ges, resules that ecting tescribed	e Vogler ally intens as were de ulting in n predict an he best a d. Compa	multipl sive for evelope nethod rea cov lternati risons	e knife-edge ruse in a propagation ed for alternative ls that are many erage over irregular ive method is of the Vogler method
	magnetic diffraction, e uency propagation, ra			ethod			diffraction, non-line-
a. REPORT Unclassified	b. ABSTRACT Unclassified	C. THIS PAGE Unclassified		UU	-DJ IRACI	10. NU	105
19a. NAME OF RESPO Christopher A. And					. PHONE N -893-529		(Include area code)